THE UNIVERSITY OF MICHIGAN
COLLEGE OF ENGINEERING
Department of Chemical and Metallurgical Engineering

Second Annual Report

ENGINEERING STUDIES ON MOVEMENT OF WATER IN CONTACT WITH NATURAL GAS

(Project NO31)

Donald L. Katz M. Rasin Tek

Maurice C. Miller Stanley C. Jones

ORA Project 02935

under contract with:

The American Gas Association
New York, New York

administered through:

OFFICE OF RESEARCH ADMINISTRATION ANN ARBOR

October 1961

Members of the Supervising Committee For American Gas Association

Research Project NO31*

J. A. Vary, Chairman	Michigan Consolidated Gas Company
O. C. Davis	Natural Gas Storage Company of Illinois
B. B. Gibbs	United Gas Corporation
E. V. Martinson	Northern Natural Gas Company
C. E. Stout	Columbia Gas System Service Corporation
S. J. Cunningham	American Gas Association
R. M. Duke, Secretary	American Gas Association

*A subcommittee of the AGA Pipeline Research Committee, R. H. Crowe, Chairman.

TABLE OF CONTENTS

	Page
LIST OF TABLES	v
LIST OF FIGURES	vii
ABSTRACT	xi
INTRODUCTION	1
PART I. CALCULATION PROCEDURES DEVELOPED, EXTENDED, AND IMPROVED DURING THE SECOND YEAR	
A. ANALYSIS OF RESERVOIR PERFORMANCE BASED ON FIELD DATA	7
1. Development of Equations	7
2. Summary of Working Equations and Stepwise Calculation Procedure	11
B. LINEAR FLOW MODEL	14
1. Constant-Pressure Case	15
2. Constant-Rate Case	16
3. Variable-Pressure Solution	17
C. EQUATIONS COMMON TO THE VARIOUS METHODS	18
1. Calculation of Bottom-Hole Pressure, Psia	18
2. Calculation of Gas in Place	19
3. Calculation of Pore-Volume Ratio	20
4. Calculation of Dimensionless Time	20
D. SUMMARY OF WORKING EQUATIONS FOR RADIAL AND THICK SAND MODELS	21
1. Radial Flow Model	21
2. Thick Sand Model	24
PART II. FIELD CASE STUDIES	
FIELD A	33
1. Geology	33
2. Field Data	33
3. Calculations	33
4. Results	41

TABLE OF CONTENTS (Concluded)

	Page
FIELD B	49
1. Geology	49
2. Field Data	49
3. Calculations	53
4. Results	57
FIELD C	63
1. Geology	63
2. Field Data	63
3. Calculations	63
4. Results	71
FIELD D	77
1. Geology	77
2. Field Data	77
3. Calculation on Field D: Example of Resistance-Function Method	80
FIELD E	95
1. Geology	95
2. Field Data	96
3. Results	96
FIELD F	111
1. Geology	111
2. Field Data	111
3. Results	111
FIELD G	123
1. Geology	123
2. Field Data	123
3. Results	123
FIELD H	135
1. Geology	135
2. Field Data	135
3. Results	135
ACKNOWLEDGMENT	147
REFERENCES	149

LIST OF TABLES

Table		Page
I.	Data Required and Used for Field Studies on Various Models.	2
II.	Dimensionless Pressure Drop vs. Dimensionless Time for Thick Sand Model	25
III.	Parameters M and A for the Thick Sand Model	25
IV.	Definition and Units of Parameters used in the Various Mathematical Models and in the Resistance Function	32
V.	Parameters used for Fit and Prediction of Field Data	146
A-1.	Gas Field A Data	35
A-2.	Gas Inventory and Pressure History for Field A	36
A-3.	Calculated Values for Field A using Radial Model	38
B-1.	Storage Field B Data	51
B-2.	Gas Inventory and Pressure History for Field B	52
B-3.	Calculated Values for Field B using Thick Sand Model	55
C-1.	Storage Field C Data	65
C-2.	Gas Inventory and Pressure History for Field C	66
C-3.	Calculated Values for Field C using Linear Model	68
D-1.	Storage Field D Data	78
D-2.	Gas Inventory and Pressure History for Field D	79
E-1.	Storage Field E Data	97
E-2.	Gas Inventory and Pressure History for Field E	98

LIST OF TABLES (Concluded)

Table		Page
F-1.	Storage Field F Data	112
F-2.	Gas Inventory and Pressure History for Field F	113
G-1.	Gas Field G Data	124
G-2.	Gas Inventory and Pressure History for Field G	125
H-1.	Storage Field H Data	136
H-2.	Gas Inventory and Pressure History for Field H	137

LIST OF FIGURES

Figure		Page
A-1.	Areal sketch showing boundary of Field A.	34
A-2.	Comparison of Field A predicted pressures, assuming no water movement with observed pressures.	42
A-3.	Comparison of Field A pressures predicted using radial model (infinite aquifer) with observed pressures.	43
A-4.	Comparison of Field A volume ratio predicted using radial model (infinite aquifer) with volume ratios calculated from field data.	44
A-5.	Comparison of Field A pressures predicted using resistance function with observed pressures.	45
A-6.	Comparison of Field A volume ratio predicted using resistance function with volume ratios calculated from field data.	46
A-7.	Resistance function vs. time for Field A.	47
B-1.	Areal sketch showing boundary of Field B.	50
B-2.	Comparison of Field B predicted pressures, assuming no water movement with observed pressures.	58
B-3.	Comparison of Field B pressures predicted using thick sand model (infinite aquifer) with observed pressures.	59
B-4.	Comparison of Field B pressures predicted using radial model (infinite aquifer) with observed pressures.	60
B-5.	Comparison of Field B volume ratio predicted using radial model (infinite aquifer) with volume ratios calculated from field data.	61
C-1.	Areal sketch showing the boundary of Field C.	64
C-2.	Comparison of Field C predicted pressures, assuming no water movement with observed pressures.	73

LIST OF FIGURES (Continued)

Figure		Page
C-3.	Comparison of Field C pressures predicted using linear model (infinite aquifer) with observed pressures.	74
C-4.	Comparison of Field C volume ratio predicted using linear model with volume ratios calculated from field data.	75
D-1.	Areal sketch showing boundary of Field D.	81
D-2.	Comparison of Field D predicted pressures, assuming no water movement with observed pressures.	89
D-3.	Comparison of Field D pressures predicted using radial model (infinite aquifer) with observed pressures.	90
D-4.	Comparison of Field D volume ratios predicted using infinite radial model with volume ratios calculated from field data.	91
D-5.	Comparison of Field D pressures predicted using resistance function with observed pressures.	92
D-6.	Comparison of Field D volume ratios predicted using resistance function with volume ratios calculated from field data.	93
D-7.	Resistance function vs. time for Field D.	94
E-1.	Areal sketch showing boundary of gas Field E.	100
E-2.	Comparison of Field E predicted pressures assuming no water movement with observed pressures for an initial pore volume of 440 million cubic feet.	101
E-3.	Comparison of Field E predicted pressures assuming no water movement with observed pressures for an initial pore volume of 520 million cubic feet.	102
E-4.	Comparison of Field E pressures predicted using thick sand model (infinite aquifer) with observed pressures.	103
E-5.	Comparison of Field E pressures predicted using radial model (infinite aquifer) with observed pressures.	104

LIST OF FIGURES (Continued)

Figure		Page
E-6.	Comparison of Field E pressures predicted using finite radial model (R=9) with observed pressures.	105
E-7.	Comparison of Field E volume ratio predicted using finite radial model (R=9) with volume ratios calculated from field data.	106
E-8.	Comparison of Field E pressures predicted using resistance function with observed pressures.	107
E-9.	Comparison of Field E volume ratio predicted using resistance function with volume ratios calculated from field data.	108
E-10.	Resistance function vs. time for Field E.	109
F-1.	Areal sketch showing boundary of Field F.	115
F-2.	Comparison of Field F predicted pressures, assuming no water movement with observed pressures.	116
F-3.	Comparison of Field F pressures predicted using radial model (infinite aquifer) with observed pressures.	117
F-4.	Comparison of Field F pressures predicted using finite radial model (R=10) with observed pressures.	118
F-5.	Comparison of Field F volume ratio predicted using finite radial model (R=10) with volume ratios calculated from field data.	119
F-6.	Comparison of Field F pressures predicted using resistance function with observed pressures.	120
F-7.	Comparison of Field F volume ratios predicted using resistance function with volume ratios calculated from field data.	121
F-8.	Resistance function vs. time for Field F.	122
G-1.	Areal sketch showing boundary of Field G.	127

LIST OF FIGURES (Concluded)

Figure		Page
G-2.	Comparison of Field G predicted pressures assuming no water movement with observed pressures.	128
G-3.	Comparison of Field G pressures predicted using radial model (infinite aquifer) with observed pressures.	129
G-4.	Comparison of Field G volume ratio predicted using radial model (infinite aquifer) with volume ratios calculated from field data.	130
G-5.	Comparison of Field G pressures predicted using resistance function with observed pressures.	131
G-6.	Comparison of Field G volume ratio predicted using resistance function with volume ratios calculated from field data.	132
G-7.	Resistance function vs. time for Field G.	133
H-1.	Areal sketch showing boundary of Field H.	139
H-2.	Comparison of Field H predicted pressures assuming no water movement with observed pressures.	140
H-3.	Comparison of Field H pressures predicted using radial model (infinite aquifer) with observed pressures.	141
H-4.	Comparison of Field H volume ratio predicted using radial model (infinite aquifer) with observed pressures.	142
H-5.	Comparison of Field H pressures predicted using resistance function with observed pressures and those calculated assuming no water movement.	143
H-6.	Comparison of Field H volume ratio predicted using resistance function with volume ratios calculated from field data.	144
H-7.	Resistance function vs. time for Field H.	145

ABSTRACT

The purpose of American Gas Association Project NO31, "Engineering Studies on Movement of Water in Contact with Natural Gas," begun at The University of Michigan in May, 1959, was to investigate the behavior of aquifers adjacent to gas storage reservoirs. The equations and procedures developed during the first year (see that year's progress report) were applied during this second year to typical cases of aquifer water-movement problems for which direct data from fields were available. This work permitted a quantitative evaluation of predictive and simulative accuracy of the equations and methods developed as well as their practical applicability to various cases.

INTRODUCTION

When water drive is present, volumetric studies of gas production or storage reservoirs, simulation of inventory gas-pressure behavior, optimization of production-pressure schedules, development of gas storage bubbles in aquifers, and of many other reservoir engineering problems of practical significance must take into account the nature and extent of the water movement at reservoir boundaries. A broad investigation of various problems encountered in the movement of water in contact with natural gas was initiated by the American Gas Association as Project NO31 in May, 1959.

The first year of the research project was devoted to defining various geometric models and problems encountered in the field and developing solutions and computational procedures permitting the prediction of water movement for various cases. This work was reported in the first annual report issued in September, 1960.

The models of gas fields and surrounding aquifers studied during the first year included:

1. horizontal radial flow;
2. radial flow with thickness parameters;
3. hemispherical flow;
4. reservoirs bounded by elliptic geometry; and
5. multilayered sands.

In addition to the above, where the geometry is the controlling factor, a generalized method for analyzing the reservoir performance from direct field data on that particular reservoir was developed and reported as a special computational procedure to be applied to actual field case studies.

To check out, test, and evaluate the equations and procedures developed for predicting the water movement, a program based on study of analysis of direct field data was initiated early during the second year of the project. Several gas storage and producing companies were contacted and visited with assistance from AGA and API. As a result, field data from several companies operating gas fields subject to water drive have been received, screened, and selected for evaluation of various theories and methods developed during the first year.

Table I below indicates the data required and used for field studies on various models. The field case studies completed during the past year included eight fields analyzed by digital computational procedures and mathematical models developed during the first year on the project. These fields are located in Michigan, Kansas, Illinois, New York, and the Gulf of Mexico.

TABLE I

DATA REQUIRED AND USED FOR FIELD STUDIES ON VARIOUS MODELS

Aquifer Characteristics

Type of formation
Lateral extent
Average thickness, variation range
Average porosity, variation range
Average permeability (core data), variation range
Permeability (in situ) from well tests
Formation and liquid compressibility (if known)
Vicsocity of liquid
Density of liquid in aquifer—undisturbed
Initial pressure or water level
Depth of the aquifer sand

Data on Producing or Storage Fields

a. Field geometry
   Location: state, county, township
   Type of formation
   Nature of structure, contour map with water level, cross sections
   Number and location of gas wells
   Number and location of observation wells

b. Gas sand formation and fluid properties
   Porosity
   Permeability
   Reservoir temperature
   Gas gravity
   Reservoir depth
   Baseconditions for gas measurement
   Gas compressibility factor data

c. Data on production-pressure history of gas reservoir
   Initial discovery pressure with datum
   Reservoir formation or well head pressures (weekly or monthly time increments)
   Inventory (cumulative) gas vs. time

Radial, Linear, and Thick Sand models and the Resistance Function method have been used to predict, compare, and evaluate the equations developed for simulating the actual reservoir behavior observed. To ascertain the nature and relative degree of effectiveness of water movement, the performance predicted for each case has been compared with performance computed on the basis of no water movement.

These field studies are described in detail in this report. It may be noticed that four sections precede the major section of this report entitled "Field Case Studies." These sections include; Analysis of Reservoir Performance Based on Field Data (The Resistance Function Method), The Linear Flow Model, Equations Common to the Various Methods, and A Summary of Working Equations for Radial and Thick Sand Models.

PART I. CALCULATION PROCEDURES DEVELOPED, EXTENDED, AND IMPROVED DURING THE SECOND YEAR

As work on field studies progressed during the second year of the project it became necessary to develop some additional calculation procedures. The first major phase of this development concerned the resistance function method, which was improved in its practical applicability and predictive accuracy since last year's report. The second phase saw the development of the Linear Model. In addition, a list of equations common to most of the methods and a summary of the calculation procedures for the Radial and Thick Sand Models are included in this section.

A. ANALYSIS OF RESERVOIR PERFORMANCE BASED ON FIELD DATA

A calculation procedure for predicting performance in water-drive fields without the usual assumptions of simplified aquifer geometry, homogeneity, and isotrophy is presented here. A characteristic curve called the "resistance function" is calculated from field-performance data. Its extrapolation allows prediction of future water movement and pressure behavior when a production-injection schedule is given or assumed.

A previous weakness of the method due to its sensitivity to small errors in pressure data has been eliminated by "fitting" the radial model for an infinite aquifer to the first few data points. The best fit of this mathematical model yields the initial portion of the resistance function. The remainder of the curve (which is less sensitive to these errors) is computed from an algebraic rearrangement of the superposition equation using field performance data directly.

Calculation of the resistance function is unstable. However, suitable damping based on theoretical restrictions on the shape of the curve restores stability at the expense of a slight loss of accuracy.

In its present form, the method is suitable for processing on a digital computer without intermediate manual operations.

1. DEVELOPMENT OF EQUATIONS

Solutions to the partial differential equations for pressure drop at the gas-water interface of an aquifer as a function of time and water influx rate for various field geometries may all be expressed in the general form:

$$\Delta P = K_1 e_w f(t_D) \qquad (1)$$

This equation gives the pressure drop for a constant rate of influx, e_w. Both K_1 and the function $f(t_D)$ are determined by the physical properties and geometry of the system and are different for each aquifer shape. They are "known" for the simplified geometries when the aquifer properties are given. For the radial model which is used in determining the initial portion of the resistance curve:

$$K_1 = 25.15\mu/(Khf) \tag{1a}$$

$$t_{D_n} = K_2 \cdot n = \frac{0.00633\ K\Delta t}{\mu\phi c r_b^2} \cdot n \tag{1b}$$

where n indicates the nth time increment, each of which has a duration of Δt days. The function $f(t_D)$ has been solved by Van Everdingen and Hurst[4] and is presented in tabular form.[1,2,4] See Table IV, page 32 for nomenclature.

For the case of a nonhomogeneous anisotropic aquifer with an irregular geometry, we assume that some function of time, $K_1 f(t_D)$, exists. The problem is to find it.

Equation (1) may be modified by the superposition principle to account for a nonconstant water influx rate:

$$\Delta P = K_1 \int_o^t e_w(t_D - \tau)\ \frac{\partial f(t_D)}{\partial \tau}\ d\tau \tag{2}$$

where t_D is "dimensionless time" and τ is a dummy variable of integration.

Equation (2) may be approximated by an equivalent finite difference form:

$$\Delta P = K_1 \sum_{j=1}^{n} e_{w_{(n+1-j)\Delta t_D}} \cdot \Delta f_{j\Delta t_D} \tag{3}$$

Any desired degree of accuracy can be obtained by reducing the size of the dimensionless time increment, Δt_D. The function $f(t_D)$ may be replaced by another function $g(t)$, where t is actual, rather than dimensionless time. If K_1 is combined with this new function inside the summation sign and Δt is taken as unity then Eq. (3) becomes:

$$\Delta P_n = \sum_{j=1}^{n} e_{w_{n+1-j}} \cdot \Delta Z_j \tag{4}$$

where $\Delta Z_n \equiv Z_n - Z_{n-1} = K_1 \Delta g_n$ and $\Delta P_n \equiv P_o - P_n$. As used in Eq. (4), e_{w_n} is the average water influx rate during the nth time interval. This rate is equal to the decrease in the volume of the gas bubble during the interval:

$$e_{w_n} = \frac{V_{n-1} - V_n}{\Delta t} = \frac{1}{\Delta t}\left\{\left(\frac{a}{P_{n-1}} + b\right)\left(\frac{V_o}{\frac{a}{P_o}+b} - \frac{P_b G_{p_{n-1}} T}{T_b}\right) - \left(\frac{a}{P_n} + b\right)\left(\frac{V_o}{\frac{a}{P_n}+b} - \frac{P_b G_{p_n} T}{T_b}\right)\right\} \tag{5}$$

The constants a and b arise from a linear approximation of the variation of the gas compressibility factor with pressure, $z = a+bP$. We can write Eq. (5) more compactly by defining a new variable, S_n:

$$S_n = \frac{V_o}{\Delta t\left(\frac{a}{P_o}+b\right)} - \frac{P_b T}{\Delta t T_b} \cdot G_{p_n} \tag{6}$$

where G_p is the cumulative gas produced, SCF at pressure and temperature bases P_b and T_b, respectively. Equation (5) now becomes:

$$e_{w_n} = (a/P_{n-1} + b)S_{n-1} - (a/P_n + b)S_n \tag{5a}$$

Our problem now is to calculate Z_n as a function of time. Toward this goal the first and last terms of the summation of Eq. (4) are removed from under the summation sign and the equation is solved for e_{w_n}:

$$e_{w_n} = \frac{1}{\Delta Z_1}\left(P_o - P_n - e_{w_1} \cdot \Delta Z_n - \sum_{j=2}^{n-1} e_{w_{n+1-j}} \cdot \Delta Z_j\right). \tag{7}$$

Now e_{w_n} is eliminated between Eqs. (5a) and (7) and the resulting equation is solved for ΔZ_n:

$$\Delta Z_n = \frac{1}{e_{w_1}}\left\{P_o - P_n^* - \sum_{j=2}^{n-1} e_{w_{n+1-j}} \cdot \Delta Z_j + \left(\frac{a}{P_n^*} + b\right)S_n \Delta Z_1 - \left(\frac{a}{P_{n-1}} + b\right)S_{n-1} \cdot \Delta Z_1\right\} \tag{8}$$

When Z is plotted vs. time the curve must pass through the origin, i.e., $Z_o = 0$; and it must have a positive slope which must either decrease or remain constant with increasing time. Therefore, theoretically, ΔZ_n cannot be greater than ΔZ_{n-1} nor less than, zero. However, small errors in the pressure data will cause violation of these rules. Since the calculation of ΔZ_n depends upon all the previous ΔZ's, these errors propagate themselves, resulting in an unstable computation. Thus it is mandatory to place restraints

on the otherwise direct calculation of the resistance function. The obvious upper limit, whenever ΔZ_n from Eq. (8) is greater than ΔZ_{n-1}, is to set ΔZ_n equal to ΔZ_{n-1}. A lower boundary is suggested by a limiting condition of the curve corresponding to the radial model for an infinite aquifer. At large times the slope of this curve is proportional to the natural log of time:

$$Z_n = A \cdot \ell n\, n + B$$

thus

$$\Delta Z_n = Z_n - Z_{n-1} = A \cdot \ell n \left(\frac{n}{n-1}\right)$$

and

$$\Delta Z_{n-1} = A \cdot \ell n \left(\frac{n-1}{n-2}\right)$$

therefore

$$\Delta Z_n = \Delta Z_{n-1} \frac{\ell n \left(\frac{n}{n-1}\right)}{\ell n \left(\frac{n-1}{n-2}\right)} \tag{9}$$

The first term of a series expansion of the ℓn terms is $(n-2)/(n-1)$; thus the lower limit for ΔZ_n is:

$$\Delta Z_n = \Delta Z_{n-1} \left(\frac{n-2}{n-1}\right) \tag{9a}$$

i.e., if ΔZ_n as calculated from Eq. (8) is less than the value calculated from Eq. (9a), then ΔZ_n is set equal to the latter value.

A moment's consideration will reveal that the above restrictions are too severe. For example, let us assume that we are generating a portion of the Z curve which should actually be a straight line, but due to an error in the pressure data, one ΔZ is less than the previous values. If the upper limit, as stated above, were applied, all the subsequent ΔZ's would have smaller values and the Z-curve could never "recover." The same argument applies to the lower boundary in addition to the fact that this particular limit does not necessarily apply to all geometries. A factor, ϵ, rectifies the situation:

(1) whenever $\Delta Z_n > (1+\epsilon)\Delta Z_{n-1}$, $\Delta Z_n = (1+\epsilon)\Delta Z_{n-1}$ (10a)

(2) or whenever $\Delta Z_n < (1-\epsilon)\Delta Z_{n-1}\left(\frac{n-2}{n-1}\right)$, $\Delta Z_n = (1-\epsilon)\Delta Z_{n-1}\left(\frac{n-2}{n-1}\right)$. (10b)

An $\epsilon = 0.02$ has been found to work satisfactorily. It should be pointed out

that condition (10a) above gives rise to the possibility of an upward-curving resistance function which violates the rule that the second derivative with respect to time, d^2Z/dt^2, be zero or negative. Whenever a positive second derivative occurred in the application of this method to field data, a straight line, tangent to the high points of the Z-curve, was drawn producing a new "smoothed" curve. Extrapolation and predictions were based on this new curve.

A programming modification is planned which will automatically produce tangents to the Z-curve, continuously back-correcting it.

Equations (5a) and (7) are combined and solved for P_n:

$$P_n^2 + \left\{\Delta Z_1\left[\left(\frac{a}{P_{n-1}} + b\right)S_{n-1} - bS_n\right] + \sum_{j=2}^{n} e_{w_{n+1-j}} \cdot \Delta Z_j - P_o\right\} P_n - aS_n\Delta Z_1 = 0$$

Let

$$B_n = \frac{1}{2}\left\{\Delta Z_1\left[\left(\frac{a}{P_{n-1}} + b\right)S_{n-1} - bS_n\right] + \sum_{j=2}^{n} e_{w_{n+1-j}} \cdot \Delta Z_j - P_o\right\}$$

and

$$C_n = aS_n\Delta Z_1$$

Therefore

$$P_n = \sqrt{B_n^2 + C_n} - B_n \qquad (11)$$

The water influx during the nth time interval is calculated using the smoothed ΔZ_n value and the corresponding calculated pressure, P_n:

$$e_{w_n} = \frac{1}{\Delta Z_1}\left(P_o - P_n - \sum_{j=2}^{n} e_{w_{n+1-j}} \cdot \Delta Z_j\right) \qquad (12)$$

2. SUMMARY OF WORKING EQUATIONS AND STEPWISE CALCULATION PROCEDURE

(1) Calculate K_1 and K_2 from best estimate of reservoir field properties

$$K_1 = 25.15\mu/(Khf)$$

$$K_2 = 0.006328\ K\Delta t/(\mu\phi c r_b^2)$$

(2) Calculate all S_n values to be used from an estimate of the initial pore volume, V_o, and cumulative gas production data, G_{p_n}

$$S_n = V_o/[(a/P_o + b)\Delta t] - [P_b T/(T_b \Delta t)] \cdot G_{p_n}$$

$$= C_1 - C_2 \cdot G_{p_n} \qquad n = 1,2,\ldots, L$$

(3) Compute dimensionless time values corresponding to the first few data points

$$t_{D_n} = K_2 \cdot n, \quad n = 1,2,\ldots, M$$

(4) Using linear interpolation and values from tables[1,2,4] calculate dimensionless pressure values:

$$p_n = p_{j=1} + \frac{(t_{D_n} - t_{D_{j-1}})}{(t_{D_j} - t_{D_{j-1}})} (p_j - p_{j-1})$$

where j and j-1 refer to the table values of $p(t_D)$ and t_D nearest to and respectively greater and less than t_{D_n}.

(5) Calculate $\Delta p_1 \ldots \Delta p_M$

$$\Delta p_n = p_n - p_{n-1}$$

(6) Compute P_n and e_{w_n} alternatively, starting with P_1:

$$P_n = \sqrt{B_n^2 + C_n} - B_n$$

where

$$B_n = \frac{1}{2}\left\{[(a/P_{n-1} + b)S_{n-1} - bS_n]K_1 \Delta p_1 - P_o + K_1 \sum_{j=2}^{n} e_{w_{n+1-j}} \cdot \Delta p_j \right\}$$

and

$$C_n = aS_n K_1 \Delta p_1$$

$$e_{w_n} = \left(P_o - P_n - K_1 \sum_{j=2}^{n} e_{w_{n+1-j}} \cdot \Delta p_j\right)/K_1 \Delta p_1$$

$$n = 1,2,\ldots, M$$

(7) Find the percentage deviation between calculated pressures and selected pressure data

$$\% \text{ deviation} = 100 \frac{\sum \left| P_{calc_i} - P_{data_i} \right|}{\sum P_{data_i}}$$

where P_i's are selected from $P_1 \ldots P_M$, but do not necessarily include all the values.

(8) Change the value of K_1 and repeat steps (6) and (7). Repeat until the minimum deviation between calculated and data pressures is obtained.

(9) Compute $\Delta Z_1 \ldots \Delta Z_M$

$$\Delta Z_n = K_{1_{optimum}} \cdot \Delta p_n$$

(10) Find ΔZ_{M+1}

$$\Delta Z_n = P_o - P_n^* - \sum_{j=2}^{n-1} e_{w_{n+1-j}} \cdot \Delta Z_j + [(a/P_n^* + b)S_n - (a/P_{n-1} + b)S_{n-1}]\Delta Z_1$$

The asterisk denotes pressure data. Pressures without it are calculated.

(11) If ΔZ_{M+1} does not fall within the following limits set it is equal to the lower value if below or to the higher limit if above:

$$(1-\epsilon)\left(\frac{n-2}{n-1}\right)\Delta Z_{n-1} \leqslant \Delta Z_n \leqslant (1+\epsilon) \cdot \Delta Z_{n-1}$$

A value of $\epsilon = 0.02$ has been found to work satisfactorily.

(12) Calculate P_{M+1} using the corrected value of ΔZ_{M+1}

$$P_n = \sqrt{B_n^2 + C_n} - B_n$$

where

$$B_n = \frac{1}{2}\left\{[(a/P_{n-1} + b)S_{n-1} - bS_n]\Delta Z_1 - P_o + \sum_{j=2}^{n} e_{w_{n+1-j}} \cdot \Delta Z_j\right\}$$

and

$$C_n = aS_n\Delta Z_1$$

(13) Compute $e_{w_{M+1}}$

$$e_{w_n} = P_o - P_n - \sum_{j=2}^{n} e_{w_{n+1-j}} \cdot \Delta Z_j \Big) / \Delta Z_1$$

(14) Repeat steps (11), (12), and (13), for n = M+2...L.

(15) "Observed" and calculated pore volume ratios may be calculated for n = 1... L

$$\left(\frac{V_n}{V_o}\right)_{obs} = \left(\frac{a}{P_n^*} + b\right) \frac{S_n \Delta t}{V_o}$$

$$\left(\frac{V_n}{V_o}\right)_{calc} = 1 - \left(\Delta t \sum_{j=1}^{n} e_{w_j}\right) / V_o$$

(16) If a finite aquifer is indicated (as has been the case in all the present field studies), i.e., if a plot of Z_n vs. n approaches a straight line as n approaches L, extrapolation is obtained by setting $\Delta Z_{L+1}...\Delta Z_N$ all equal to ΔZ_L. Otherwise

$$\Delta Z_{n+1} = \Delta Z_n \cdot \frac{n-1}{n} \text{ for } n = L... N.$$

(17) Calculate $S_{L+1}...S_N$ (see step 2) using projected gas production schedule.

(18) Predict pressures and water influx rates using the extrapolated ΔZ_n values in steps (12) and (13).

B. LINEAR FLOW MODEL

The partial differential equation governing one-dimensional, unsteady-state flow of a compressible liquid through porous media is

$$\frac{\partial^2 p}{\partial x^2} = \frac{\mu \phi c}{K} \frac{\partial p}{\partial t} \tag{1}$$

Definition of the new variables

$$P = p - p_o \tag{2}$$

$$\theta = Kt/(\mu \phi c) \tag{3}$$

where p_o is initial aquifer pressure, allows (1) to be written

$$\frac{\partial^2 P}{\partial x} = \frac{\partial P}{\partial \theta} \tag{4}$$

The solutions to Eq. (4) for constant boundary pressure and constant water influx rate across the boundary are obtained as follows.

1. CONSTANT-PRESSURE CASE

Here the initial and boundary conditions for solution of Eq. (4) are

$$P(x,0) = 0 \tag{5}$$
$$P(\infty,\theta) = 0 \tag{6}$$
$$P(0,\theta) = \Delta p \tag{7}$$

If $\bar{P}(x,s)$ denotes the Laplace Transform of $P(x,\theta)$ with respect θ, then transformation of Eq. (4) yields

$$\frac{d^2\bar{P}}{dx^2} - s\bar{P} = 0 \tag{8}$$

for which the solution satisfying Eqs. (6) and (7) is

$$\bar{P} = \frac{\Delta p}{s} e^{-\sqrt{s}\, x} \tag{9}$$

The rate of water influx into the reservoir (at x = 0) is

$$q = \frac{KA}{\mu} \frac{\partial p}{\partial x}\Big)_{x=o} = \frac{KA}{\mu} \frac{\partial P}{\partial x}\Big)_{x=o} = q(\theta)$$

where A is the cross-sectional area of the linear flow system.

The Laplace Transform of q is

$$\bar{q}(s) = \frac{KA}{\mu} \left.\frac{\partial \bar{P}}{\partial x}\right)_{x=o} \tag{10}$$

The cumulative water influx into the reservoir is $W_e = \int_o^t q\,dt$ or

$$W_e = \frac{\mu\phi c}{K} \int_o^\theta q\,d\theta \ . \tag{11}$$

The Laplace Transform of W_e is $\bar{W}_e$

$$\bar{W}_e = \frac{\mu\phi c}{K} \frac{1}{s} \bar{q} = \frac{\mu\phi c}{K} \frac{KA}{\mu} \frac{1}{s} \left.\frac{\partial \bar{P}}{\partial x}\right)_{x=o} \tag{12}$$

Inserting $\left.\frac{\partial \bar{P}}{\partial x}\right)_{x=o}$ from Eq. (9) into Eq. (11) yields

$$\bar{W}_e = -\phi cA \frac{\Delta p}{s^{3/2}} \tag{13}$$

and taking the inverse transform of this expression yields

$$W_e = \frac{2}{\sqrt{\pi}} \phi cA(p_o - p) \sqrt{\theta} \tag{14}$$

which is the constant-pressure-case solution of Eq. (4). Thus the cumulative water influx W_e is proportional to the square root of time.

2. CONSTANT-RATE CASE

The initial and boundary conditions for the constant-rate case are

$$P(x,0) = 0 \tag{15}$$

$$P(\infty,0) = 0 \tag{16}$$

$$\left.\frac{\partial P}{\partial x}\right)_{x=o} = \frac{q\mu}{AK} \tag{17}$$

where q is the constant rate of water influx into the reservoir.

The solution to Eq. (8) for these conditions is

$$\bar{P}(x,s) = -\frac{q\mu}{AK}\frac{1}{s^{3/2}}e^{-\sqrt{s}\,x} \tag{18}$$

and the inverse transformation of this function is

$$P(x,\theta) = -\frac{q\mu}{AK}2\sqrt{\frac{\theta}{\pi}}\,e^{-\frac{x^2}{4\theta}}$$

The reservoir pressure at x = 0 is thus given as

$$p_o - p = \frac{2}{\sqrt{\pi}}\frac{q\mu}{AK}\sqrt{\theta} \tag{19}$$

When field units are used, $\theta = \frac{0.006328\ Kt}{\mu\phi c}$, t in days, c vol/vol psi, ϕ is a fraction, q is in ft^3/day, A in ft^2, μ in cp, K in md, and Eq. (19) becomes

$$p_o - p = 178\frac{q\mu}{AK}\sqrt{\theta} \tag{20}$$

which is the constant-rate-case solution of (4).

3. VARIABLE-PRESSURE SOLUTION

When the reservoir pressure is not constant but rather a specified function of time, the superposition principle can be applied to (14) to obtain

$$W_{e_j} = \frac{1}{\sqrt{\pi}}\phi cA\sqrt{\Delta\theta}\sum_{i=0}^{i=j-1}\Delta p_i\sqrt{(j-i)} \tag{21}$$

where

W_{e_j} = cumulative water influx at time $j\Delta t$, ft^3

$\Delta\theta$ = transformed time increment, $\frac{0.006328K}{\mu\phi c}\Delta t$

Δp_i = $p_{i-1} - p_{i+1}$; $p_{-1} = p_o$

p_i = reservoir pressure at time $i\Delta t$, psia

Δt = time increment, days.

Equation (21) gives comulative water influx for any known or specified pressure schedule, p_0, p_1, p_2,....

4. VARIABLE-RATE CASE

Application of the superposition principle to the constant-rate-case solution, (20), yields

$$p_o - p_j = \frac{178\mu\sqrt{\Delta\Theta}}{AK\Delta t} \sum_{i=0}^{i=j-1} \Delta V_i \sqrt{j-i} \qquad (22)$$

where

p_j = reservoir boundary pressure at time $j\Delta t$, psia

Δt = time increment, days

ΔV_i = $2V_i - V_{i+1} - V_{i-1}$; $\Delta V_o = V_o - V_1$

V_i = reservoir pore volume at time $i\Delta t$, ft^3

Equation (22) gives reservoir pressure p_j whenever the schedule of pore-volume variation is known or specified.

C. EQUATIONS COMMON TO THE VARIOUS METHODS

Equations used to calculate terms common in several programs are included below. These calculations concern:

(1) bottom-hole pressures when wellhead pressures are given;
(2) inventory gas in place (lb-moles) from initial pore volume and production-injection history;
(3) pore-volume ratios from calculated and observed pressures;
(4) dimensionless time; and
(5) prediction of pressure when no water movement is assumed.

1. CALCULATION OF BOTTOM-HOLE PRESSURE, PSIA

Field-pressure data are usually expressed in psig or psia (wellhead). The pressure in the reservoir is determined by the following procedure. If the data are given as psig (wellhead), add 14.7 to obtain psia (wellhead) and calculate bottom-hole pressure by

$$P_{bhp} = P_{wh}\, e^{Mh/(144\ zRT)} \qquad (1)$$

where

P_{bhp} = bottom-hole pressure, psia

P_{wh} = wellhead pressure, psia

M = molecular weight of gas = gas gravity x 29

h = depth gas well below surface, feet

R = 10.73 $(psia)(ft)^3(lb\text{-}mole)^{-1}(°R)^{-1}$

T = reservoir temperature, °R

z = gas compressibility factor

2. CALCULATION OF GAS IN PLACE

The number of pound moles initially in a gas reservoir, n_o, is calculated by

$$n_o = \frac{P_o V_o}{zRT} = \frac{P_o V_o}{(a+bP_o)RT} = \frac{V_o}{(\frac{a}{P_o}+b)RT} \qquad (2)$$

where

n_o = initial gas present in field, pound-moles

V_o = initial pore volume, ft^3

a,b = constants in correlation

$$z = a + bP$$

The cumulative gas in place, n_j, for any time step "j" is given by

$$n_j = n_o - \frac{P_{base}\, G_{p_j}}{RT_{base}}$$

where

P_{base} = base pressure for measurement of gas, psia

T_{base} = base temperature for measurement of gas, °R

G_{p_j} = cumulative gas produced (gas injected is defined as negative production), standard cubic feet

j = "j" time step

3. CALCULATION OF PORE-VOLUME RATIO

The ratio of the pore volume at any time step "j" to the initial pore volume is determined as follows:

$$\frac{V_j}{V_o} = \frac{zn_jRT}{P_jV_o} = \frac{(a+bP_j)n_jRT}{P_jV_o} \tag{4}$$

where P_j may be either an observed or calculated pressure.

4. CALCULATION OF DIMENSIONLESS TIME

Dimensionless time, t_D, and the incremental dimensionless time, Δt_D, used in the radial, thick sand, and hemispherical models are given in terms of field units by

$$t_D = \frac{0.00633\ Kt}{\mu\phi cr_b^2} \tag{5}$$

and

$$\Delta t_D = \frac{0.00633\ K\Delta t}{\mu\phi cr_b^2} \tag{6}$$

where

t_D = dimensionless time

Δt_D = incremental dimensionless time

K = permeability, millidarcys

t = time, days

Δt = time per increment, days

μ = viscosity, centipoise

ϕ = porosity, fraction

c = compressibility of aquifer rock and water, vol/vol psi

r_b = radius of gas reservoir or inner radius of aquifer, feet

Note that

$$t_j = j\Delta t \tag{7}$$

and

$$t_{Dj} = j\Delta t_D \tag{8}$$

5. PREDICTION OF PRESSURE ASSUMING NO WATER MOVEMENT

Pressures assuming no water movement are calculated from the gas law.

$$P_j = \frac{zn_jRT}{V_o} = \frac{(a+bP_j)n_jRT}{V_o} \tag{9}$$

Solving (9) for P_j yields

$$P_j = \frac{an_jRT}{V_o - bn_jRT} \tag{10}$$

D. SUMMARY OF WORKING EQUATIONS FOR RADIAL AND THICK SAND MODELS

The developments of the Radial Flow Model and Thick Sand Model were presented in our 1960 annual report. The Radial Flow Model has been modified to correct for the expansion and contraction of water under the gas bubble. A brief development of the working equations in their present form is given below.

1. RADIAL FLOW MODEL

Water influx for the constant terminal pressure case is calculated by superposing the effects of each constant time step, giving

$$W_{ej} = \pi\phi c r_b^2 hf \sum_{i=0}^{i=j-1} \Delta P_i \, Q_{(j-1)\Delta t} + \pi h\phi c r_b^2 f_1 (P_o - P_j) \tag{1}$$

where

$$\Delta P_i = P_{i-1} - P_{i+1}$$

and

$$P_{-1} = P_o \tag{2}$$

The first term on the right-hand side of Eq. (1) gives the water influx into the reservoir boundary; the second term represents the compression or expansion of water under the gas reservoir.

The dimensionless cumulative influx $Q_{(t_D)}$ is tabulated in the papers by Van Everdingen and Hurst,[4] Chatas,[1] and the Handbook of Natural Gas Engineering[2] [Tables (10-4)-(10-8), p. 426]. The dimensionless time is given by

$$t_D = \frac{0.00633\ Kt}{\mu \phi c r_b^2} \tag{3}$$

In Eqs. (1), (2), and (3) above, the terms in field units are given by

ϕ = fractional porosity

c = formation and water compressibility, vol/vol psi

h = formation thickness, ft

K = formation permeability, millidarcys

t = actual time, days

μ = water viscosity, centipoise

r_b = inner aquifer radius, ft

f = fraction of complete circle represented by reservoir

f_1 = fraction of cylinder $\pi r_b^2 h$ of water under gas reservoir

W_{e_j} = cumulative water influx at time $j\Delta t$

A volumetric balance gives

$$V_j = V_o - W_{e_j} \tag{4}$$

where V_o is the initial pore volume and V_j the pore volume at the j time step. V_j may be calculated using the gas law

$$V_j = \frac{z_j n_j RT}{P_j} \tag{5}$$

and the gas compressibility constant z; by

$$z_j = a+bP_j \tag{6}$$

Combining (1), (2), (4), (5), and (6) we obtain

$$\frac{a+bP_j}{P_j} n_j RT = V_o - \pi h\phi c r_b^2 f \sum_{i=0}^{j-2} \Delta p_i Q_{j-i}$$

$$- \pi h\phi c r_b^2 f\, P_{j-2} Q_1 - \pi h\phi c r_b^2 f_1\, P_o \tag{7}$$

$$+ P_j(\pi h\phi c r_b^2 f\, Q_1 + \pi h\phi c r_b^2 f_1)$$

Solving (7) for P_j yields

$$P_j = C_1 + \sqrt{C_1^2 + C_2} \tag{8}$$

where

$$C_1 = \frac{\pi h\phi c r_b^2 \left[f \sum_{i=0}^{j-2} \Delta P_i\, Q_{j-i} + f Q_1\, P_{j-2} + f_1 P_o\right] + b n_j RT - V_o}{2\pi h\phi c r_b^2 f\, Q_1 + 2\pi h\phi c r_b^2 f_1} \tag{9}$$

and

$$C_2 = \frac{a n_j RT}{[\pi h\phi c r_b^2 f\, Q_1 + \pi h\phi c r_b f_1^2]} \tag{10}$$

2. THICK SAND MODEL

The superposition principle applied to the equation governing the reservoir pressure drop for the thick sand model, constant-terminal-rate case, results in

$$P_o - P_j = \frac{50.2\mu}{Kr_b\sqrt{K_R}} \sum_{i=0}^{i=j-1} \Delta\bar{e}_i \, \bar{P}_{(j-i)} \qquad (11)$$

where

P_j = reservoir pressure at time $t = j\Delta t$, psia

$\Delta\bar{e}_i$ = $(\bar{e})_{i+1} - (\bar{e})_i$

$(\bar{e})_i$ = average rate of water influx during the time increment from $(i-1)\Delta t$ to $i\Delta t$ = $V_{i-1}-V_i$, ft^3/day

$\bar{P}_{j-i}$ = the value of P at dimensionless time $t_D = (j-i)\Delta t_D$

Δt = time increment chosen for representation of e_w as a step function of time, days

Δt_D = $(.00633\ K\Delta t)/\mu\phi c r_b^2$, dimensionless time increment

The dimensionless pressure drop, $\bar{P}_j$, is listed as a function of dimensionless time in Table II for t_D less than 10. For dimensionless time t_D greater than 10, $\bar{P}$ can be calculated from the equation

$$\bar{P} = A + \frac{1}{4M} \ln t_D \qquad (12)$$

where the value of the constant A is dependent upon M, as given in Table III.

M is defined by

$$M = h/(r_b K_R) \qquad (13)$$

where K_R is the ratio of vertical to horizontal permeability in aquifer (dimensionless).

Substituting the equivalent for $\Delta\bar{e}_i$, $(2V_i-V_{i+1}-V_{i-1})/\Delta t$, in Eq. (11), combining this with the equation of state for gases, and solving for P_j, one obtains:

$$P_j = C_1 + \sqrt{C_1^2 - C_2} \qquad (14)$$

TABLE II

DIMENSIONLESS PRESSURE DROP VS. DIMENSIONLESS TIME FOR THICK SAND MODEL

t_D = dimensionless time = $Kt/\mu\phi cr_b^2$ $\qquad$ $M = h/(r_b K_R)$

t_D	P						
	M = .05	M = .1	M = .3	M = .5	M = .7	M = .9	M = 1.0
.1	1.433	.741	.329	.287	.285	.285	.285
.2	2.675	1.362	.536	.412	.383	.377	.377
.3	3.649	1.849	.699	.509	.454	.436	.436
.4	4.464	2.257	.835	.591	.512	.483	.483
.5	5.166	2.608	.952	.661	.562	.522	.521
1	7.693	3.871	1.373	.914	.743	.663	.648
2	10.590	5.319	1.856	1.204	.950	.824	.792
3	12.442	6.245	2.164	1.389	1.082	.927	.885
4	13.789	6.919	2.389	1.523	1.178	1.001	.952
5	14.848	7.448	2.565	1.629	1.254	1.060	1.005
6	15.722	7.885	2.711	1.717	1.316	1.109	1.049
7	16.465	8.257	2.835	1.791	1.369	1.150	1.086
9	17.684	8.866	3.038	1.913	1.456	1.218	1.147
10	18.198	9.123	3.123	1.964	1.493	1.246	1.173

TABLE III

PARAMETERS M AND A FOR THE THICK SAND MODEL

M	A
.05	6.5644
.10	3.3065
.30	1.1846
.50	0.8010
.70	0.6622
.90	0.6000
1.00	0.5911

where

$$C_1 = -\frac{1}{2}\left(\frac{-50.2\mu}{Kr_b\sqrt{K_r}\,\Delta tf}\right)\left\{\sum_{i=0}^{j-2}\Delta V_i\bar{P}_{j-i} + (2V_{j-1} - V_{j-2})\bar{P}_1 - \bar{P}_1\,RTn_jb - P_o\right. \tag{14a}$$

and

$$C_2 = \left(\frac{-50.2\mu}{Kr_b\sqrt{K_r}\,\Delta tf}\right)\bar{P}_1\,RTn_ja \tag{14b}$$

and

$$\Delta V_i = 2V_i - V_{i+1} - V_{i-1} \tag{14c}$$

where

V_i = reservoir pore volume at time $t = i\Delta t$, ft.^{3}

If t_D is less than 10 and the value for M is not given in the table, dimensionless pressure, $\bar{P}$, can be calculated by a LaGrangian polynomial fit of three table values (Table II) whose values of M are nearest to the actual M:

$$\bar{P} = \frac{(M-M_2)(M-M_3)}{(M_1-M_2)(M_1-M_3)}\cdot\bar{P}_1 + \frac{(M-M_1)(M-M_3)}{(M_2-M_1)(M_2-M_3)}\bar{P}_2 + \frac{(M-M_1)(M-M_2)}{(M_3-M_1)(M_3-M_2)}\bar{P}_3 \tag{15}$$

Equation (15) is applied twice, the first time for t_D (Table II) less than the actual value, and then for t_D greater. Finally the dimensionless pressure drop corresponding to the required M and t_D is obtained by linear interpolation.

As an example, suppose that M = 0.65, and t_D = 3.5. First table values of $\bar{P}$ corresponding to t_D = 3 and M = .5, .7, and .9; 1.389, 1.082, and 0.927, respectively, are used in Eq. (15). Thus:

$$M = 0.65$$

$$M_1 = 0.5, \quad \bar{P}_1 = 1.389$$

$$M_2 = 0.7, \quad \bar{P}_2 = 1.082$$

$$M_3 = 0.9, \quad \bar{P}_3 = 0.927$$

and $\bar{P}$ for M = 0.65 and t_D = 3 is found from Eq. (15). Then the same equation is used to solve for $\bar{P}$ at t_D = 4:

$$M = 0.65$$

$$M_1 = 0.5, \quad \bar{P}_1 = 1.523$$

$$M_2 = 0.7, \quad \bar{P}_2 = 1.178$$

$$M_3 = 0.9, \quad \bar{P}_3 = 1.001$$

The $\bar{P}$ for t_D = 3.5 is, by linear interpolation, midway between the two values calculated using Eq. (15).

PART II. FIELD CASE STUDIES

The eight fields studied individually and in detail by methods developed during the first year will be referred in the following as Fields A, B, C, etc., without specific mention of the names, location, and without designating the particular operating company. The descriptions of each of these fields include all the available data on geology, geometry, and past production-pressure history. The mathematical procedures and specific calculations are shown in detail once for every mathematical model.

A summary of parameters used in the application of the models and resistance function to these field studies is presented in Table IV. A summary of the values of these parameters is presented at the end of the report in Table V (see page 146). It may be noted that two K_1 values are listed for each model in Table V. The first value is estimated from physical parameters of the field and aquifer and the second value is that which gave the best prediction of the reservoir behavior.

TABLE IV

DEFINITION AND UNITS OF PARAMETERS USED IN THE VARIOUS MATHEMATICAL MODELS AND IN THE RESISTANCE FUNCTION

Model	Case	K_1	K_2
Radial	CTP	$h\phi cr_b^2$, $(ft)^3\ (psi)^{-1}$	$K/(\mu\phi cr_b^2)$, $(md)(cp)^{-1}(psi)(ft)^{-2}$
Thick Sand	CTR	$\mu/(Kr_b\sqrt{Kr}\ \Delta t\phi)$, $(cp)(md)^{-1}(ft)^{-1}(days)^{-1}$(time interval)	$K/(\mu\phi cr_b^2)$, $(md)(cp)^{-1}(psi)(ft)^{-2}$
Hemispherical	CTP	$\pi r_b^3\phi c$, $(ft)^3(psi)^{-1}$	$K/(\mu\phi cr_b^2)$, $(md)(cp)^{-1}(psi)(ft)^{-2}$
Linear	CTP	$(\phi cA/\sqrt{\pi})\sqrt{\frac{.00633\ K\Delta t}{\mu\phi c}} = (md)^{1/2}(cp)^{-1/2}(psi)^{-1/2}(ft)^2(\text{time interval})^{1/2}$	
Radial as used in resistance function	CTR	$25.15\ \mu/(Khf\Delta t)$, $(psi)(ft)^{-3}$(time interval)	$0.006328\ K\Delta t/(\mu\phi cr_b^2)$, $(\text{time interval})^{-1}$

Nomenclature

A	Area open to flow, ft^2
CTP	Constant Terminal Pressure
CTR	Constant Terminal Rate
f	Fraction of a "pie" occupied by gas bubble, dimensionless
h	Aquifer thickness, ft
K	Permeability, millidarcys
Kr	Ratio of vertical to horizontal permeabilities, dimensionless
r_b	Radius of gas bubble, ft
Δt	Number of days per time interval
ϕ	Aquifer porosity, expressed as a fraction
μ	Liquid viscosity, cp
π	3.1416
c	Combined liquid and formation compressibility, vol/vol-psi

FIELD A

Field A, one of two large gas reservoirs located under the Gulf of Mexico off the coast of Louisiana, was discovered in 1951. The two fields we located on opposite sides of a fault running through a structural dome and have a 400-foot vertical displacement with no pressure or aquifer communication across the fault. The discovery pressure of Field A has declined from 3745 psia (bottom hole) to 3175 psia after producing over 172 billion standard cubic feet of gas. To date, this field has only been produced and its location makes conversion to storage operation doubtful. Figure A-1 shows a plan sketch of Field A.

1. GEOLOGY

Field A is a structural dome bounded by a fault, located 7400 ft below the Gulf of Mexico. The pay is fine- to medium-grained, moderately cemented sandstone separated b several shale lenses. The shale has numerous breaks and cannot be correlated from well to well. The location of this field makes drilling and coring operations very expensive; thus the available geological information is limited.

2. FIELD DATA

The reservoir and fluid properties of Field A are given in Table A-1 and the production-pressure history in Table A-2.

The initial pore volume was found by comparing the predicted and observed pressure for several selected initial pore volumes. The best estimate for the initial pore volume using both the radial model and resistance function method is 3850 million cubic feet.

3. CALCULATIONS

(a) Application of Radial Model to Field A.—The data needed for the application of the Radial Model to Field A are taken from Tables A-1 and A-2 and listed below.

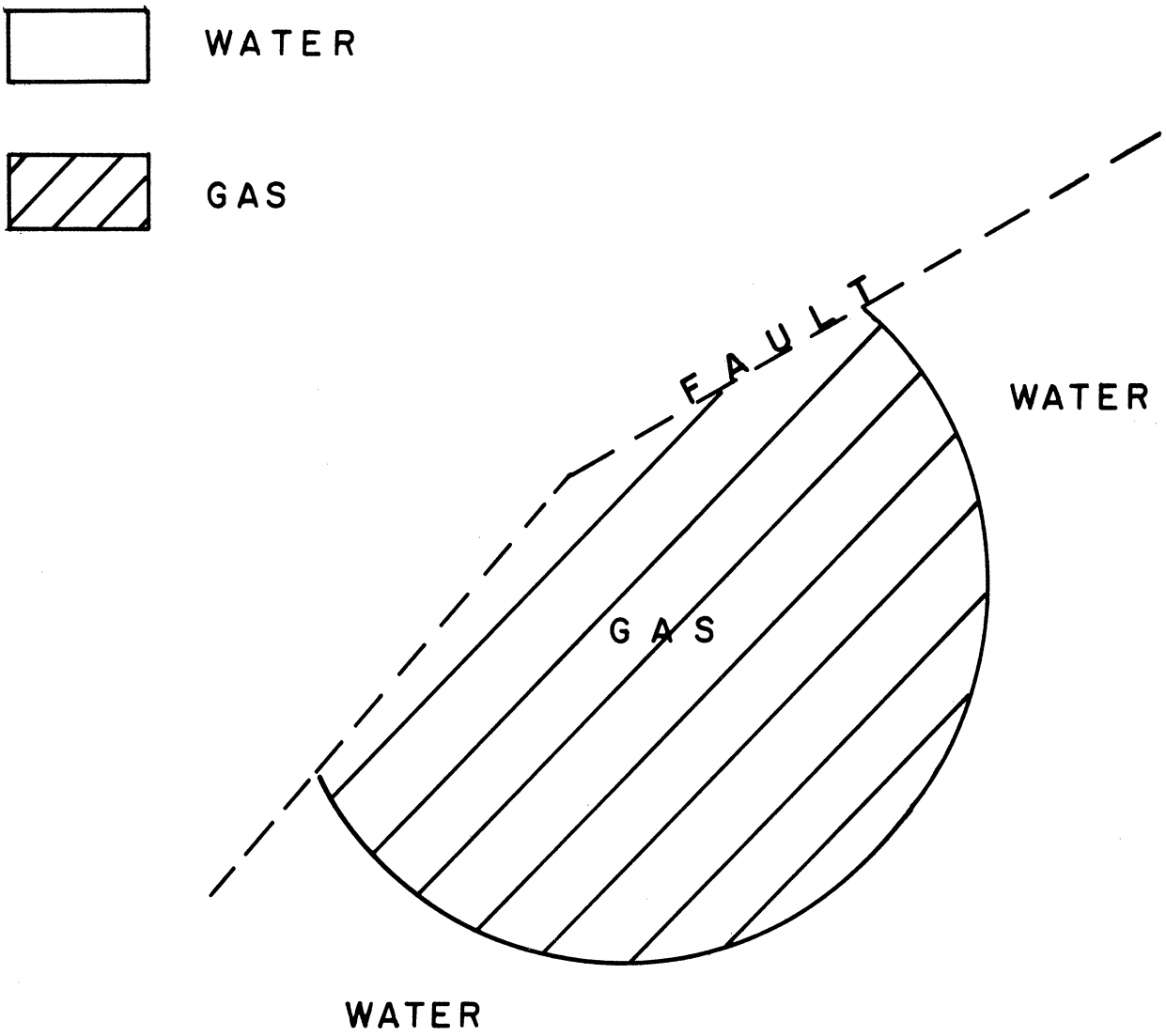

Fig. A-1. Areal sketch showing boundary of Field A.

TABLE A-1

GAS FIELD A DATA

Aquifer Characteristics

Type of formation	Sandstone
Porosity	29%
Permeability	1474 millidarcys
Thickness	170 ft
Depth to top of aquifer	7929 ft
Viscosity of liquid in aquifer	0.5 centipoise
Compressibility of brine and aquifer	7×10^{-6} vol/vol-psi

Data on Gas Field

a. Field geometry

Location	Gulf of Mexico
Type of formation	Sandstone
Nature of structure	Structural dome

b. Gas-sand formation and fluid properties

Gas compressibility correlation, $z = a + bP$	
Constant a	0.776
Constant b	4.17×10^{-5} psi^{-1}
Depth to top of sand	7800 ft
Reservoir temperature	640°F
Reservoir thickness	129 ft
Base conditions for gas measurements	P_b = 14.7 psia
	T_b = 520°R

c. History of gas reservoir

Discovery date	1951
Initial discovery pressure	3745 psia (bottom hole)
Initial pore volume	3850×10^6 cu ft

TABLE A-2

GAS INVENTORY AND PRESSURE HISTORY FOR FIELD A

Pressure Base = 14.7 psia
Temperature Base = 520°R

Date	Cumulative Gas Production MMSCF at End of Month	P, Well Bottom, psia at End of Month
1951 Feb		3745
Aug	2,680	3731
1952 Feb	7,254	3708
Aug	12,342	3688
1953 Feb	17,497	3670
Aug	23,162	3645
1954 Feb	30,898	3621
Aug	39,909	3595
1955 Feb	49,474	3555
Aug	60,471	3508
1956 Feb	74,126	3470
Aug	88,523	3430
1957 Feb	103,237	3383
Aug	117,024	3324
1958 Feb	135,775	3265
Aug	154,123	3220
1959	172,591	3175

ϕ = .29
h_{gas} = 129 ft
$h_{aquifer}$ = 170 ft
c = 7×10^{-6} vol/vol psi
K = 1474 millidarcys
μ = 0.5 cp
a = 0.776
b = $4.17 \times 10^{-5} (psi)^{-1}$
Δt = 182.5 days
f = .425
f_1 = (170-129/170) = 0.24
T_r = 640°R
V_o = 3850×10^6 ft^3
r_b^2 = 77×10^6 ft^2

Δt_D is calculated from

$$\Delta t_D = \frac{0.00633\ K\Delta t}{\mu \phi c r_b^2} = \frac{0.00633(1474(182.5)}{(0.5)(.29)(7\times10^{-6})(77\times10^6)} = 22$$

and t_D for each time step is determined by

$$t_D(1) = j(\Delta t) = 1(22) = 22$$

$$t_D(2) = 2(22) = 44$$

$$t_D(3) = 3(22) = 66, \text{ etc.}$$

The values of $Q_{i\Delta t_D}$ for an infinite radial model corresponding to the above t_D values are interpolated from Table 10-4 in the Handbook of Natural Gas Engineering and are listed in Table A-3.

The initial number of lb moles, n_o, is calculated from

$$n_o = \frac{V_o}{RT\left(\frac{a}{P_o}+b\right)} = \frac{3890\times10^6}{(10.73)(640)\left(\frac{1776}{3746}+0.0000417\right)}$$

$$= 2.252\times10^9 \text{ lb moles}$$

TABLE A-3

CALCULATED VALUES FOR FIELD A USING RADIAL MODEL

Time Step, N	Dimensionless, Q	Cumulative Gas Produced, MMSCF	Cumulative Gas in Place, lb moles	Pressures Predicted Using Radial Model, psia	Pressures Predicted Assuming No Water Movement, psia	Pressure Data, psia	Volume Ratios Using Predicted Pressures (radial model)	Volume Ratios Using Observed Pressures
0	0	0	2252×10^6	3745.0	3745.0	3745.0	1.0000	1.0000
1	13.2	2680	2245	3730.9	3732.0	3731.0	0.9998	1.0000
2	22.4	7250	2233	3706.9	3711.3	3708.0	0.9990	0.9998
3	30.7	12340	2220	3680.2	3690.2	3688.0	0.9977	0.9982
4	39.7	17500	2206	3653.3	3670.7	3670.0	0.9960	0.9962
5	46.3	23160	2191	3623.8	3650.3	3645.0	0.9939	0.9951
6	53.6	30900	2171	3583.6	3621.4	3621.0	0.9912	0.9913
7	70.0	39910	2147	3537.0	3588.8	3595.0	0.9879	0.9864
8	68.0	49470	2122	3487.7	3556.1	3555.0	0.9838	0.9840
9	75.1	60470	2093	3431.3	3518.8	3508.0	0.9790	0.9815
10	81.8	74130	2057	3361.6	3471.2	3470.0	0.9733	0.9736
11	88.6	88520	2019	3288.7	3423.6	3430.0	0.9665	0.9650
12	95.1	103200	1980	3214.7	3377.5	3383.0	0.9589	0.9576
13	101.5	117000	1944	3145.7	3338.8	3324.0	0.9505	0.9541
14	107.9	135800	1895	3052.7	3277.2	3265.0	0.9412	0.9441
15	114.3	154100	1846	2962.4	3221.7	3220.0	0.9306	0.9310
16	120.6	172600	1798	2872.3	3168.4	3175.0	0.9190	0.9174

and the cumulated gas in place for each succeeding time step from

$$n_j = n_o - \frac{P_{base}\, G_{p_j}}{RT_{base}}$$

$$n_1 = 2.252\text{x}10^9 - \frac{(14.7)(2.68\text{x}10^9)}{(10.73)(520)} = 2.245\text{x}10^9 \text{ lb moles}$$

$$n_2 = 2.252\text{x}10^9 - \frac{(14.7)(7.254\text{x}10^9)}{(10.73)(520)} = 2.233\text{x}10^9 \text{ lb moles}$$

The remaining values for the gas inventory are tabulated in Table A-3.

The pressure can now be predicted from Eqs. (17), (18), and (19) for j greater than 1. For j = 0, 1,

$$P_o(\text{calc}) = P_o(\text{initial}) = 3745 \text{ psia}$$

$$P_j(\text{calc}) = C_1 + \sqrt{C_1^2 + C_2}$$

$$C_1 = \frac{\pi K_1(fQP_{j-2}+f_1P_o)+bn_jRT-V_o}{2\pi K_1(fQ_1+f_1)}$$

$$C_2 = \frac{an_jRT}{\pi K_1(f_1Q_1+f_1)}$$

where $K_1 = h\phi cr_b^2$. The value of K_1 was varied until the absolute deviation observed and calculated pressures was a minimum. Calculations for $K_1 = 3750$, the optimum value, are given below.

$$P_1 = C_1 + \sqrt{C_1 + C_2}$$

$$C_1 = \pi(3750)\{(.425)(13.17)(3745) + .24(3745)\}$$

$$+ (4.17\text{x}10^{-5})(2.245\text{x}10^9)(10.73)(640) - 3850\text{x}10^6/$$

$$[(2\pi)(3750)\{(.425)(13.17) + .24\}]$$

$$C_2 = \frac{(0.776)(2.245\text{x}10^9)(10.73)(420)}{\pi(3750)\{(.425)(13.17)+.24\}}$$

$$P_1 = 3732.0 \text{ psia}$$

$$P_2 = C_1 + \sqrt{C_1^2 + C_2}$$

$$C_1 = \frac{\pi K_1\{f\Delta P_o \bar{Q}_2 + f\bar{Q}_1 P_o + f_1 P_o\} + bn_j RT - V_o}{2\pi K_1(fQ_1 + f_1)}$$

$$C_2 = \frac{an_j RT}{\pi K_1(fQ_1 + f_1)}$$

$$\Delta P_o = P_o - P_1 = 3745 - 3732 = 13$$

$$C_1 = \pi(3750)\ [.425(13)(22.4)$$

$$+ .425(13.17)(3745) + .24(3745)]$$

$$+ 4.17\text{x}10^{-5}(2.233\text{x}10^{9})(10.73)(640) - 3850\text{x}10^{6}/$$

$$[2\pi(3750)\{(.425)(13.17) + .24\}]$$

$$C_2 = \frac{.776(2.233)(10.73(640)}{[\pi(3750)(.425)(13.17) + \pi(3750)(.24)]}$$

$$P_2 = 3711.3 \text{ psia}$$

This procedure is repeated until all pressures are calculated (see Table A-3).

The pore volume ratio is predicted by

$$\frac{V_j}{V_o} = \left\{\frac{a+bP_j}{P_j}\right\} n_j RT/V_o$$

$$\frac{V_1}{V_o} = \left\{\frac{.776 + 4.17\text{x}10^{-5}(3732)}{3732}\right\} (2.245\text{x}10^{9})(10.73)(640)/3850\text{x}10^{6} = 0.998$$

The remaining pore volumes, calculated for the predicted and observed pressure, for each time step with the respective gas volume (lb mole), are also tabulated in Table A-3.

The pressures, assuming no water movement, were calculated from Eq. (10).

$$P_j \text{ (no water movement)} = \frac{an_jRT}{V_o - bn_jRT}$$

$$P_1 = \frac{(.776)(2.245\times10^9)(10.73)(640)}{3850\times10^6-(4.17\times10^{-5})(2.245\times10^9)(10.73)(640)} = 3730.9$$

A summary of all the numbers calculated in processing Field A data by the radial model is given in Table A-3.

4. RESULTS

The performance predicted for a producing reservoir in which water movement is not considered shows lower pressures than actually observed (Fig. A-2).

Application of the radial model, the closest approximation of the reservoir shape (Fig. A-1), with an infinite aquifer to the field data gave a predicted performance almost identical to that observed (Fig. A-3). This agreement is also reflected in the volume ratios calculated from these pressures (Fig. A-4). As all the predicted pressures are in good agreement with the observed, the aquifer is either infinite or the boundary of the aquifer has not had time to influence the pressure history.

The resistance function method (see Field D for example calculation (Fig. A-5) also gave close agreement between the calculated and observed pressures. This agreement was also reflected in the corresponding pore volume ratios (Fig. A-6). The slope of the resistance curve of Field A becomes constant toward the end of the history, indicating that the reservoir if of finite extent. However, the effect of the boundary is just beginning to be felt, and the deviation from infinite aquifer behavior is not significant. The resistance curve for Field A is shown in Fig. A-7.

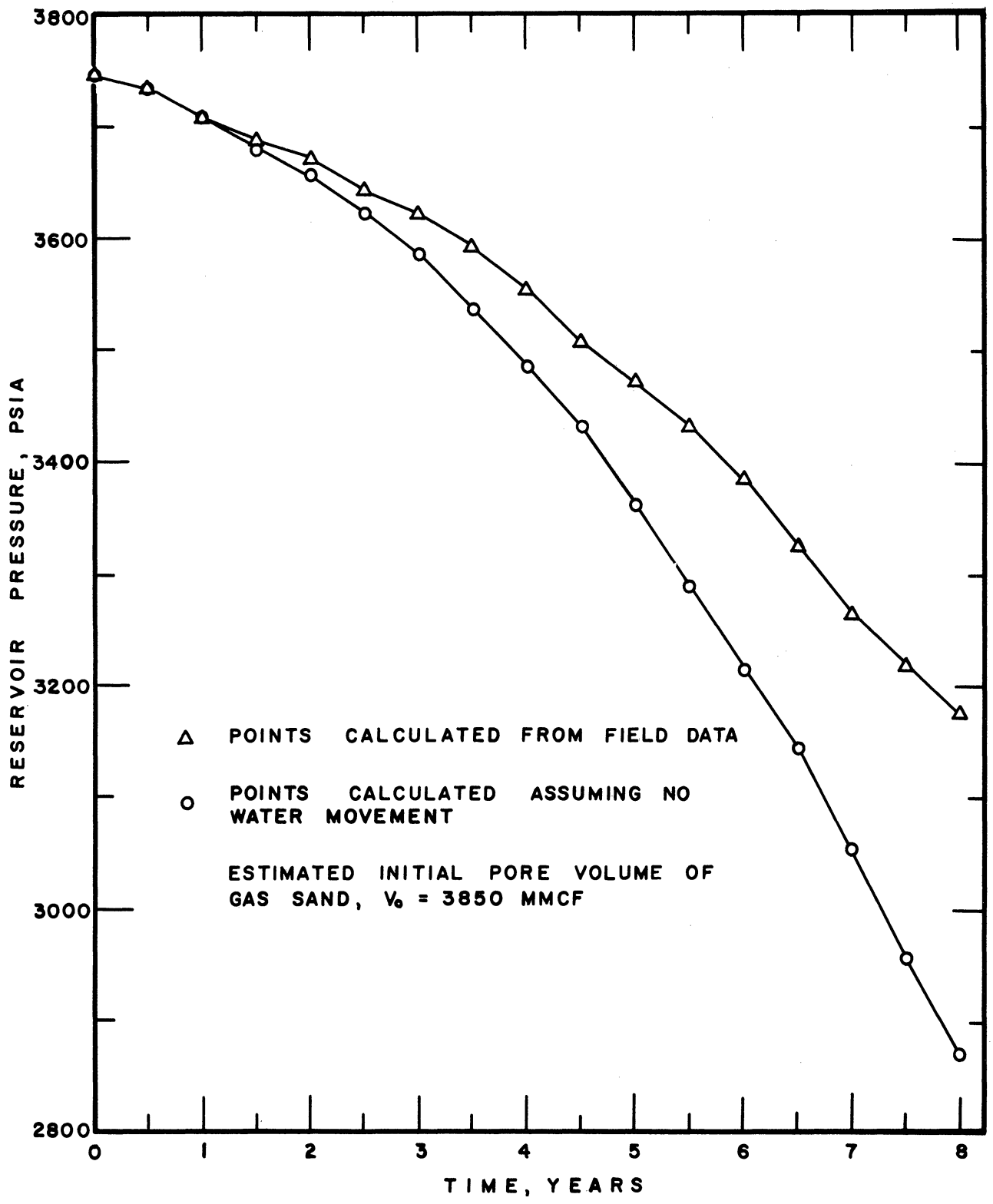

Fig. A-2. Comparison of Field A predicted pressures, assuming no water movement with observed pressures.

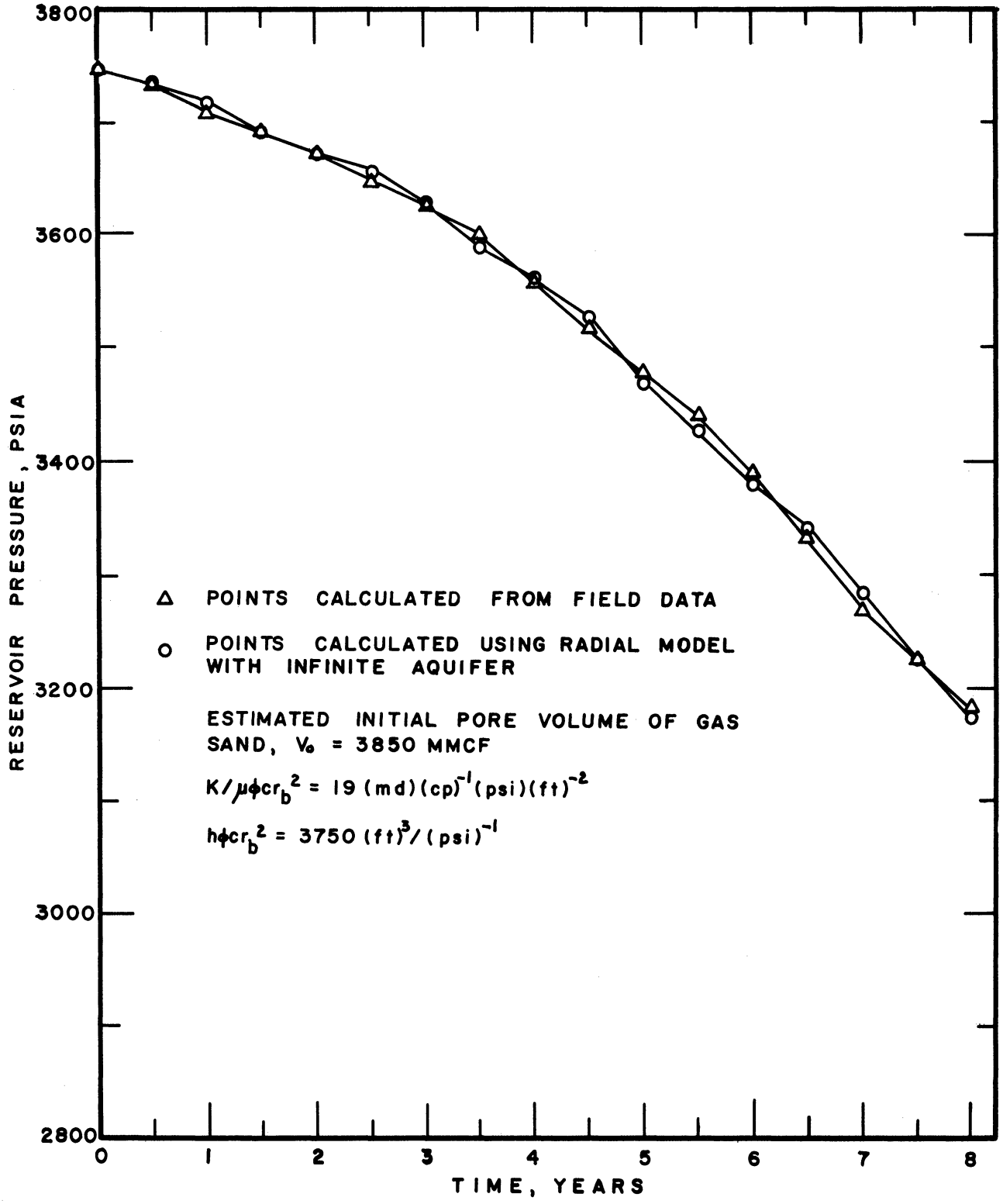

Fig. A-3. Comparison of Field A pressures predicted using radial model (infinite aquifer) with observed pressures.

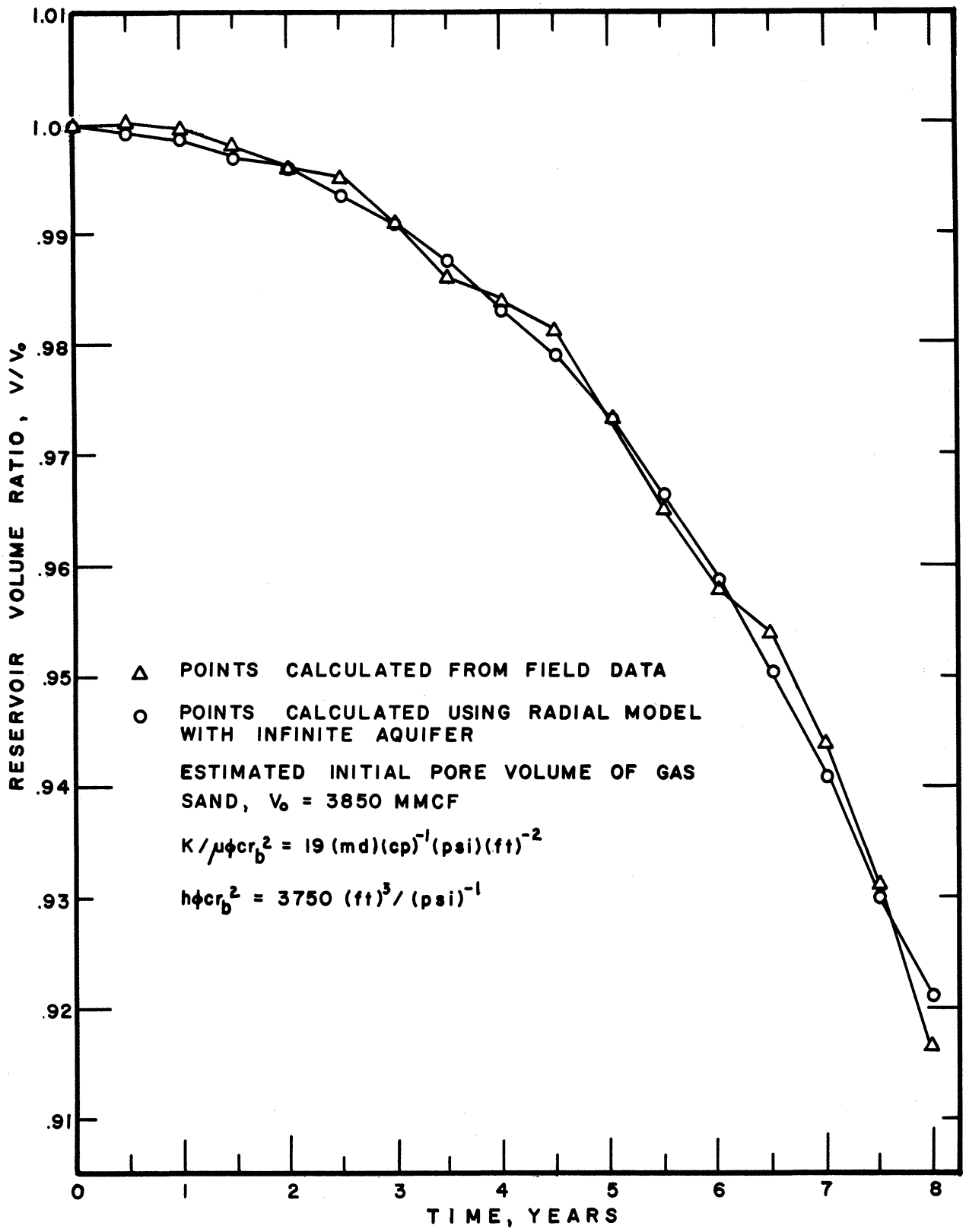

Fig. A-4. Comparison of Field A volume ratio predicted using radial model (infinite aquifer) with volume ratios calculated from field data.

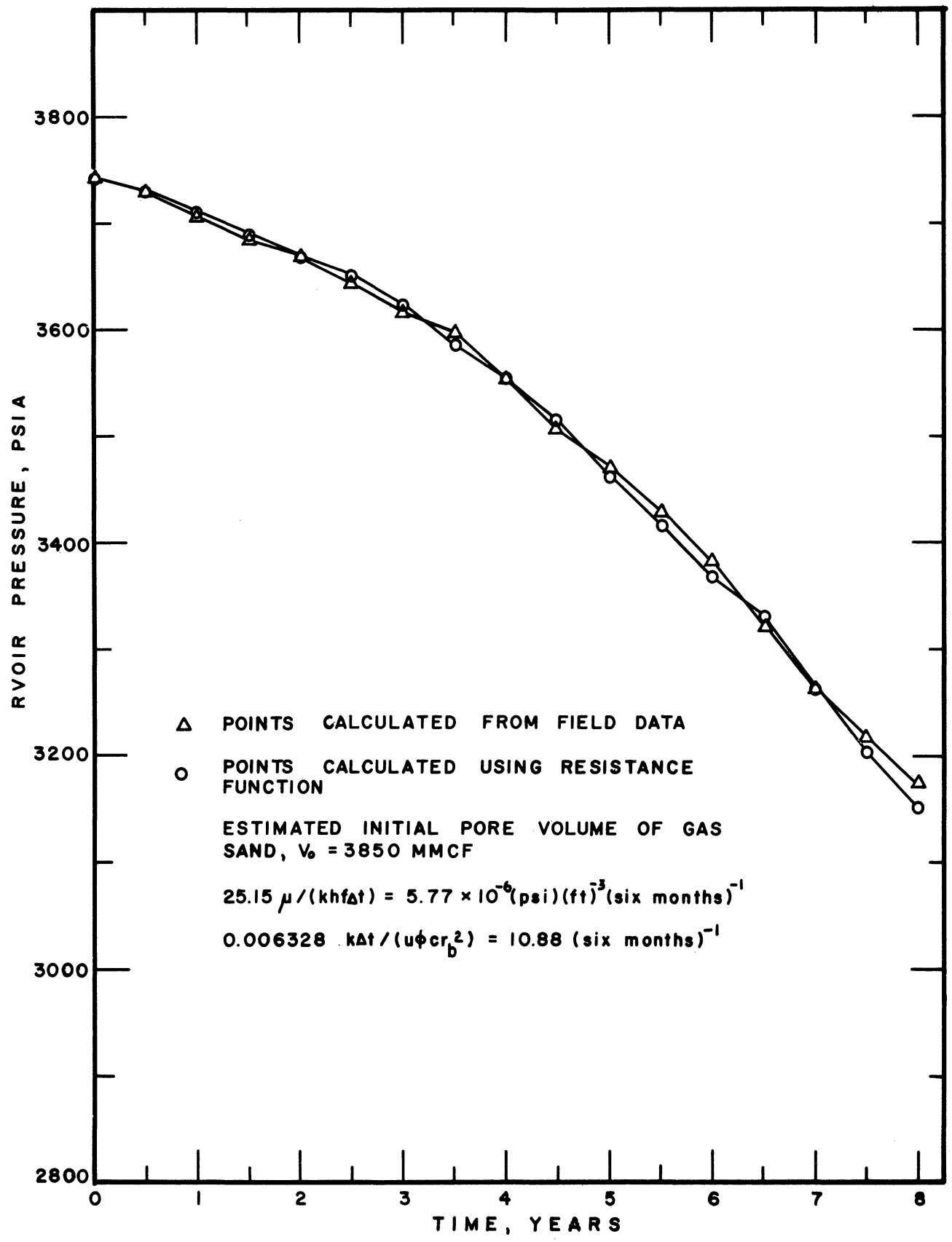

Fig. A-5. Comparison of Field A pressures predicted using resistance function with observed pressures.

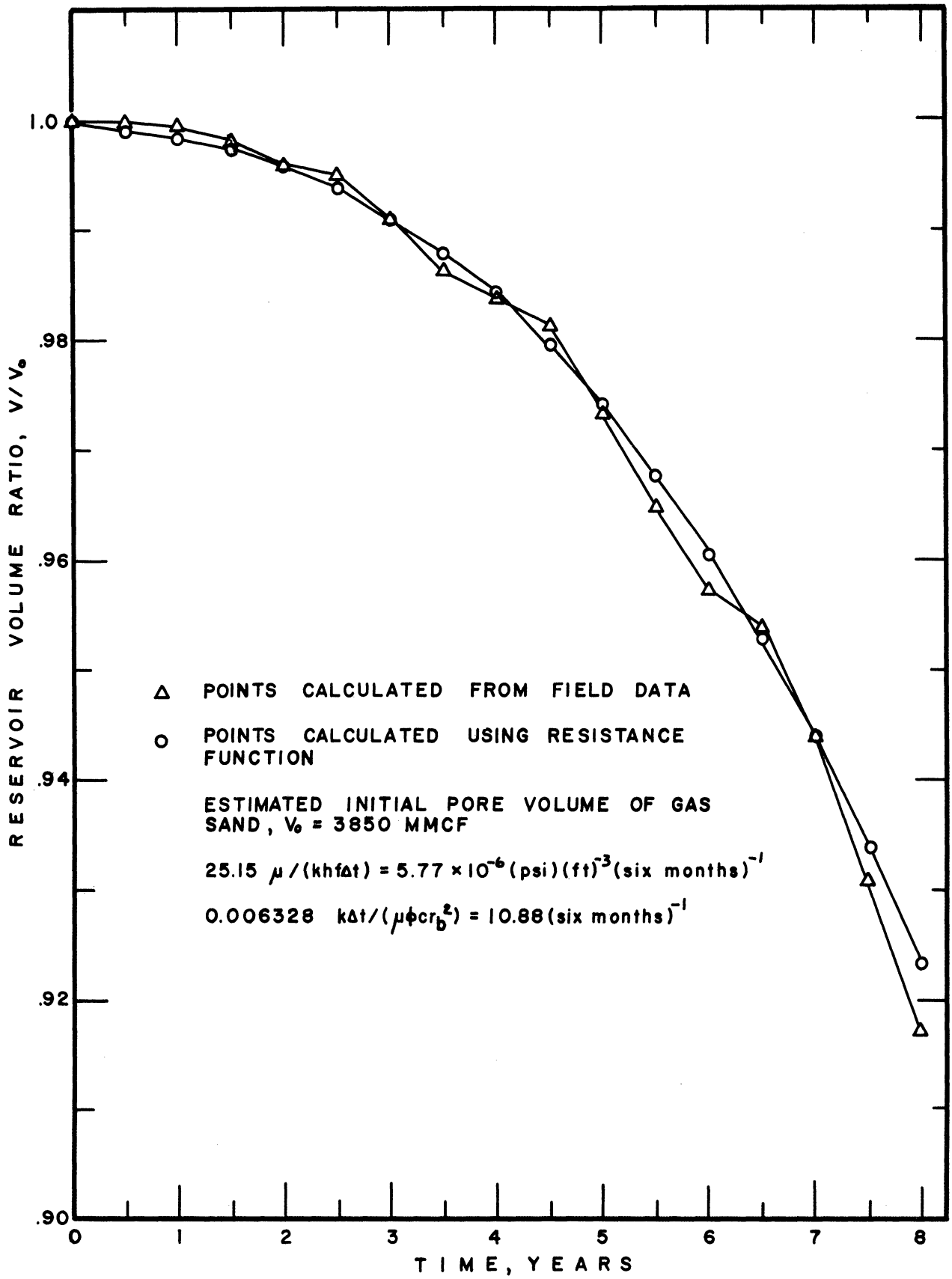

Fig. A-6. Comparison of Field A volume ratio predicted using resistance function with volume ratios calculated from field data.

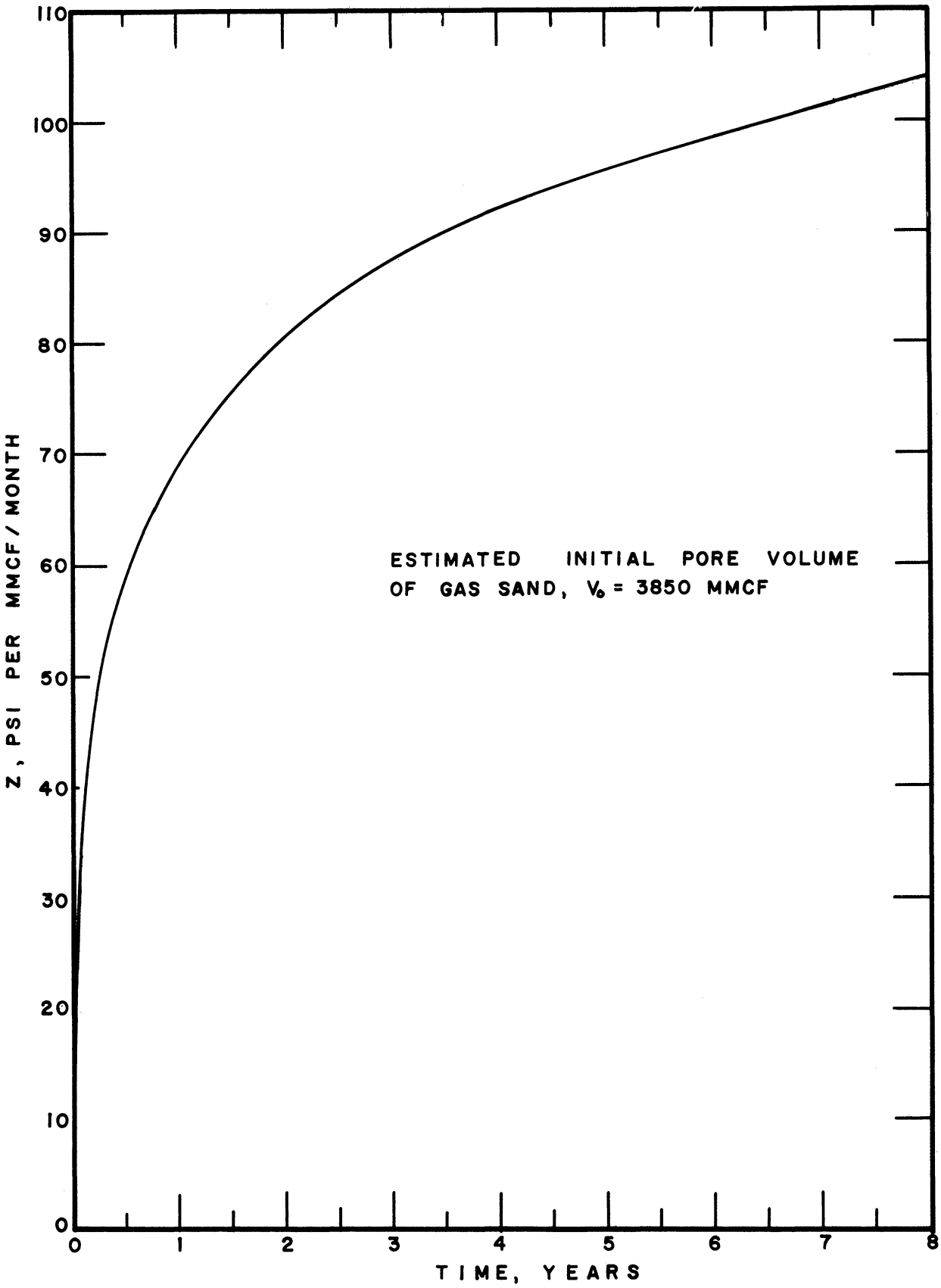

Fig. A-7. Resistance function vs. time for Field A.

FIELD B

Field B, a northern Illinois storage reservoir, was formed by injecting gas into a sandstone aquifer initially containing only water. Development of the reservoir for gas storage was initiated in early 1957 and gas injection started on Nov. 30, 1957. By December 5, 1960, 16,339,900 MCF of gas had been injected. A plan sketch, Fig. B-1, shows a horizontal view of this field.

1. GEOLOGY

The storage sand, encounted at an average depth of 2450 feet below the surface, is 2500 feet thick. This sand consists of alternate layers of fine- to very-coarse-grained sandstone with several randomly spaced, non-continuous, thin, green shale laminations.

Imprevious layers of dolomite and shale form the cap rock. The lower two layers of dolomite and shale in this cap rock are more than twenty and forty feet thick, respectively.

No faults are known to exist in the immediate vicinity of the aquifer. Although geological information indicates an "infinite" aquifer, this cannot be ascertained without analysis of field-performance data.

2. FIELD DATA

A summary of the reservoir and aquifer properties is given in Table B-1 and the production-pressure history is tabulated in Table B-2.

Although the configuration of the aquifer and gas bubble does not conform to any of the present mathematical models, the field's performance can be approximated by the radial or thick sand model.

The mathematical models used impose the restriction that the radius of the gas-water interface may not change with time. Hence one is forced with an awkward situation for an "aquifer" storage field, i.e., one in which the initial gas bubble radius is zero. It is necessary to create some pseudo initial conditions or assign a later time in the field's history, when the gas bubble has grown to a finite size, as the starting point for analysis. The latter route was chosen for field B.

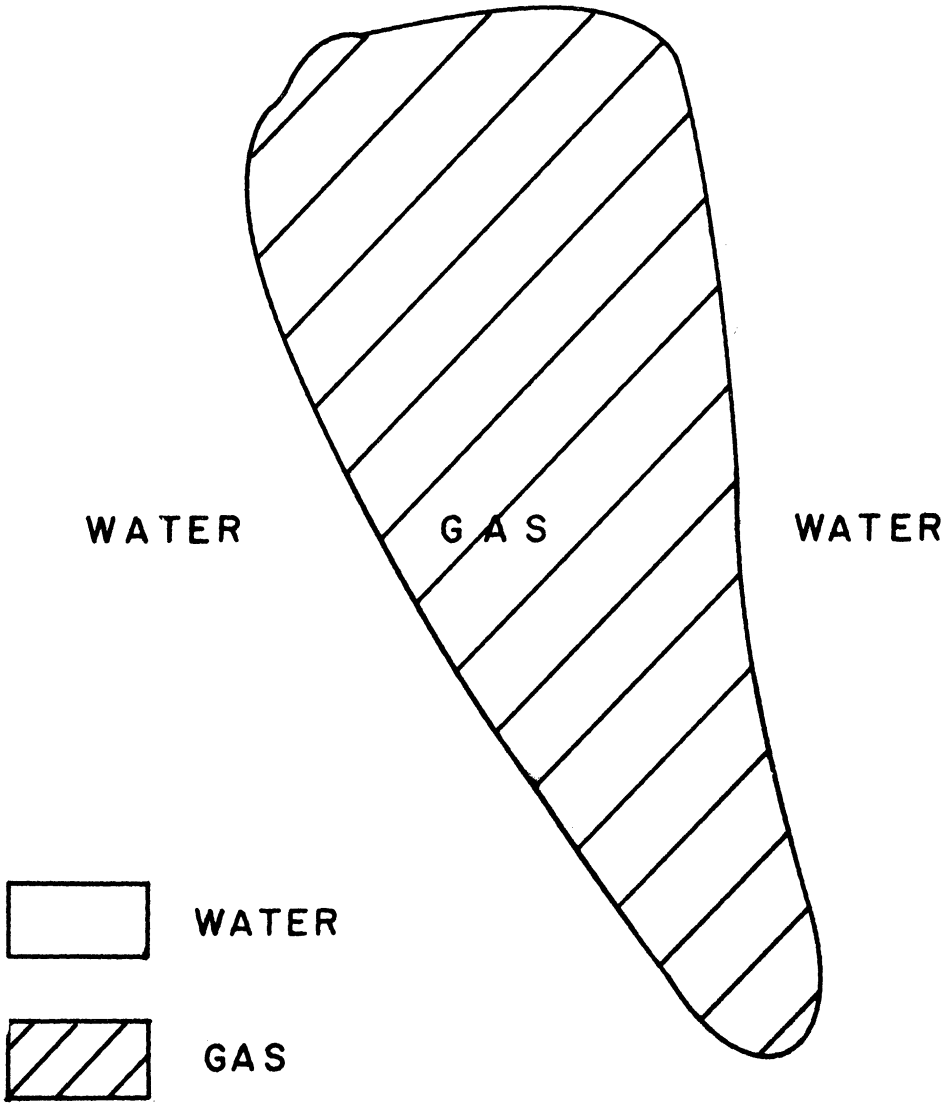

Fig. B-1. Areal sketch showing boundary of Field B.

TABLE B-1

STORAGE FIELD B DATA

Aquifer Characteristics

Type of formation	Sandstone
Porosity	14.8%
Permeability	100 millidarcys
Thickness	2500 ft
Depth to top of aquifer	2490 ft
Viscosity of liquid in aquifer	1 centipoise
Compressibility of brine and formation	8×10^{-6} vol/vol-psi

Data on Storage Field

a. Field geometry

Location	Northern Illinois
Type of formation	Sandstone
Nature of structure	Structural dome

b. Gas-sand formation and fluid properties

Gas compressibility correlation, $z = a + bP$	
Constant a	0.98
Constant b	-0.000083
Depth to top of sand	2450 ft
Reservoir temperature	530°R
Reservoir thickness	40 ft
Base conditions for mas measurements	P_b = 14.65 psia
	T_b = 520°R

c. History of gas reservoir

Date storage operations started	November 30, 1957*
Initial discovery pressure	1097.4 psia* (well bottom)
Initial pore volume	110×10^6 cu ft

*March 26, 1960, used as initial time in this study.

TABLE B-2

GAS INVENTORY AND PRESSURE HISTORY FOR FIELD B

Pressure Base = 1465 psia
Temperature Base = 520°R

Date	Cumulative Gas Production, MMSCF	P, Well Bottom, psia
1960 Mar 26	0	1097
Apr 2	- 204	1147
9	- 348	1169
16	- 633	1212
23	- 871	1231
30	-1092	
May 7	-1292	1252
14	-1404	1239
21	-1603	1251
28	-1789	1252
June 4	-1978	1256
11	-2166	1258
18	-2346	1259
25	-2526	1259
July 2	-2730	1264
9	-2932	-263
16	-3131	1264
23	-3320	1261
30	-3532	1265
Aug 6	-3730	1265
13	-3935	1265
20	-4147	1267
27	-4352	1266
Sept 3	-4507	1257
10	-4737	1264
17	-4953	1265
24	-5147	1262
Oct 1	-5375	1266
8	-5591	1265
15	-5797	1260
22	-5927	1237
29	-6173	1263
Nov 5	-6406	1264
12	-6605	1260
19	-6843	1265
26	-7074	1265
Dec 3	-7207	1247
10	-7282	1226
17	-7282	1204
24	-7282	1189
31	-7019	1115
1961 Jan 7	-6874	1129
14	-5707	1084
21	-6569	1080
28	-6521	1091
Feb 4	-6338	1069
11	-6073	1020
18	-5907	1002
25	-5673	1002
Mar 4	-5673	1028
11	-5673	1028

By March 26, 1960, after more than nine billion SCF of gas had been injected, the field was shut in for about a month and the pressure stabilized to a value near the discovery pressure of the aquifer. This date was selected as the initial time, t_D. The "initial" pore volume was calculated from the quantity of gas injected and the field pressure.

3. CALCULATIONS

(a) Application of Thick Sand Model to Field B.—The data required for the application of the Thick Sand Model to Field B are taken from Tables B-1 and B-2 and are listed below.

$$
\begin{aligned}
\phi &= .148 \\
h_{gas} &= 40 \text{ ft} \\
h_{aquifer} &= 2500 \text{ ft} \\
c &= 8\text{x}10^{-6} \text{ vol/vol-psi} \\
K &= 100 \text{ millidarcys} \\
\mu &= 1 \text{ centipoise} \\
a &= 0.98 \\
b &= -0.000083 \text{ psi}^{-1} \\
\Delta t &= 7 \text{ days} \\
T_r &= 530^\circ\text{R} \\
V_o &= 110\text{x}10^6 \text{ ft}^3 \\
r_b^2 &= 5.9\text{x}10^6 \text{ ft}^2 \\
K_r &= 1 \\
M &= .963 \\
M_1 &= .7 \\
M_2 &= .9 \\
M_3 &= 1.0
\end{aligned}
$$

The incremental delta time is calculated from

$$\Delta t_D = \frac{0.00633\ K\Delta t}{\mu\phi c r_b^2}$$

$$= \frac{0.00633(100)(7)}{(1)(.148)(8\text{x}10^{-6})(5.9\text{x}10^6)} = .64$$

and t_D for each time by

$$(t_D)_j = j\Delta t$$

$$
\begin{aligned}
t_D(1) &= 1(.64) = .64 \\
t_D(2) &= 2(.64) = 1.28 \\
t_D(3) &= 3(.64) = 1.92
\end{aligned}
$$

The values of dimensionless pressure $\bar{P}_j$ are calculated by Eq. (15), page , when t_D was less than 10, and Eq. (12), page , when t_D was larger than 10. An example calculation is shown for $\bar{P}_1$ using 0.7, 0.9, 1.0 for M_1, M_2, M_3, respectively.

$$\bar{P}_1 = \frac{(.963-.9)(.963-1.0)}{(.7-.9)(.7-1.0)}(.616)$$

$$+ \frac{(.963-.7)(.963-1.0)}{(.9-.7)(.9-1.0)}(.560)$$

$$+ \frac{(.963-.7)(.963-.9)}{(1.0-.7)(1.0-.9)}(.550)$$

$$= .55622$$

The remaining values for $\bar{P}_j$ are given in Table B-3.

The cumulative gas in place is found by:

$$n_o = \frac{V_o}{(\frac{a}{P_o}+b)RT}$$

$$= \frac{110\text{x}10^6}{(\frac{0.98}{1097.4}-0.000083)(10.73)(530)}$$

$$= 2.382\text{x}10^7 \text{ lb moles}$$

and

$$n_j = n_o - \frac{P_{base}\, G_{pj}}{RT_{base}}$$

$$n_1 = 2.382\text{x}10^7 - \frac{(14.7)(-204\text{x}10^6)}{(10.73)(520)}$$

$$= 2.436\text{x}10^7 \text{ lb moles}$$

TABLE B-3

CALCULATED VALUES FOR FIELD B USING THICK SAND MODEL

Time, Step, N	Dimensionless, P	Cumulative Gas Produced, MMSCF	Cumulative Gas in Place, lb moles	Pressures Predicted Using Thick Sand Model, psia	Pressure Data, psia	Volume Ratios Using Predicted Pressures (thick sand model)	Volume Ratios Using Observed Pressures
0	0	0	2.382×10^7	1097.4	1097.4	1.0000	1.0000
1	0.5562	-0.204×10^9	2.436	1115.7	1147.0	1.0039	0.9737
2	0.6929	-0.348	2.474	1126.1	1169.0	1.0092	0.9682
3	0.7885	-0.633	2.549	1147.7	1211.8	1.0180	0.9584
4	0.8546	-0.871	2.611	1162.3	1230.6	1.0285	0.9652
5	0.9109	-1.092	2.669	1173.9	1245.9	1.0398	0.9731
6	0.9551	-1.292	2.722	1182.6	1251.9	1.0517	0.9870
7	0.9927	-1.404	2.751	1183.1	1238.7	1.0625	1.0095
8	1.0268	-1.603	2.803	1191.4	1250.6	1.0743	1.0178
9	1.0560	-1.789	2.852	1197.7	1252.0	1.0866	1.0342
10	1.0823	-1.978	2.902	1203.7	1256.4	1.0994	1.0481
11	1.1067	-2.166	2.951	1209.2	1258.4	1.1125	1.0640
12	1.1280	-2.346	2.998	1213.6	1259.1	1.1257	1.0804
13	1.1483	-2.526	3.046	1217.7	1258.7	1.1391	1.0978
14	1.1674	-2.730	3.099	1223.4	1263.9	1.1631	1.1119
15	1.1846	-2.932	3.152	1228.5	1262.5	1.1675	1.1324
16	1.2001	-3.131	3.205	1232.9	1263.6	1.1821	1.1500
17	1.2158	-3.320	3.254	1236.3	1260.6	1.1967	1.1709
18	1.2306	-3.532	3.310	1241.1	1265.1	1.2119	1.1862
19	1.2447	-3.730	3.362	1244.6	1264.9	1.2271	1.2051
20	1.2580	-3.935	3.416	1248.4	1265.1	1.2425	1.2241
21	1.2707	-4.147	3.471	1252.4	1267.1	1.2583	1.2419
22	1.2827	-4.352	3.525	1255.6	1266.4	1.2741	1.2619
23	1.2943	-4.507	3.566	1255.2	1256.6	1.2893	1.2877
24	1.3053	-4.737	3.626	1260.2	1264.1	1.3053	1.3008
25	1.3159	-4.953	3.683	1263.8	1265.2	1.3215	1.3198
26	1.3261	-5.147	3.734	1265.6	1262.0	13376	1.3419
27	1.3359	-5.375	3.375	1269.7	1266.1	1.3542	1.3585
28	1.3453	-5.591	3.850	1272.6	1265.2	1.3708	1.3799
29	1.3544	-5.797	3.905	1274.7	1260.2	1.3875	1.4055
30	1.3633	-5.927	3.939	1271.9	1236.8	1.4031	1.4478
31	1.3718	-6.173	4.003	1277.0	1262.5	1.4197	1.4381
32	1.3800	-6.406	4.064	1280.8	1263.7	1.4367	1.4585
33	1.3880	-6.605	4.117	1282.1	1260.4	1.4535	1.4816
34	1.3957	-6.843	4.179	1285.8	1265.2	1.4708	1.4977
35	1.4033	-7.074	4.240	1288.8	1265.2	1.4882	1.5194
36	1.4106	-7.207	4.275	1285.7	1246.6	1.5046	1.5575
37	1.4177	-7.282	4.294	1279.7	1225.5	1.5195	1.5948
38	1.4246	-7.282	4.294	1269.9	1203.5	1.5325	1.6273
39	1.4314	-7.282	4.294	1261.4	1189.0	1.5442	1.6494
40	1.4379	-7.019	4.225	1238.0	1114.6	1.5515	1.7434
41	1.4443	-6.894	4.193	1225.1	1128.8	1.5575	1.7058
42	1.4506	-6.707	4.143	1209.5	1084.3	1.5615	1.7623
43	1.4567	-6.569	4.107	1198.0	1079.8	1.5644	1.7549
44	1.4627	-6.521	4.095	1192.5	1090.6	1.5675	1.7305
45	1.4685	-6.338	4.047	1179.2	1068.6	1.5687	1.7490
46	1.4742	-6.073	3.977	1161.8	1020.3	1.5673	1.8084
47	1.4798	-5.907	3.933	1151.6	1001.5	1.5654	1.8253
48	1.4853	-5.800	3.905	1145.4	1002.4	1.5634	1.8105
49	1.4906	-0.5673	3.872	1138.2	1001.6	1.5810	1.7966
50	1.4959	-5.673	3.872	1139.0	1028.2	1.5597	1.7458

$$n_2 = 2.382\text{x}10^7 - \frac{(14.7)(-348\text{x}10^6)}{(10.73)(520)}$$

$$= 2.474\text{x}10^7 \text{ lb moles}$$

The values for n_3 through n_{50} are listed in Table B-3.

The value for K_3

$$K_3 = \frac{50.2\mu}{Kr_b \sqrt{K_r}\ \Delta tf}$$

was varied until the sum of the absolute differences between the predicted and observed pressures was a minimum. The value found for K_3 was 0.00007591.

The pressures can now be calculated from Eq. (14), page .

$$P_o(\text{predicted}) = P_o(\text{observed}) = 1097.4$$

$$P_1 = C_1 + \sqrt{C_1^2 - C_2}$$

$$C_1 = -\frac{1}{2}(K_3)\{V_o\bar{P}_1 - \bar{P}_1 RTn_1 b\} - P_o$$

$$= -\frac{1}{2}(0.00007591)\{(110\text{x}10^6)(.55622)$$

$$- .55622(10.73)(530)(2.436\text{x}10^7)(-.000083)\}$$

$$- 1097.4$$

$$C_2 = -K_3\bar{P}_1 RTn_1 a$$

$$= -(0.00007591)(.55622)(10.73)(530)(2.436\text{x}10^7)(.98)$$

$$P_1 = 1115.7$$

The pressures assuming no water movement are determined by:

$$P_j = \frac{an_jRT}{V_o - bn_jRT}$$

$$P_1 = \frac{(.98)\ (2.436\text{x}10^7)(10.73)(530)}{110\text{x}10^6 + .000083(2.436\text{x}10^7)(10.73)(530)}$$

$$= 1119.7$$

The pore volume ratio is determined by

$$V_j/V_o = \frac{(a+bP_j)n_jRT}{P_jV_o}$$

$$V_1/V_o\ (\text{calc}) = \frac{\{.98-.000083(1115.7)\}(2.436\text{x}10^7)(10.73)(530)}{(1115.7)(110\text{x}10^6)}$$

$$= 1.0039$$

The remaining values are tabulated in Table B-3.

(b) Application of Radial and Resistance-Function Method.—Examples of the Application of the Radial Model and Resistance-Function method are given in Field A and Field D, respectively.

4. RESULTS

Calculations based on the following were performed for Field B:

1. no water movement;
2. thick sand model, infinite aquifer; and
3. radial model, infinite aquifer.

The comparisons between predicted and observed pressure performance for these cases are plotted in Figs. B-2-B-4, respectively. The predictions obtained using the models are all considerably better than the prediction based on the assumption of no water movement. The thick sand model gave the best prediction, but was only slightly better than that of the radial model. However, the correspondence between the predicted and observed performance leaves much to be desired. The volume ratios predicted using the thick sand model are shown in Fig. B-5.

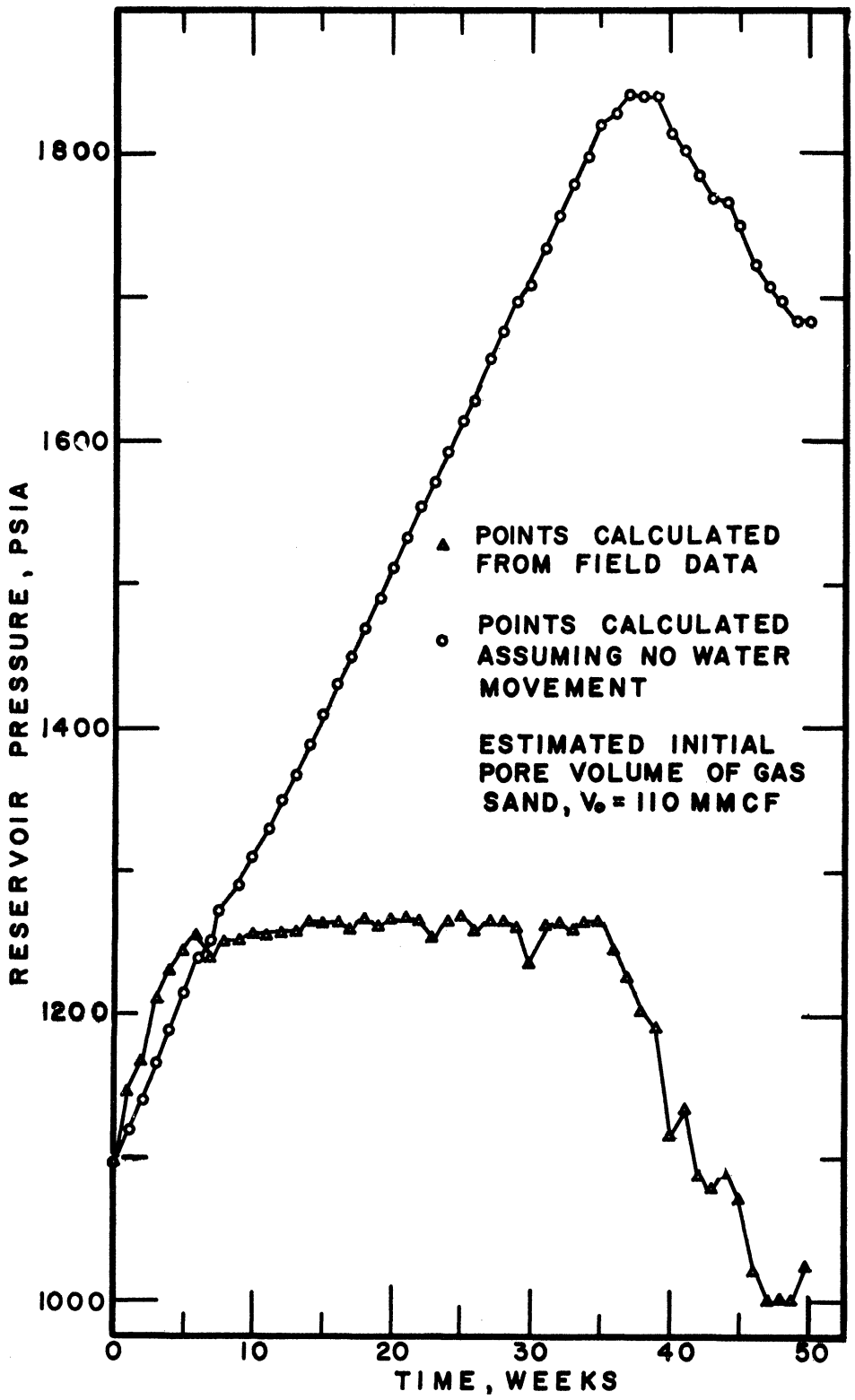

FIg. B-2. Comparison of Field B predicted pressures, assuming no water movement with observed pressures.

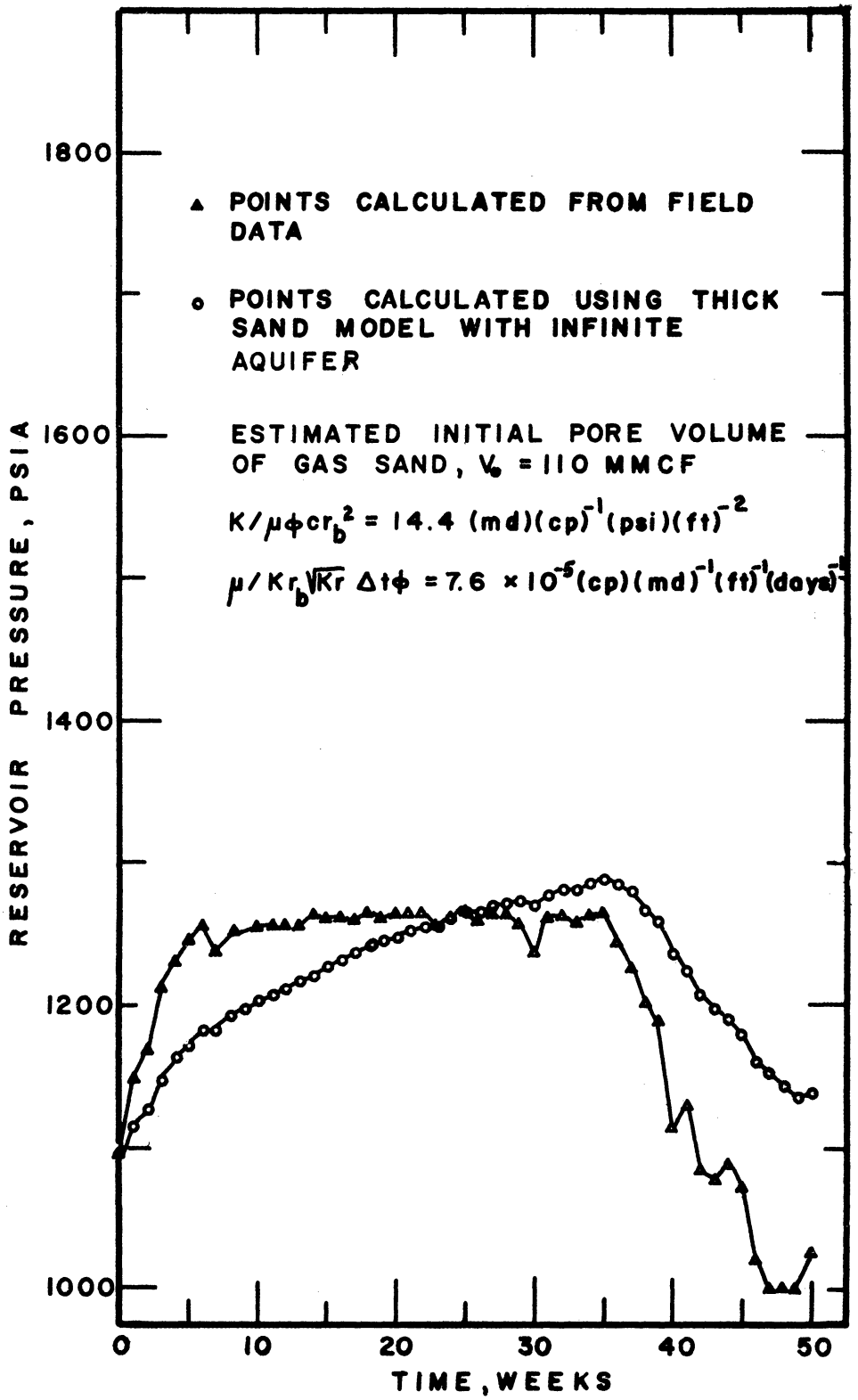

Fig. B-3. Comparison of Field B pressures predicted using thick sand model (infinite aquifer) with observed pressures.

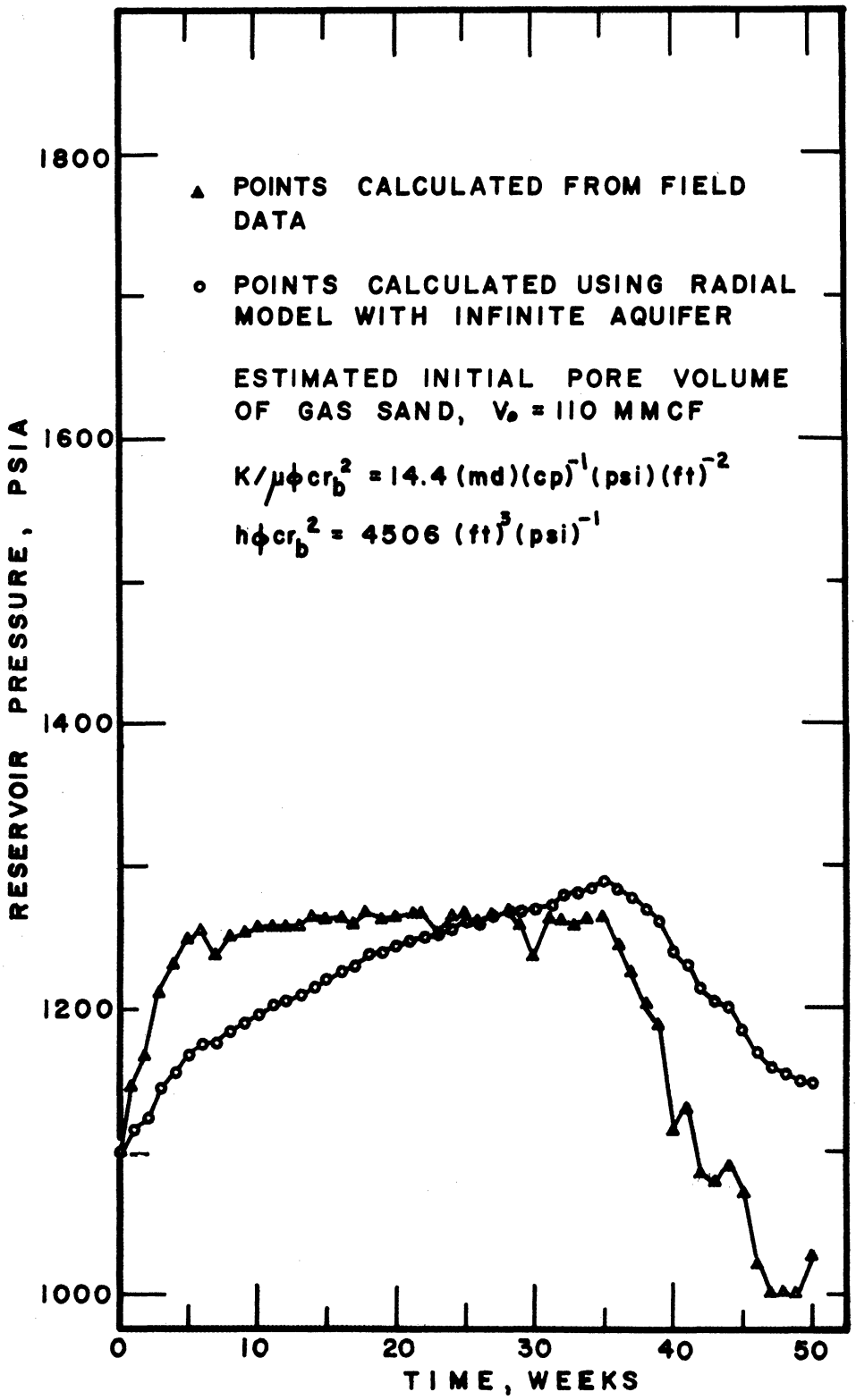

Fig. B-4. Comparison of Field B pressures predicted using radial model (infinite aquifer) with observed pressures.

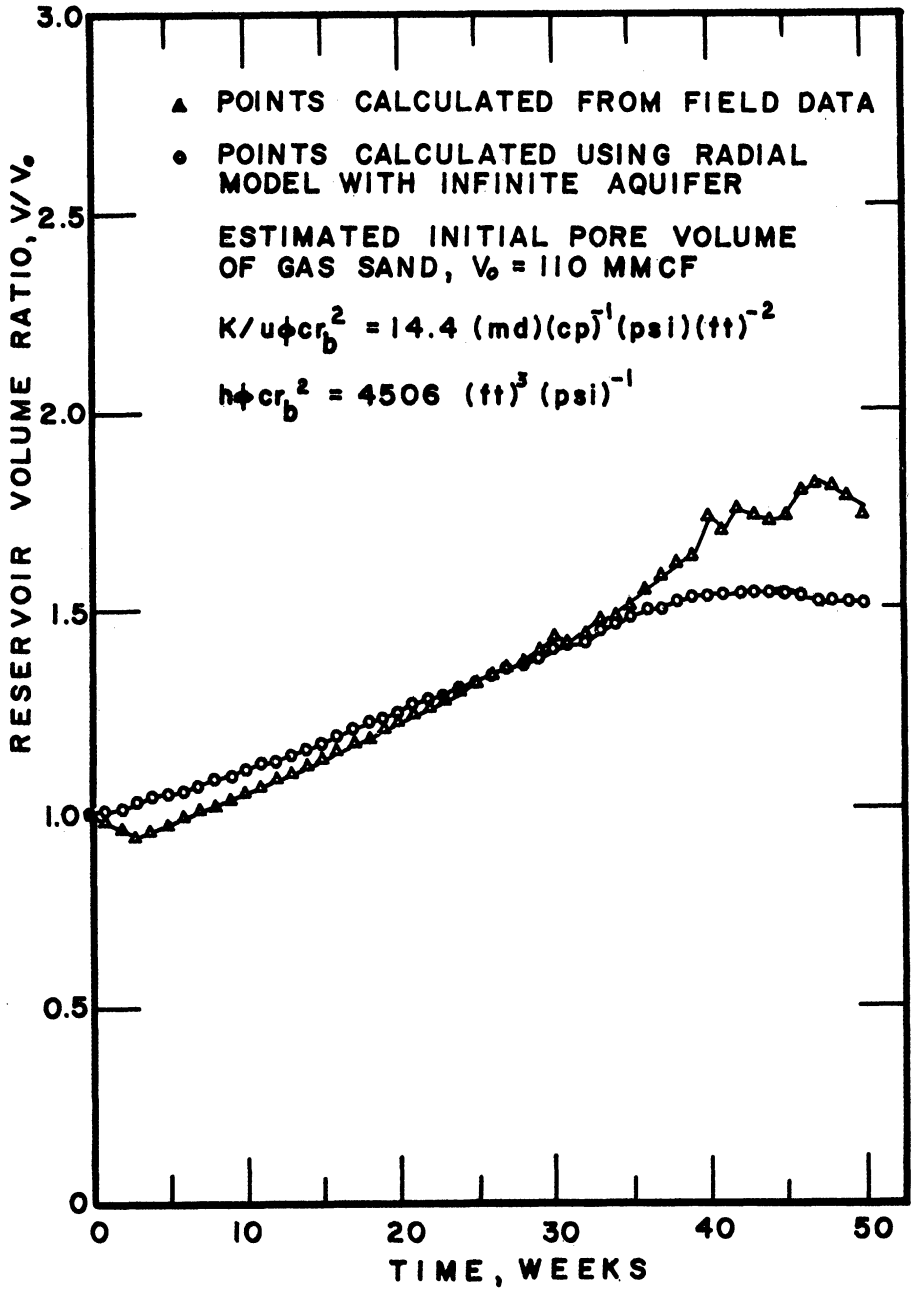

Fig. B-5. Comparison of Field B volume ratio predicted using radial model (infinite aquifer) with volume ratios calculated from field data.

FIELD C

Field C, a western New York storage reservoir discovered in 1934, produced gas for eight years prior to conversion to gas-storage operation. The reservoir was nearly depleted during the initial eight years when 3,582 million standard cubic feet were produced accompanied by a wellhead pressure decline from an initial value of 2124 to 247 psia.

1. GEOLOGY

This field, 4555 feet below the surface, consists of weakly cemented sandstone. Extensive coring operations were unsuccessful because the cementing material was not strong enough to hold the sand grains together. The rock is composed of fairly coarse to medium-grained quartz sandstone, open in texture, with small amounts of secondary silica and calcite as cementing material.

The sandstone was deposited during a rapidly westward advancing sea; the old shore deposits were reworked during temporary interruptions of this encroachment. This sand is found throughout central and western New York in lenticular beds.

The structure of this field is a small structural dome, elongated east and west, and bracketed by two paralleled reverse faults to the north and south. The presence of these faults suggests that the linear model would best approximate this reservoir. An areal sketch of the gas and water boundary is shown in Fig. C-1.

2. FIELD DATA

The reservoir and fluid properties are summarized in Table C-1 and the production-pressure history tabulated in Table C-2.

3. CALCULATIONS

(a) Application of Linear Model to Field C.—The location of Field C between two parallel faults suggested that the Linear Model would be the most suitable choice for analyzing the data from this field.

The following data from Tables C-1 and C-2 were used:

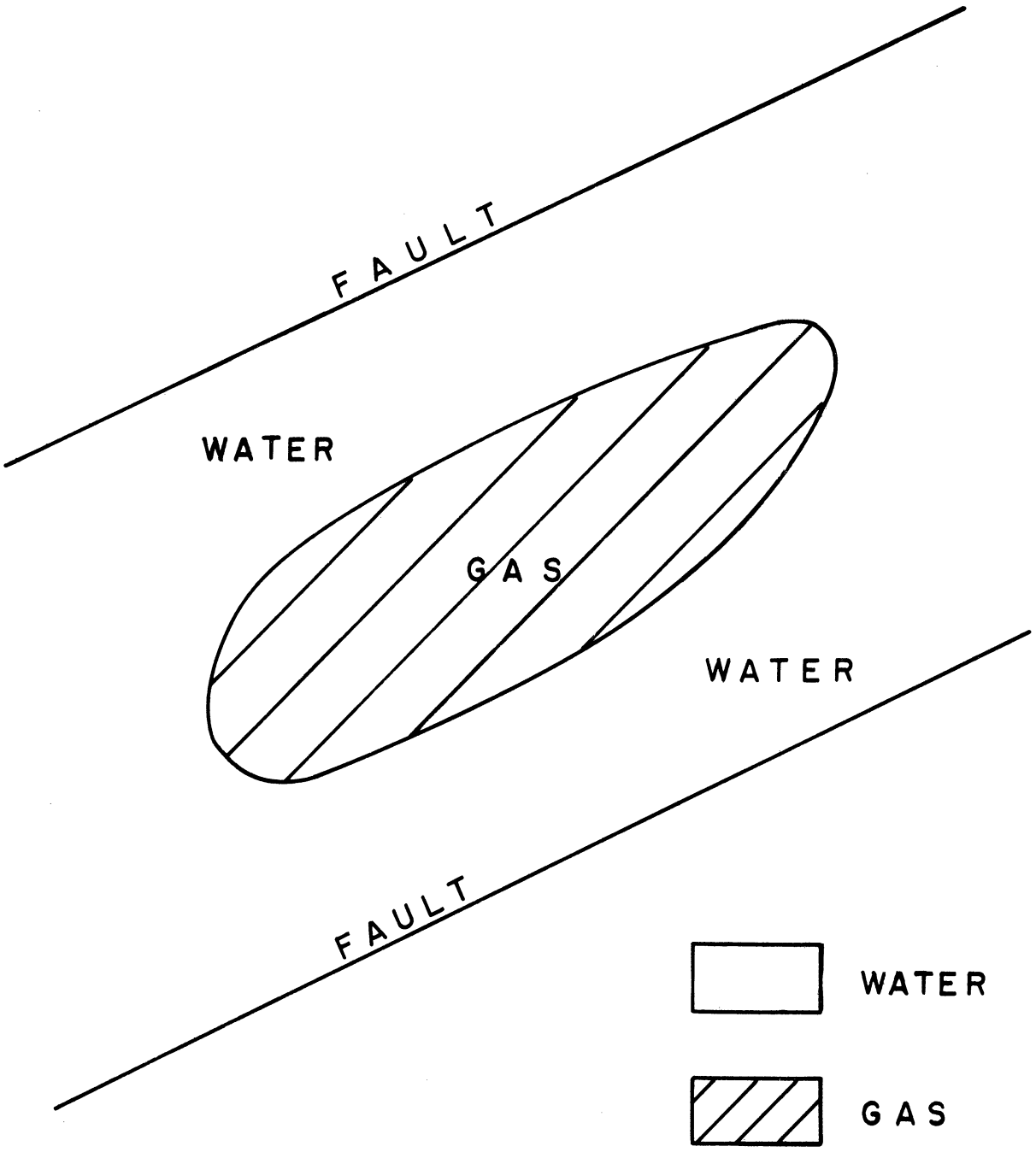

Fig. C-1. Areal sketch showing the boundary of Field C.

TABLE C-1

STORAGE FIELD C DATA

Aquifer Characteristics

Type of formation	Sandstone
Porosity	8%
Permeability	50 millidarcys
Thickness	14 ft
Depth to top of aquifer	4555 ft
Viscosity of liquid in aquifer	1 centipoise
Compressibility of brine and formation	7×10^{-6} vol/vol-psi

Data on Storage Field

a. Field geometry

Location	Western New York
Type of formation	Sandstone
Nature of structure	Structural dome

b. Gas-sand formation and fluid properties

Gas compressibility correlation, $z = a + bP$	
Constant a	0.983
Constant b	-0.000081
Reservoir temperature	582°R
Reservoir thickness	5 ft
Base conditions for gas measurements	P_b = 14.75 psia
	T_b = 520°R

c. History of gas reservoir

Discovery date	1934
Initial discovery pressure	1900 psig (wellhead)
Initial pore volume	24×10^6 cu ft
Date converted to gas storage	1942

TABLE C-2

GAS INVENTORY AND PRESSURE HISTORY FOR FIELD C

Pressure Base 14.75 psia
Temperature Base = 520°R

Date	Cumulative Gas Production, MMSCF	P, Wellhead, psig, at End of Month
Initial		1900
1934 Nov	2.0	--
Dec	33.4	--
1935 Jan	79.8	--
Feb	99.9	--
Mar	113.3	--
Apr	124.6	1855
May	138.6	--
June	140.1	1825
July	143.7	1825
Aug	143.7	1820
Sept	149.5	1850
Oct	152.5	1840
Nov	152.5	1830
Dec	182.2	1825
1936 Jan	211.5	1825
Feb	244.7	--
Mar	260.2	1825
Apr	262.4	1825
May	262.4	1825
June	262.4	--
July	262.4	--
Aug	280.2	--
Sept	280.2	--
Oct	280.2	1770
Nov	297.3	1770
Dec	318.8	1740
1937 Jan	319.8	--
Feb	320.3	--
Mar	320.3	--
Apr	320.3	--
May	320.3	--
June	320.3	--
July	320.3	--
Aug	320.3	1750
Sept	320.3	--
Oct	321.3	1745
Nov	321.3	--
Dec	373.2	1725
1938 Jan	384.5	1720
Feb	384.5	1725
Mar	386.8	1725
Apr	386.8	1725
May	386.8	1725
June	386.8	1730
July	386.8	1725
Aug	386.8	--
Sept	392.0	1725
Oct	401.0	1725
Nov	432.4	1715
Dec	458.8	1685
1939 Jan	611.1	--
Feb	878.5	--
Mar	1192	--
Apr	1424	1250
May	1614	1180
June	1794	1085
July	2026	990
Aug	2230	910
Sept	2280	905
Oct	2432	--
Nov	2608	--
Dec	2791	--
1940 Jan	2944	--
Feb	3059	--
Mar	3161	--
Apr	3221	--
May	3247	--
June	3253	385
July	3256	385
Aug	3256	395
Sept	3257	400
Oct	3276	395
Nov	3328	--
Dec	3381	360
1941 Jan	3432	--
Feb	3481	--
Mar	3528	--
Apr	3562	217
May	3580	212
June	3580	226
July	3580	238
Aug	3580	253
Sept	3580	265
Oct	3580	--
Nov	3580	--
Dec	3580	305
1942 Jan	3580	--
Feb	3580	--
Mar	3580	--
Apr	3581	330
May	3582	350
June	3582	370
July	3574	385
Aug	3537	423
Sept	3480	477
Oct	3456	530
Nov	3456	--
Dec	3458	548
1943 Jan	3469	--
Feb	3488	530
Mar	3504	--
Apr	3504	530
May	3504	535
June	3475	560
July	3460	589
Aug	3436	616
Sept	3399	643
Oct	3359	670
Nov	3359	680
Dec	3389	--
1944 Jan	3414	645
Feb	3439	--
Mar	3462	610
Apr	3470	--
May	3461	--
June	3429	650
July	3392	688
Aug	3361	720
Sept	3342	--
Oct	3324	--
Nov	3324	770
Dec	3370	--
1945 Jan	3424	--
Feb	3458	--
Mar	3458	665
Apr	3458	680
May	3458	685
June	3458	700
July	3458	--
Aug	3458	--
Sept	3458	--
Oct	3458	720
Nov	3458	730
Dec	3476	--
1946 Jan	3496	--
Feb	3502	680
Mar	3502	--
Apr	3502	--
May	3502	675
June	3502	695
July	3502	710
Aug	3502	--
Sept	3503	--
Oct	3504	--
Nov	3504	--
Dec	3540	--
1947 Jan	3576	680
Feb	3617	--
Mar	3642	607
Apr	3642	--
May	3642	630
June	3639	651
July	3599	693
Aug	3583	728
Sept	3576	--
Oct	3552	--
Nov	3545	--
Dec	3550	--
1948 Jan	3568	--
Feb	3591	--
Mar	3618	--
Apr	3633	1015
May	3633	--
June	3609	--
July	3585	--
Aug	3562	--
Sept	3536	--
Oct	3531	--
Nov	3511	--
Dec	3492	--
1949 Jan	3492	--
Feb	3492	--
Mar	3492	--
Apr	3492	--
May	3492	--
June	3492	--
July	3446	--
Aug	3381	--
Sept	3308	--
Oct	3235	1290
Nov	3217	--
Dec	3226	--
1950 Jan	3267	--
Feb	3324	--
Mar	3360	1110
Apr	3392	--
May	3337	--
June	3283	--
July	3229	--
Aug	3173	--
Sept	3117	1420
Oct	3074	--
Nov	3088	--
Dec	3176	--
1951 Jan	3246	--
Feb	3319	--
Mar	3332	1180
Apr	3286	--
May	3223	--
June	3152	--
July	3078	--
Aug	3008	--
Sept	2945	--
Oct	2889	--
Nov	2899	1595
Dec	2978	--
1952 Jan	3067	--
Feb	3108	--
Mar	3152	1336
Apr	3161	--
May	3115	--
June	3054	--
July	2989	--
Aug	2928	--
Sept	2874	1650
Oct	2854	--
Nov	2835	--
Dec	2920	--
1953 Jan	2975	--
Feb	3014	--
Mar	3064	1440
Apr	3062	--
May	3004	--
June	2927	--
July	2847	--
Aug	2769	--
Sept	1776	--
Oct	2661	--
Nov	2658	--
Dec	2701	--
1954 Jan	2780	--
Feb	2792	--
Mar	2798	1629
Apr	2794	--
May	2753	--
June	2691	--
July	2617	--
Aug	2545	--
Sept	2479	1877
Oct	2437	--
Nov	2483	--
Dec	2638	--
1955 Jan	2764	--
Feb	2845	--
Mar	2903	--
Apr	2865	1527
May	2810	--
June	2744	--
July	2677	--
Aug	2614	--
Sept	2556	1804
Oct	2495	--
Nov	2567	--
Dec	2792	--
1956 Jan	2909	--
Feb	3073	--
Mar	3186	1049
Apr	3145	--
May	3081	--
June	3016	--
July	2938	--
Aug	2866	--
Sept	2811	1625

ϕ = .08
h_{gas} = 5 ft
$h_{aquifer}$ = 14 ft
c = 7×10^{-6} vol/vol psi
K = 50 millidarcys
μ = 1 centipoise
a = 0.983
b = -0.000081 psi^{-1}
Δt = 30.45 days/time interval
T_r = 582°R
V_o = 24.0×10^6 ft^3
Gas gravity = 0.577
Gas well depth = 4,600 ft

Since wellhead pressures, psig, were reported, the bottom hole pressures were calculated by:

$$P_{bhp} = P_{wh} e^{Mh/144\ zRT}$$

$$P_o = (1900 + 14.7) e^{\{(29)(.577)\}(4,600)/\{(144)(10.73)(582)\}}$$

$$= 2124.3$$

$$P_6 = (1855 + 14.7) e^{\{(29)(.577)\}(4,600)/\{(144)(10.73)(582)\}}$$

$$= 2073.4$$

The remaining values for the first ten points are summarized in Table C-3.

As in the previous example of calculations, the cumulative gas in place was calculated by:

$$n_o = \frac{V_o}{(\frac{a}{P_o}+b)RT}$$

$$= \frac{24.0 \times 10^6}{(\frac{.983}{2124.3}-.000081)(10.73)(582)}$$

$$= 1.008 \times 10^7 \text{ lb moles}$$

TABLE C-3

CALCULATED VALUES FOR FIELD C USING LINEAR MODEL

Time Step, N	Dimensionless, Q	Cumulative Gas Produced, MMSCF	Cumulative Gas in Place, lb moles	Pressures Predicted Using Linear Model, psia	Pressures Predicted Assuming No Water Movement, psia	Pressure Data, psia	Volume Ratios Using Predicted Pressures (linear model)	Volume Ratios Using Observed Pressures
0	0	2.0	10.08×10^6	2124.3	2124.3	2124.3	1.0000	1.0000
1	4140	33.4	10.07	2123.4	2123.4	--	1.0000	--
2	5855	79.8	9.99	2109.7	2108.9	--	0.9995	--
3	7177	99.9	9.86	2090.2	2087.5	--	0.9984	--
4	8281	113.3	9.81	2083.1	2078.1	--	0.9971	--
5	9258	124.6	9.78	2078.7	2071.9	--	0.9960	--
6	10142	138.6	9.75	2075.1	2066.7	2073.4	0.9951	0.9961
7	10954	140.1	9.71	2070.3	2060.2	--	0.9941	--
8	11711	143.7	9.71	2071.0	2059.5	2039.5	0.9933	1.0118
9	12421	143.7	9.70	2070.5	2057.8	2039.5	0.9926	1.0108
10	13093	149.5	9.70	2071.6	2057.8	2033.9	0.9920	1.0141

and

$$n_j = n_o - \frac{P_{base}\, G_{p_j}}{RT_{base}}$$

$$n_1 = 1.008\text{x}10^7 - \frac{(14.7)(2{,}016{,}000)}{(10.73)(520)}$$

$$n_1 = 1.007\text{x}10^7 \text{ lb moles}$$

$$n_2 = 1.008\text{x}10^7 - \frac{14.7(33{,}440{,}000)}{(10.73)(520)}$$

$$= 9.987\text{x}10^6 \text{ lb moles}$$

The remaining values of cumulative gas in place are given in Table C-3.

The pressure assuming no water movement is given by:

$$P_j = \frac{an_jRT}{V_o - bn_jRT}$$

$$P_1 = \frac{(.983)(1.007\text{x}10^7)(10.73)(582)}{(24\text{x}10^6) - (.000081)(1.007\text{x}10^7)(10.73)(582)}$$

$$= 2123.4$$

The pressures were predicted using the water influx equation for the constant-terminal-pressure case,

$$W_{e_j} = \frac{\phi cA\sqrt{\theta}}{\sqrt{\pi}} \sum_{i=0}^{i=j-1} \Delta P_i \sqrt{j-i}$$

From a mass balance,

$$V_j = V_o - W_{e_j}$$

where V_j = reservoir volume at time step j, ft^3 the gas low

$$V_j = \frac{z_j n_j RT}{P_j} = \frac{a+bP_j}{P_j} n_j RT$$

and an expansion of the water influx equation,

$$\frac{a+bP_j}{P_j} n_j RT = V_o - \phi cA\sqrt{\frac{\Delta\theta}{\pi}} \sum_{i=0}^{j-2} \Delta P_i \sqrt{j-i} - \phi cA\sqrt{\frac{\Delta\theta}{\pi}} P_{j-2} + \phi cA\sqrt{\frac{\Delta\theta}{\pi}}$$

Let

$$K_4 = \phi cA\sqrt{\frac{\Delta\theta}{\pi}} = \phi cA\sqrt{\frac{0.00633\ K\Delta t}{\pi\mu\phi c}}$$

Solving the above equation for P_j yields

$$P_j = C_1 + \sqrt{C_1^2 + C_2}$$

where

$$C_1 = \frac{K_4\left[\left(\sum_{i=0}^{j-2} \Delta P_i \sqrt{(j-i)}\right) + P_{j-2}\right] + bn_j RT - V_o}{2K_4}$$

$$C_2 = \frac{an_j RT}{K_4}$$

$$\Delta P_j = P_{i-1} - P_{i+1};\quad P_{-1} \equiv P_o$$

The value for K_4 was varied until the difference between the observed pressures and predicted pressures was a minimum. This value was $K_4 = 689$.

$$P_o(\text{calc}) = P_o(\text{observered})$$

$$= 2124.3 \text{ psia}$$

$$P_1 = C_1 + \sqrt{C_1^2 + C_2}$$

$$C_1 = \frac{K_4 P_o + bn_j RT - V_o}{2K_4}$$

$$= \frac{689(2124.3) - .000081(1.007\text{x}10^7)(10.73)(583) - 24\text{x}10^6}{2(689)}$$

$$C_2 = \frac{an_1RT}{K_4}$$

$$= \frac{0.983(1.007x107)(10.73)(582)}{(689)}$$

$P_1 = 2123.4$

$P_2 = C_1 + \sqrt{C_1^2 + C_2}$

$$\Delta P_o = P_{-1} - P_1$$

$$= 2124.3 - 2123.4$$

$$= 0.9 \text{ psi}$$

$$C_1 = \frac{K_4\{\Delta P_o \sqrt{2} + P_o\} + bn_2RT - V_o}{2K_4}$$

$$= 689\{0.9 \sqrt{2} + 2124.3\} - .00008(9.987x10^6)(10.73)(582)$$

$$-24.0x10^6/\{2(689)\}$$

$$C_2 = \frac{an_2RT}{K_4}$$

$$= \frac{0.983(9.987x10^6)(10.73)(582)}{689}$$

$P_2 = 2109.7$

See Table C-3 for the remaining values predicted using the Linear Model.

4. RESULTS

Nearly all the virgin gas of Field C was produced prior to the date of storage conversion. This quantity of gas, converted to the initial reservoir

temperature and pressure, was used as a lower limit for estimating the initial pore volume. This limit (V_o = 23.8 million cubic feet) was close to the value which gave the minimum deviation between calculated and observed pressures, 24.0 million cubic feet.

Pressures calculated, assuming no water movement, are considerably lower than the observed pressures after the initial drawdown of Field C (Fig. C-2). Considerable improvement is obtained when the rate of water movement is determined by use of the linear model (Fig. C-3). A comparison of the reservoir volume ratios calculated from these pressures is given in Fig. C-4. Note that at one point about 85% of the volume originally occupied by the gas had been replaced by water.

The resistance-function method in its present form did not give a satisfactory prediction for this field. Future work is planned to overcome the difficulties encountered.

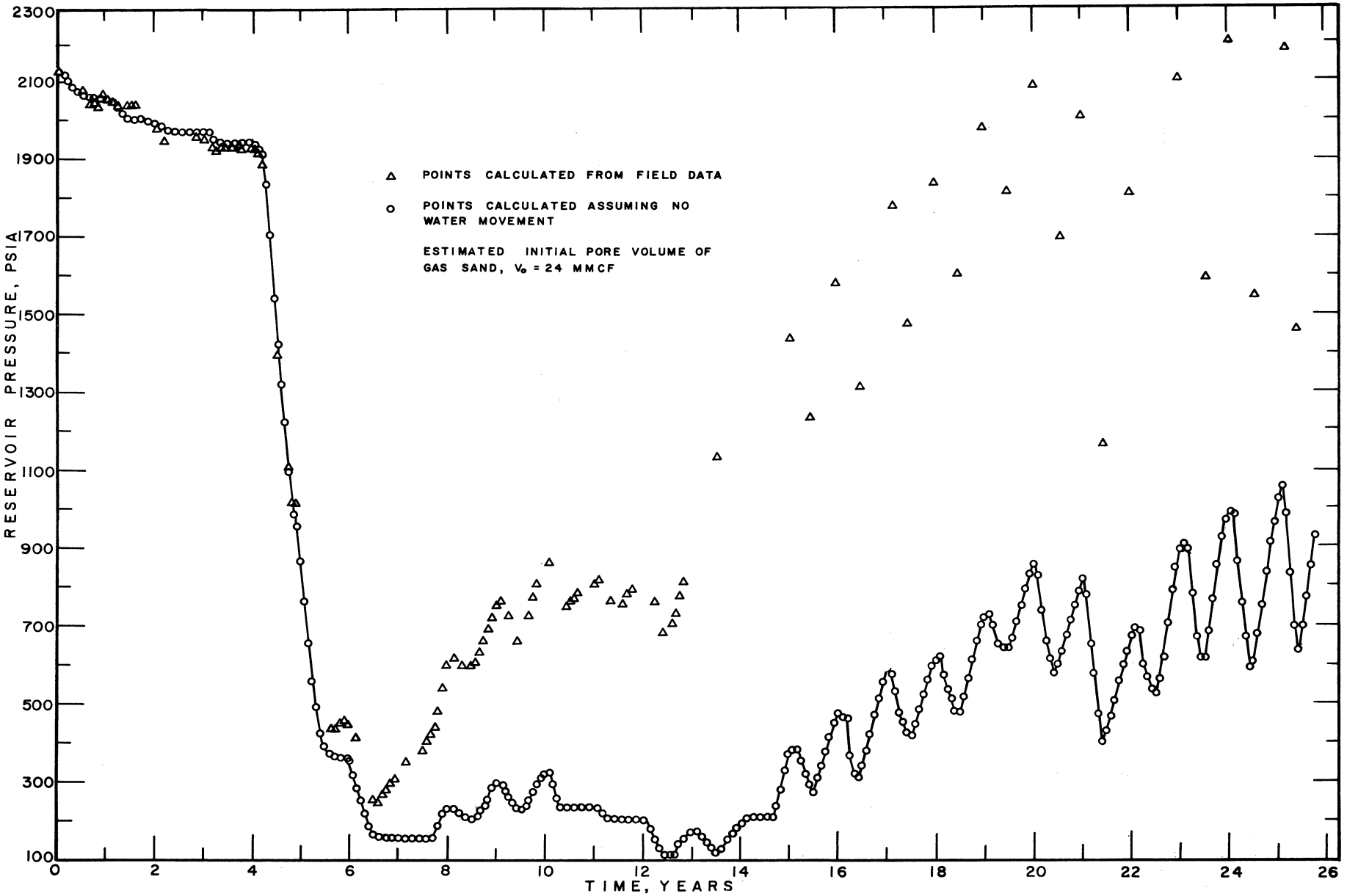

Fig. C-2. Comparison of Field C predicted pressures, assuming no water movement with observed pressures.

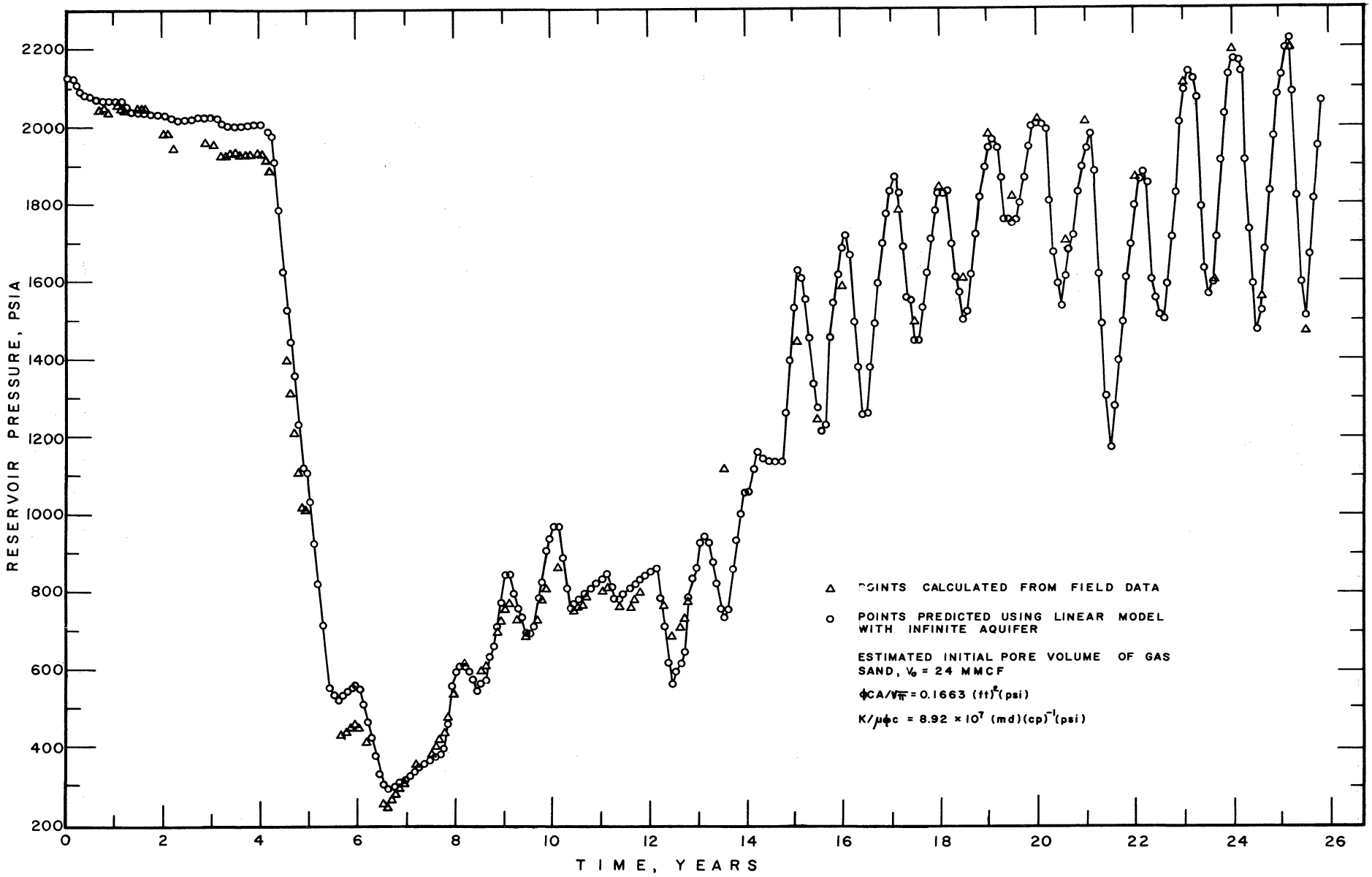

Fig. C-3. Comparison of Field C pressures predicted using linear model (infinite aquifer) with observed pressures.

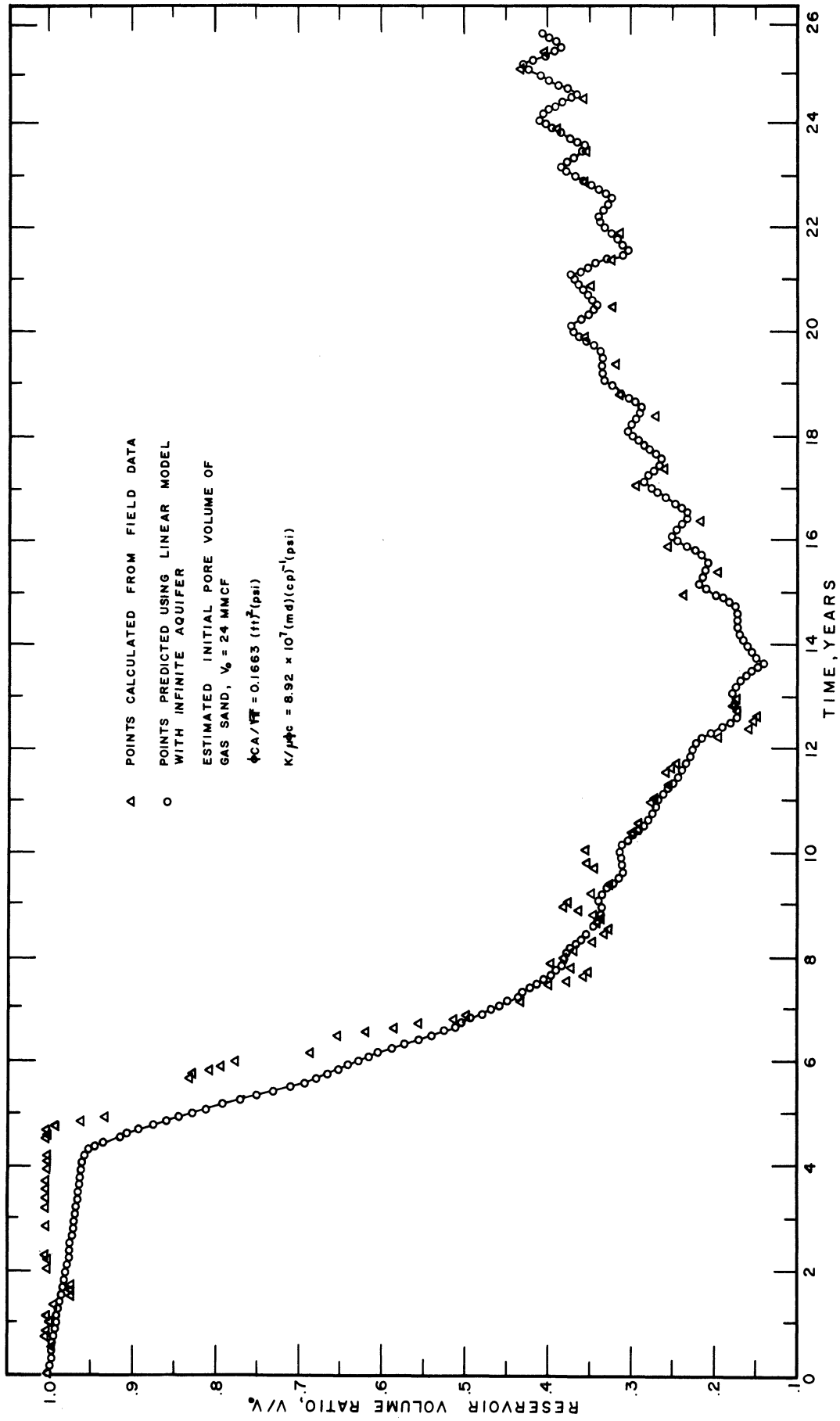

Fig. C-4. Comparison of Field C volume ratio predicted using linear model with volume ratios calculated from field data.

FIELD D

Field D, a Kansas gas reservoir, was recently converted to storage operations. The first well in the field was completed in July, 1918, with an open flow capacity of 10,000 MCF per day from a sand 1340 ft below the surface. The initial wellhead shut-in pressure was 520 psig, and the reserve originally contained 24,264,356 MCF (14.65 psia base) of gas.

Prior to conversion to gas storage in May, 1958, water had encroached the depleted areas of the field and had successively drowned out the lower-lying properties.

The ability to move water out of the storage area and to inject gas in quantities sufficient to make this field commercially acceptable has been established.

1. GEOLOGY

The gas-bearing sand that comprises Field C is an anticlinal structure with closure exhibited to the limits of the gas field. This structure appears to be of sufficient magnitude to have held the original volume in place. The sand body grades up-dip to the northeast into shaley sands and shales which effectively seal off up-dip migration of the gas; while to the south, the sand extends a considerable distance beyond the southern limit of the field. Thick shale beds overlie this storage sand. This sand rests directly upon the Mississippi Lime throughout most of the field. In a few wells a thin shale bed was found between the storage sand and Mississippi Lime. The storage sand is uniform in texture and composed of round, medium-sized grains.

2. FIELD DATA

The reservoir and aquifer properties are given in Table D-1 and the production-pressure history is tabulated in Table D-2.

The initial pore volume of the gas sand was determined from the production history prior to the conversion of the field to storage operation. Since the field had been shut in for several years, the initial pore volume used in this study is the volume at the time the field was converted to storage operation and <u>not</u> the original volume when the field was discovered in 1918. This value, V_o = 30 MMCF, also gave the best results when the mathematical models and resistance-function method were applied to the field data.

TABLE D-1

STORAGE FIELD D DATA

Aquifer Characteristics

Type of formation	Sandstone and limestone
Porosity	30%
Permeability	500 millidarcys
Thickness	10 ft
Depth to top of aquifer	1364 ft
Viscosity of liquid in aquifer	1 centipoise
Compressibility of brine and formation	7×10^{-6} vol/vol-psi

Data on Storage Field

A. Field geometry

Location	Kansas
Type of formation	Sandstone
Nature of structure	Anticlinal

b. Gas-sand formation and fluid properties

Gas compressibility correlation, $z = a + bP$	
Constant a	0.9975
Constant b	-1.25×10^{-4}
Reservoir temperature	560°R
Reservoir depth	1354 ft
Base conditions for gas measurements	P_b = 14.65 psia
	T_b = 520°R

c. History of gas reservoir

Discovery date	July 1918
Initial discovery pressure	408 psia (wellhead)
Initial pore volume	30×10^6 cu ft
Date converted to gas storage	1958

TABLE D-2

GAS INVENTORY AND PRESSURE HISTORY FOR FIELD D

Pressure Base = 1465 psia
Temperature Base = 520°R

Date	Cumulative Gas Production, MMSCF at 23rd of Month	P, Wellhead, psia, at 23rd of Month
Initial		408
1958 May	- 757	560
June	-1319	572
July	-1877	589
Aug	-2506	602
Sept	-3140	610
Oct	-3763	614
Nov	-4349	613
Dec	-4481	585
1959 Jan	-4417	552
Feb	-4229	527
Mar	-3936	503
Apr	-4317	534
May	-5505	601
June	-6531	627
July	-7131	627
Aug	-7664	626
Sept	-8176	626
Oct	-8628	626
Nov	-8658	601
Dec	-7571	536
1960 Jan	-6126	466
Feb	-4582	396
Mar	-3353	353
Apr	-5261	533
May	-7751	614
June	-8873	626
July	-9561	627

An areal sketch of the gas-water interface, Fig. D-1, and the field properties, Table D-1, indicate that the radial model should be applicable for analyzing water movement in this thin, pie-shaped reservoir.

3. CALCULATION ON FIELD D: EXAMPLE OF RESISTANCE-FUNCTION METHOD

Find the resistance function for Field D. It has been decided to fit the first ten data points with the radial model, constant-rate case. The following data are available for Field D.

n	P(well bottom psia)	G_p(MMSCF)
1	592.1	-757
2	604.5	-1319
3	622.1	-1877
4	635.5	-2506
5	643.8	-3140
6	647.9	-3763
7	646.9	-4349
8	618.0	-4481
9	583.9	-4417
10	558.1	-4229
11	533.3	-3969
12	565.3	-4317
13	634.5	-5505
14	661.4	-6531
15	661.4	-7131
16	660.3	-7664
17	660.3	-8176
18	660.3	-8628
19	634.5	-8658
20	567.4	-7571
21	495.1	-6126
22	422.9	-4582
23	378.6	-3353
24	564.3	-5261
25	647.9	-7751
26	660.3	-8873
27	661.4	-9561

P_o = 435.3 psia
V_o = 30.0 MMCF
h = 10 ft
ϕ = 0.30
μ = 1.0 cp
K = 500 md
f = 0.25

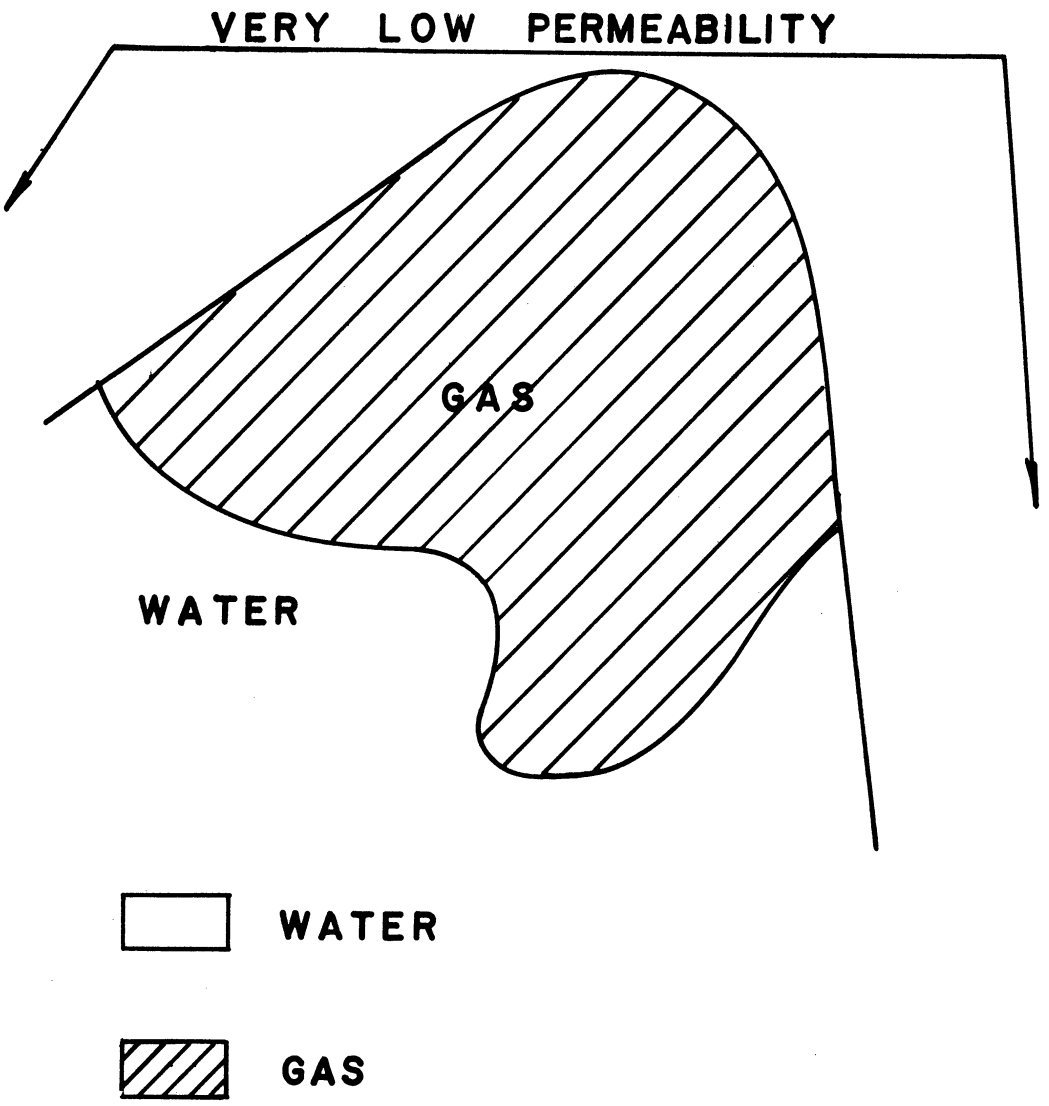

Fig. D-1. Areal sketch showing boundary of Field D.

P_b = 14.65 psia
T_b = 520°R
c = 7×10^{-6} vol/vol psia
T = 560°R
a = 0.9975
b = -.000125 psi^{-1}
Δt = 30.45 days/time interval.

(1) Calculate K_1 and K_2:

$$K_1 = \frac{25.15\mu}{Khf} = \frac{25.15 \times 1.0}{500 \times 10 \times 1.0} = .005030$$

$$K_2 = \frac{0.006328\ K\Delta t}{\mu\phi c r_b^2} = \frac{0.006328\ K\Delta t \pi hf}{\mu c V_o}$$

$$= \frac{0.006328(500)(30.45)(3.1416)(10)(1.0)}{(1.0)(7 \times 10^{-6})(30 \times 10^6)}$$

$$= 14.413$$

(2) Calculate S_o ... S_{27}:

$$S_n = \frac{V_o}{(\frac{a}{P_o}+b)\Delta t} - \left(\frac{P_b T}{T_b \Delta t}\right) \cdot G_{p_n}$$

$$S_o = \frac{30 \times 10^6}{(\frac{.9975}{435.3}-.000125)30.45} - \left(\frac{14.65 \times 560}{5w0 \times 30.45}\right)(0)$$

$$= 4.547 \times 10^8 - 0.5181(0) = 4.547 \times 10^8$$

$$S_1 = 4.547 \times 10^8 - (0.5181)(-757 \times 10^6) = 8.4697 \times 10^8, \text{ etc.}$$

(3) Calculate dimensionless time, t_{D_1} ... $t_{D_{10}}$:

$$t_{D_n} = K_2 \cdot n$$

$$t_{D_1} = (14.413)(1) = 14.413$$

$$t_{D_2} = (14.413)(2) = 28.826$$

etc.

(4) Find corresponding dimensionless pressure values from tables[1,2,4] using linear interpolation.

$$p_n = p_{j-1} + \frac{t_{D_n} - t_{D_{j-1}}}{t_{D_j} - t_{D_{j-1}}} (p_j - p_{j-1})$$

$$p_1 = 1.6509 + \frac{14.413-10.000}{15.000-10.000} (1.8294-1.6509)$$

$$= 1.8084$$

$$p_2 = 2.1251$$

$$p_3 = 2.3167, \text{ etc.}$$

(5) Compute $\Delta p_1 \ldots \Delta p_{10}$:

$$\Delta p_n = p_n - p_{n-1}$$

$$\Delta p_1 = 1.8084-0 = 1.8084$$

$$\Delta p_2 = 2.1251-1.8084 = 0.3167$$

$$\Delta p_3 = 2.3167-2.1251 = 0.1916, \text{ etc.}$$

(6) Compute P_1, e_{w_1}; P_2, e_{w_2}, ... P_{10}, $e_{w_{10}}$ (see below).

(7) Find percentage deviation between calculated and "observed" pressures.

(8) Change the value of K_1 and repeat steps (6) and (7). For purposes of this example calculation the "optimum" value only of K_1 will be used to illustrate steps (6) and (7). Its value, 1.983×10^{-4}, was found by trial and error using a modified half interval method. Starting with the value of K_1 calculated in step (1), the optimum value was obtained after 15 trials.

$$P_n = \sqrt{B_n^2 + C_n} - B_n$$

where

$$B_n = \frac{1}{2}\left\{\left[\left(\frac{a}{P_{n-1}}\right) + b\,S_{n-1} - bS_n\right]K_1\Delta p_1 - P_o + K_1\sum_{j=2}^{n} e_{w_{n+1-j}}\cdot\Delta p_j\right\}$$

and

$$C_n = aS_nK_1\Delta p_1$$

$$B_1 = \frac{1}{2}\left\{\left[\left(\frac{.9975}{435.3} - .000125\right)4.5475\text{x}10^8 + .000125\text{x}8.4697\text{x}10^8\right]\right.$$

$$\left.1.983\text{x}10^{-4}\text{x}1.8084 - 435.3 + 1.983\text{x}10^{-4}(0)\right\}$$

$$C_1 = (0.9975)(8.4697\text{x}10^8)(1.983\text{x}10^{-4})(1.8084)$$

$$P_1 = \sqrt{B_1^2 + C_1} - B_1 = 573.0 \text{ psia}$$

$$e_{w_n} = (P_o - P_n - K_1\sum_{j=2}^{n} e_{w_{n+1-j}}\cdot\Delta p_j)/(K_1\Delta p_1)$$

$$e_{w_1} = (435.3 - 573.0 - 1.983\text{x}10^{-4}(0))/(1.983\text{x}10^{-4}\text{x}1.8084)$$

$$= -383.349 \text{ MCF/day}$$

Similar calculations yield the following results.

n	P_n(data), psia	P_n(calc), psia	e_{w_n} MCF/day	$\Delta Z_n x10^5$, psia/(ft^3/day)
1	592.1	573.0	-383.349	35.900
2	604.5	598.3	-386.669	6.272
3	622.1	613.4	-387.422	3.775
4	635.5	631.4	-407.816	2.740
5	643.8	643.7	-415.172	2.131
6	647.9	651.6	-414.745	1.735
7	646.9	654.9	-405.681	1.461
8	618.0	623.8	-306.600	1.126
9	583.9	588.6	-213.300	1.126
10	558.1	553.7	-130.147	1.126

The percentage deviation is found by dividing the sum of the absolute values of the differences between columns 2 and 3 by the sum of column 2 and multiplying by 100:

$$\% \text{ deviation} = \frac{100 \sum_{n=2}^{10} \left| P_n(\text{calc}) - P_n(\text{data}) \right|}{\sum_{n=2}^{10} P_n(\text{data})} = 0.82\%$$

(9) Compute $\Delta Z_1 \ldots \Delta Z_{10}$:

$$\Delta Z_n = K_1 \text{ (optimum)} \cdot \Delta p_n$$

$$\Delta Z_1 = (1.983 \times 10^{-4})(1.8084) = 3.585 \times 10^{-4} \text{ psi/(ft}^3\text{/day)}$$

$$\Delta Z_2 = (1.983 \times 10^{-4})(0.3167) = 0.629 \times 10^{-4}, \text{ etc.}$$

(10) Find ΔZ_{11}

$$\Delta Z_n = \left\{ P_o - P_n^* - \sum_{j=2}^{n-1} e_{w_{n+1-j}} \cdot \Delta Z_j + [(a/P_n^* + b)S_n - (a/P_{n-1} + b)S_{n-1}]\Delta Z_1 \right\} / e_{w_1}$$

$$\Delta Z_{11} = \Big\{ 435.3 - 533.3 - [(-130.15 \times 10^3)(6.273 \times 10^{-5}) + (-213.30 \times 10^3)(3.776 \times 10^{-5}) + \ldots$$
$$+ (-386.70 \times 10^3)(1.127 \times 10^{-5})] + \Big[\left(\frac{.9975}{533.3} - .000125 \right) 25.112 \times 10^8 - \left(\frac{.9975}{553.7} - .000125 \right) 26.459 \times 10^8 \Big] 3.590 \times 10^{-4} \Big\} / (383.38 \times 10^3) = 1.398 \times 10^{-4}$$

Note that the asterisk on P_n^* denotes data rather than calculated pressure.

(11) Set ΔZ_{11} so that it satisfies the following:

$$(1-\epsilon)\left(\frac{n-2}{n-1}\right)\Delta Z_{n-1} \leqslant \Delta Z_n \leqslant (1+\epsilon)\Delta Z_{n-1}$$

$$(1-.02)\left(\frac{11-2}{11-1}\right)(1.126\text{x}10^{-5}) \leqslant \Delta Z_{11} \leqslant (1+.02)(1.126\text{x}10^{-5})$$

$$.991\text{x}10^{-5} \leqslant \Delta Z_{11} \leqslant 1.147\text{x}10^{-5}$$

From the above equation, ΔZ_{11} is too high. Therefore it is set equal to $(1.02)(\Delta Z_{10}) = 1.147\text{x}10^{-5}$.

(12) Calculate P_{11}:

$$P_n = \sqrt{B_n^2 + C_n} - B_n$$

where

$$B_n = \frac{1}{2}\left\{[(a/P_{n-1} + b)S_{n-1} - bS_n]\Delta Z_1 - P_o + \sum_{j=2}^{n} e_{W_{n+1-j}} \cdot \Delta Z_j\right\}$$

and

$$C_n = aS_n\Delta Z_1$$

$$B_{11} = \frac{1}{2}\left\{\left[\left(\frac{.9975}{553.7} - .000125\right)26.459\text{x}10^8 + .000125\text{x}25.112\right]3.950\text{x}10^{-4}\right.$$

$$\left. -435.3 + [(-130.14\text{x}10^3)(6.273\text{x}10^{-5}) + \ldots + (-383.38\text{x}10^3)(1.147\text{x}10^{-5})]\right\}$$

$$C_{11} = (.9975)(25.112\text{x}10^8)(3.590\text{x}10^{-4})$$

$$P_{11} = 521.0 \text{ psia.}$$

(13) Calculate $e_{w_{11}}$:

$$e_{w_n} = (P_o - P_n - \sum_{j=2}^{n} e_{w_{n+1-j}} \cdot \Delta Z_j)/\Delta Z_1$$

$$e_{w_{11}} = \frac{435.3-521.0-[(-130.15\times10^3)(6.273\times10^{-5})+\ldots+(-383.4\times10^3)(1.147\times10^{-5})]}{3.950\times10^{-4}}$$

$$= -58.236\times10^3 \text{ ft}^3/\text{day}.$$

(14) Repetition of steps 10 through 13 yield the following results:

n	P_n(data), psia	P_n(calc), psia	e_{w_n} MCF/day	$\Delta Z_n \times 10^5$, psi/(ft^3/day)
11	533.3	521.0	- 58.236	1.147
12	565.3	540.7	-134.548	1.157
13	634.5	613.5	-334.801	1.187
14	661.4	654.1	-410.144	1.218
15	661.4	659.3	-385.553	1.248
16	660.3	660.9	-366.489	1.157
17	660.3	662.2	-353.845	1.066
18	660.3	660.9	-338.341	1.005
19	634.5	639.4	-271.592	0.944
20	567.4	566.3	- 73.268	0.944
21	495.1	483.1	123.458	0.974
22	422.9	398.2	306.706	1.005
23	378.6	332.3	426.509	1.005
24	564.3	471.7	- 22.646	1.035
25	647.9	613.6	-379.582	1.035
26	660.3	650.9	-401.579	1.066
27	661.4	661.1	-337.397	1.096

The resistance curve is required by the problem in the sum of the ΔZ's.

$$Z_n = Z_{n-1} + \Delta Z_n$$

$$Z_1 = 35.900\times10^{-5} \text{ psi/(ft}^3\text{/day)}$$

$$Z_2 = 35.900\times10^{-5} + 6.273\times10^{-5} = 42.173\times10^{-5}, \text{ etc.}$$

These points are plotted in Fig. D-7. Note that the units for Z have been changed in Fig. D-7 to psi/(MMCF/month).

Pressure calculations based on the assumption of no water movement are thousands of pounds in error as shown in Fig. D-2. This is a good example of a field for which it is imperative to take water movement into account.

Application of both the radial model and the resistance function to Field D resulted in good agreement between observed and calculated pressures for its entire history (Figs. D-3 and D-5). Volume ratios calculated from the predicted pressures are shown in Figs. D-4 and D-6 for the two methods, respectively. Note that the percentage error is necessarily the same for a volume ratio prediction as for corresponding pressure prediction.

The straight line exhibited by the latter portion of the resistance curve (Fig. D-7) indicates that the aquifer's outer boundary is influencing the field's pressure behavior, i.e., that the aquifer is finite. However, due to the limited data, the extent of the aquifer cannot be accurately determined since a nearly identical prediction was obtained using the infinite radial model. Although the effect of the aquifer boundary is small now, its importance will progressively increase with time.

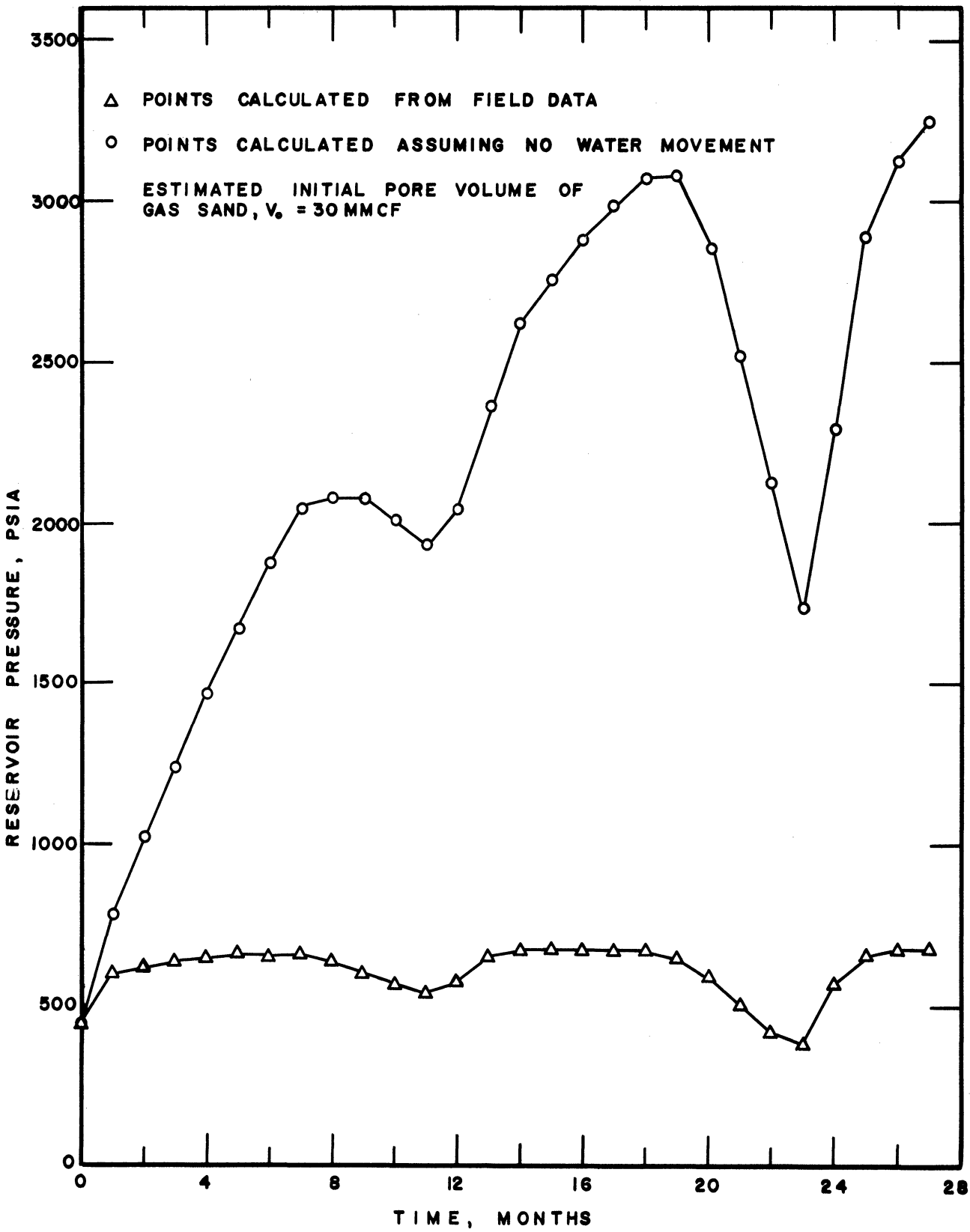

Fig. D-2. Comparison of Field D predicted pressures, assuming no water movement with observed pressures.

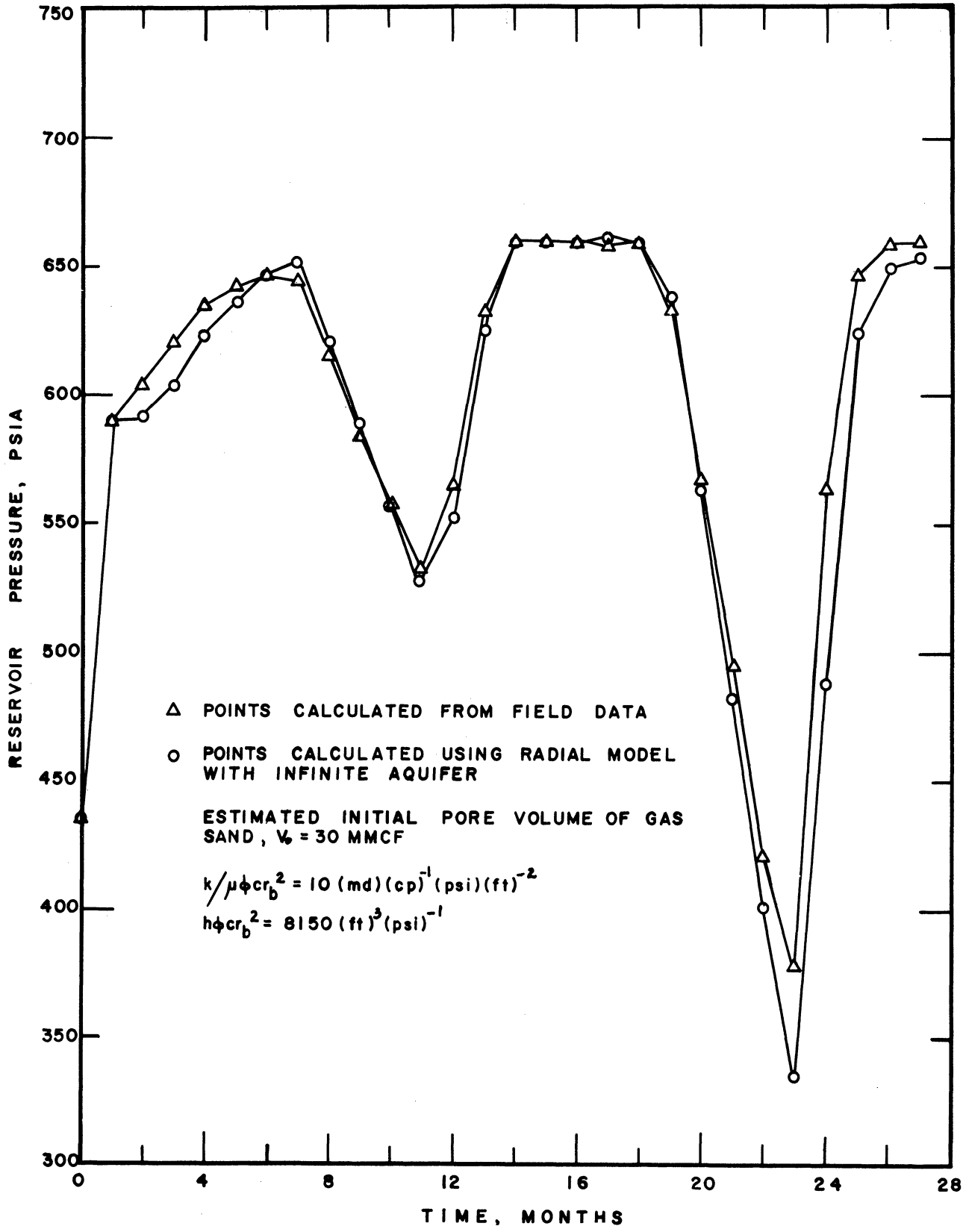

Fig. D-3. Comparison of Field D pressures predicted using radial model (infinite aquifer) with observed pressures.

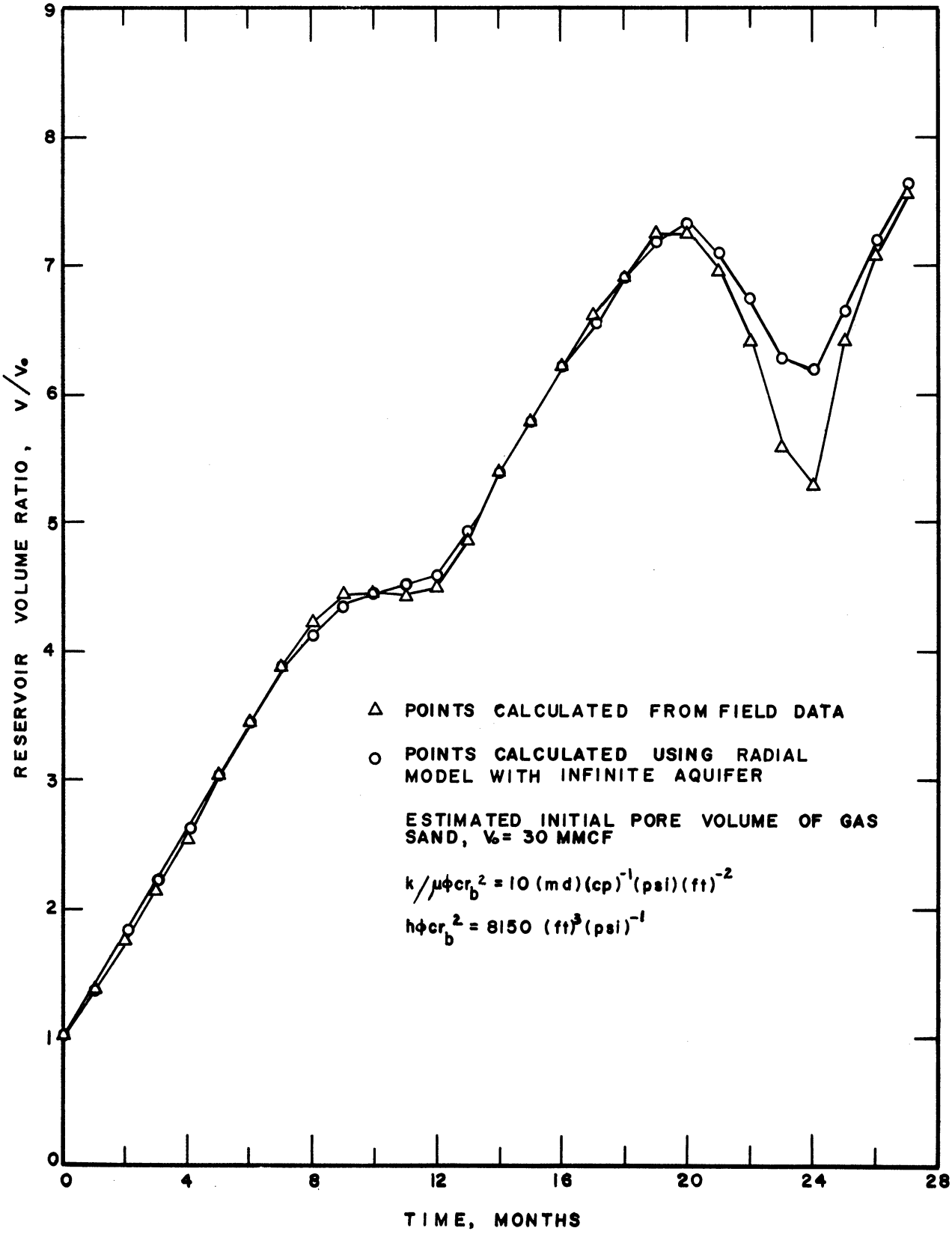

Fig. D-4. Comparison of Field D volume ratios predicted using infinite radial model with volume ratios calculated from field data.

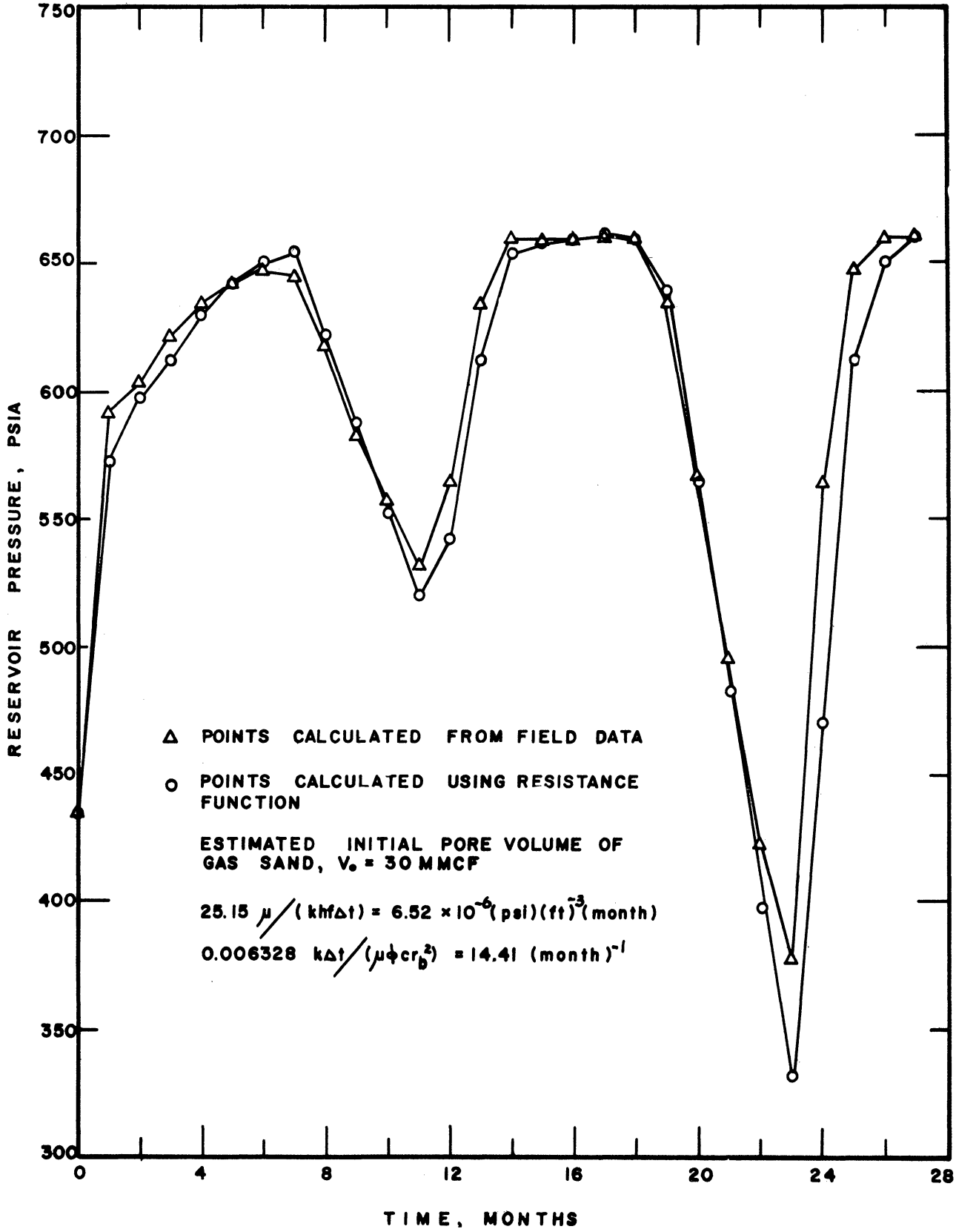

Fig. D-5. Comparison of Field D pressures predicted using resistance function with observed pressures.

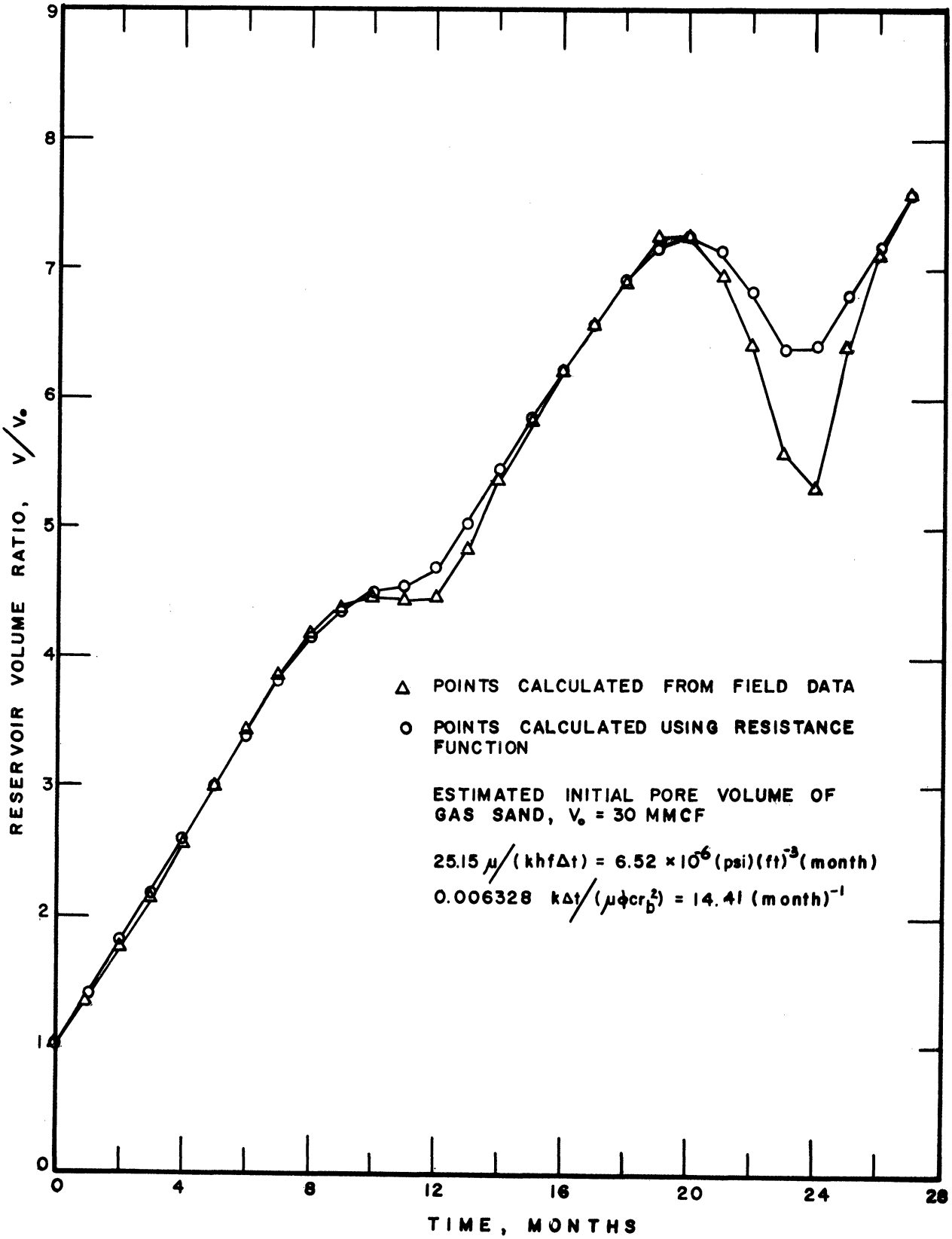

Fig. D-6. Comparison of Field D volume ratios predicted using resistance function with volume ratios calculated from field data.

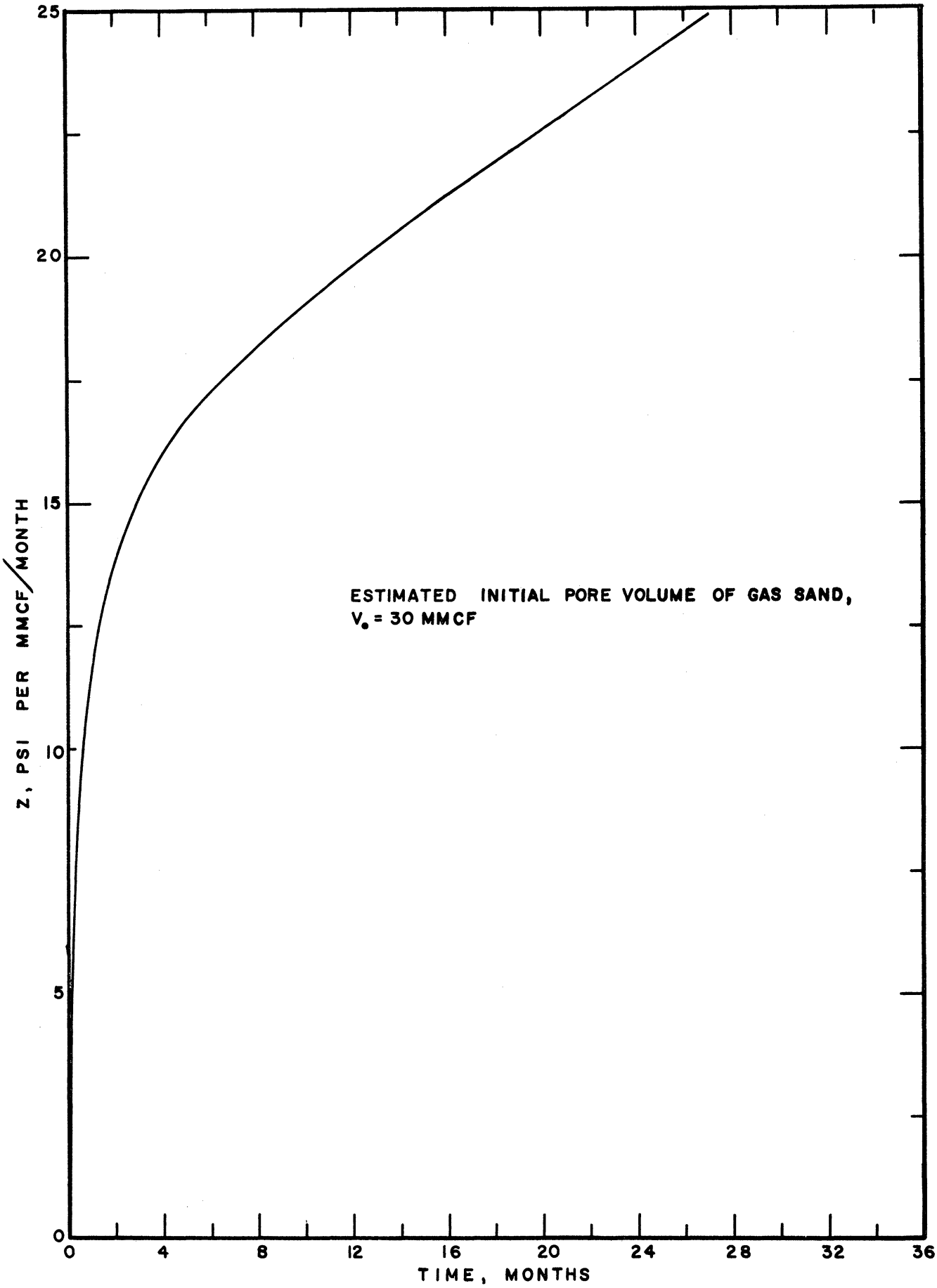

Fig. D-7. Resistance function vs. time for Field D.

FIELD E

Field E was discovered in Michigan in 1941 and produced for six years before being converted to gas-storage operation in 1947. During this period, 8,026,657 MCF of gas were produced accompanied by a pressure decline of 435 psia to 267 psia (wellhead). Recovery of pressure over short periods of high production indicated the gas-water interface was mobile. This field is one of the several gas storage fields which supplies gas to Michigan consumers during periods of high gas demand. Gas is replaced during the summer months, thereby enabling the gas pipeline to operate during periods of low demand.

1. GEOLOGY

Field E is one of several Michigan gas reservoirs found in the Michigan stray sand. This sand is a series of disconnected lenses located at random rather than a continuous layer of sandstone. For this reason, the formation has been designated as stray sand. The sand was deposited during the geologic time known as the "Michigan" and is an integral part of the Michigan formation.

The Michigan stray sand is an ancient sand bar deposited in a shallow sea at the beginning of the Michigan time. During this period, the level of the lake changed frequently and some folding of the rocks caused formation of long, narrow, irregular, gentle arches with wide troughs forming shoals in the shallow sea. Erosion of a land mass located nearby, along with waves and currents, resulted in the deposition of sand lenses, along with mud and ooze, which became discontinuous shale streaks. The ridges located near the surface caught the sand as it rolled along the sea floor forming the sand bars which later became structural domes of which Field E is one.

The sea floor was sinking with respect to the land mass during this period so that eventually sand was no longer deposited from the nearby shore, and a thick layer of mud and ooze from farther inland was deposited on the sand bar. Water was later squeezed out by the weight of overlying beds compacting the mud and calcareous ooze into impermeable layers of shale and limestone, while compacting the sand bar into a sandstone. The layers of shale and limestone are several hundred feet thick and form a good cap rock for the sandstone bar.

Underlying the stray sand is the Marshall formation, a porous and permeable sandstone like the stray. Although several shale lenses are found between the stray and Marshall formations, no consistent thickness of sealing shale is found between the two structures. In many places water in the Marshall is free to migrate into the stray if the pressure within the stray is reduced.

The invasion of the Marshall water into the stray helps maintain the pressure in the stray. Providing that the movement of this water is controlled and is not allowed to come into a production well, thereby waterlogging the well, the water is beneficial.

2. FIELD DATA

A summary of reservoir and fluid properties is given in Table E-1 and the production-pressure history is tabulated in Table E-2. A sketch showing the boundary of storage field is shown in Fig. E-1.

3. RESULTS

Predicted pressures assuming no water movement are compared with the observed field pressure history in Fig. E-2. The deviation between these two curves is considerable during the first ten years' operation but decreases after gas storage begins. This improvement may be attributed in part to the cycling of the pressures about the discovery pressure.

It must be realized that the degree of apparent water movement is related to the assumed initial gas-in-place. The pressure behavior of a large reservoir with no water movement is similar to that of a smaller reservoir with water drive. Figure E-3 shows that with a suitable choice of V_o for Field E the pressures calculated, assuming no water movement, compare reasonably well with the observed pressure history.

Pressures predicted using the thick sand model with an infinite aquifer are in good agreement with the observed pressures during the production period as shown in Fig. E-4. This agreement was not maintained during the storage cycles where the predicted pressures are higher than the observed.

The results from the radial model with an infinite aquifer (Fig. E-5) are nearly identical with those from the thick sand model. The high prediction during the latter portion of the field historyindicate that the aquifer may be finite rather than of infinite extent. Therefore the finite radial model with several values of R, the ratio of the aquifer radius to the gas bubble radius was tried. Good agreement for the entire history was obtained for R = 9. This is shown in Fig. E-6.

The variation with time of the reservoir volume ratio, V/V_o (the present gas bubble volume divided by the initial gas volume), calculated from field data and also the radial model (R = 9), is shown in Fig. E-7.

The prediction of Field E by the resistance function method also gave close agreement between predicted and observed pressures (Fig. E-8) and

TABLE E-1

STORAGE FIELD E DATA

Aquifer Characteristics

Type of formation	Marshall sandstone
Porosity	20%
Permeability	200 millidarcys
Thickness	100 ft
Depth to top of aquifer	1120 ft
Viscosity of liquid in aquifer	1 centipoise
Compressibility of brine and formation	7×10^{-6} vol/vol-psi

Data on Storage Field

a. Field geometry

Location	Michigan
Type of formation	Michigan stray sandstone
Nature of structure	Structural dome

b. Gas-sand formation and fluid properties

Gas compressibility correlation, $z = a + bP$	
Constant a	0.998
Constant b	-0.00016 psi^{-1}
Reservoir temperature	530°R
Reservoir thickness	20 ft
Base conditions for gas measurements	P_b = 15.025 psia
	T_b = 520°R

c History of gas reservoir

Discovery date	1941
Initial discovery pressure	453 psia (wellhead)
Initial pore volume	$(440 \text{ to } 470) \times 10^6$ cu ft
Date converted to gas storage	1947

TABLE E-2

GAS INVENTORY AND PRESSURE HISTORY FOR FIELD E

Pressure Base = 15.025 psia
Temperature Base = 520°R

Date	Cumulative Gas Production, MMSCF	P, Wellhead, psia, at End of Month
Initial		453
1941 Sept	152	
Oct	305	
Nov	505	
Dec	784	
1942 Jan	1044	434
Feb	1281	425
Mar	1581	417
Apr	1708	412
May	1814	409
June	2001	406
July	2200	404
Aug	2402	-
Sept	2680	-
Oct	2964	-
Nov	3238	376
Dec	3388	374
1943 Jan	3542	-
Feb	3671	364
Mar	3805	364
Apr	3976	351
May	4188	-
June	4373	343
July	4511	340
Aug	4653	333
Sept	4803	330
Oct	4991	328
Nov	5172	326
Dec	5306	323
1944 Jan	5417	319
Feb	5534	313
Mar	5663	304
Apr	5732	308
May	5842	309
June	5950	305
July	6023	295
Aug	6032	300
Sept	6047	303
Oct	6077	305
Nov	6115	298
Dec	6138	-
1945 Jan	6139	295
Feb	6140	-
Mar	6141	-
Apr	6142	-
May	6142	-
June	6142	-
July	6142	-
Aug	6142	309
Sept	6180	315
Oct	6349	-
Nov	6510	294
Dec	6679	-
1946 Jan	6850	287
Feb	7001	-
Mar	7149	-
Apr	7291	274
May	7438	270
June	7573	268
July	7690	263
Aug	7822	262
Sept	7927	254
Oct	8007	254
Nov	8011	256
Dec	8014	258
1947 Jan	8016	255
Feb	8018	252
Mar	8020	251
Apr	8022	251
May	8023	258
June	8024	260
July	8025	264
Aug	8026	267
Sept	8006	266
Oct	7937	268
Nov	7899	267
Dec	7883	267
1948 Jan	7873	270
Feb	7830	269
Mar	7767	273
Apr	7497	288
May	7420	291
June	7317	294
July	7101	302
Aug	6921	308
Sept	6838	311
Oct	6785	312
Nov	6757	313
Dec	6755	314
1949 Jan	6800	312
Feb	6901	308
Mar	6941	307
Apr	6968	306
May	6953	307
June	6931	309
July	6900	310
Aug	6863	312
Sept	6836	313
Oct	6878	311
Nov	6954	307
Dec	7035	304
1950 Jan	7117	302
Feb	7189	298
Mar	7273	295
Apr	7353	293
May	7219	299
June	7041	307
July	6933	311
Aug	6898	316
Sept	4774	375
Oct	2336	451
Nov	2143	462
Dec	2352	449
1951 Jan	4539	382
Feb	5349	353
Mar	5565	364
Apr	4328	384
May	2587	439
June	- 360	519
July	-1817	558
Aug	-3883	614
Sept	-5072	637
Oct	-5689	649
Nov	-3975	599
Dec	-2917	565
1952 Jan	- 671	507
Feb	345	478
Mar	501	468
Apr	- 17	485
May	-1994	540
June	-4172	597
July	-6595	657
Aug	-7470	676
Sept	-7839	682
Oct	-7199	659
Nov	-6361	636
Dec	-5096	602
1953 Jan	-2586	536
Feb	- 770	488
Mar	356	452
Apr	450	455
May	- 129	469
June	- 347	480
July	-2974	548
Aug	-5286	609
Sept	-6247	631
Oct	-6857	638
Nov	-6018	620
Dec	-4001	564
1954 Jan	-1174	491
Feb	362	448
Mar	1237	422
Apr	937	422
May	- 236	465
June	-1725	509
July	-3170	546
Aug	-5015	592
Sept	-6079	618
Oct	-6007	615
Nov	-4428	573
Dec	- 929	482
1955 Jan	1633	411
Feb	3347	357
Mar	4290	348
Apr	4363	322
May	4403	344
June	1237	425
July	-2199	512
Aug	-4927	580
Sept	-5523	596
Oct	-5520	605
Nov	-2686	535
Dec	748	446
1956 Jan	2915	390
Feb	5160	328
Mar	6196	290
Apr	6087	292
May	5738	291
June	4470	
July	2697	395
Aug	581	449
Sept	-1096	517
Oct	-1222	508
Nov	-1918	513
Dec	- 499	482
1957 Jan	2495	407
Feb	3774	372
Mar	3258	337
Apr	2243	404
May	778	442
June	-1085	491
July	-4039	562
Aug	-7200	638
Sept	-7255	649
Oct	-6987	631
Nov	-6050	610
Dec	-3844	557
1958 Jan	-1587	487
Feb	274	435
Mar	1975	390
Apr	1575	406
May	-1473	501
June	-4395	581
July	-5208	596
Aug	-5966	599
Sept	-6335	615
Oct	-6228	608
Nov	-5634	589
Dec	-1543	483
1959 Jan	1836	389
Feb	4136	316
Mar	4643	292
Apr	3359	361
May	1136	423
June	-1019	485
July	-2896	562
Aug	-6096	613
Sept	-7040	632
Oct	-7001	618
Nov	-4014	547
Dec	- 964	464
1960 Jan	1120	400
Feb	2830	356
Mar	4178	313
Apr	4655	295
May	1993	388
June	377	447
July	-1659	499
Aug	-3071	539
Sept	-6197	619
Oct	-6850	625
Nov	-5512	565
Dec	-2547	470

volume ratios (Fig. E-9). It should be noted that the best results were obtained with V_o = 470 MMCF rather than 440 MMCF used in the above model studies.

The initial portion of the resistance curve was generated by the infinite radial model using field data from the first five years. The remainder of the curve was produced directly from the observed field data without the use of any model. However, the curve was concave upward in this portion violating one of the conditions of the resistance function. Thus a smoothed Z-curve was drawn as a straight line passing through the final point of the unsmoothed curve and tangent to it at a previous time step as shown in Fig. E-10, satisfying all restrictions imposed by the method.

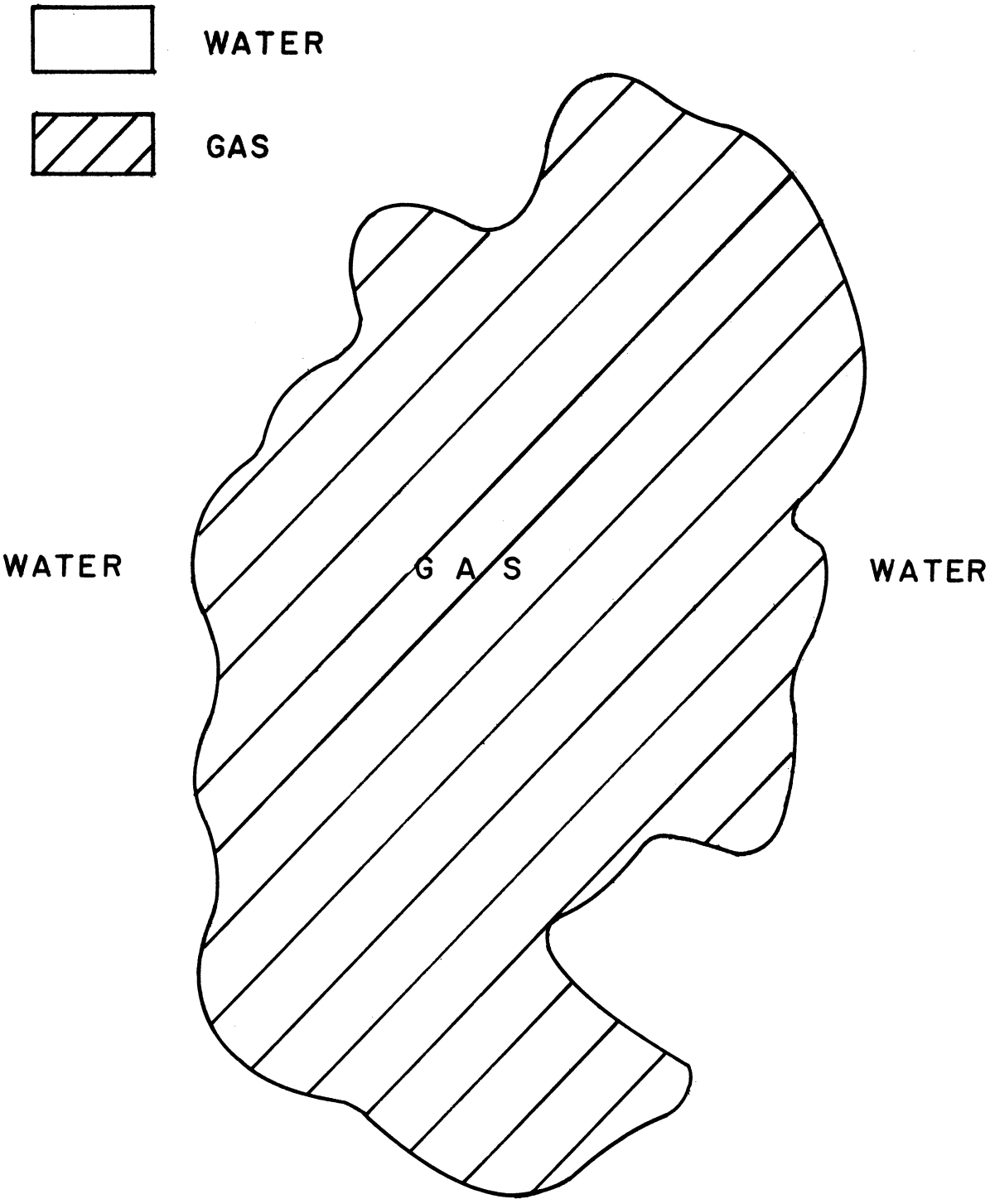

Fig. E-1. Areal sketch showing boundary of gas Field E.

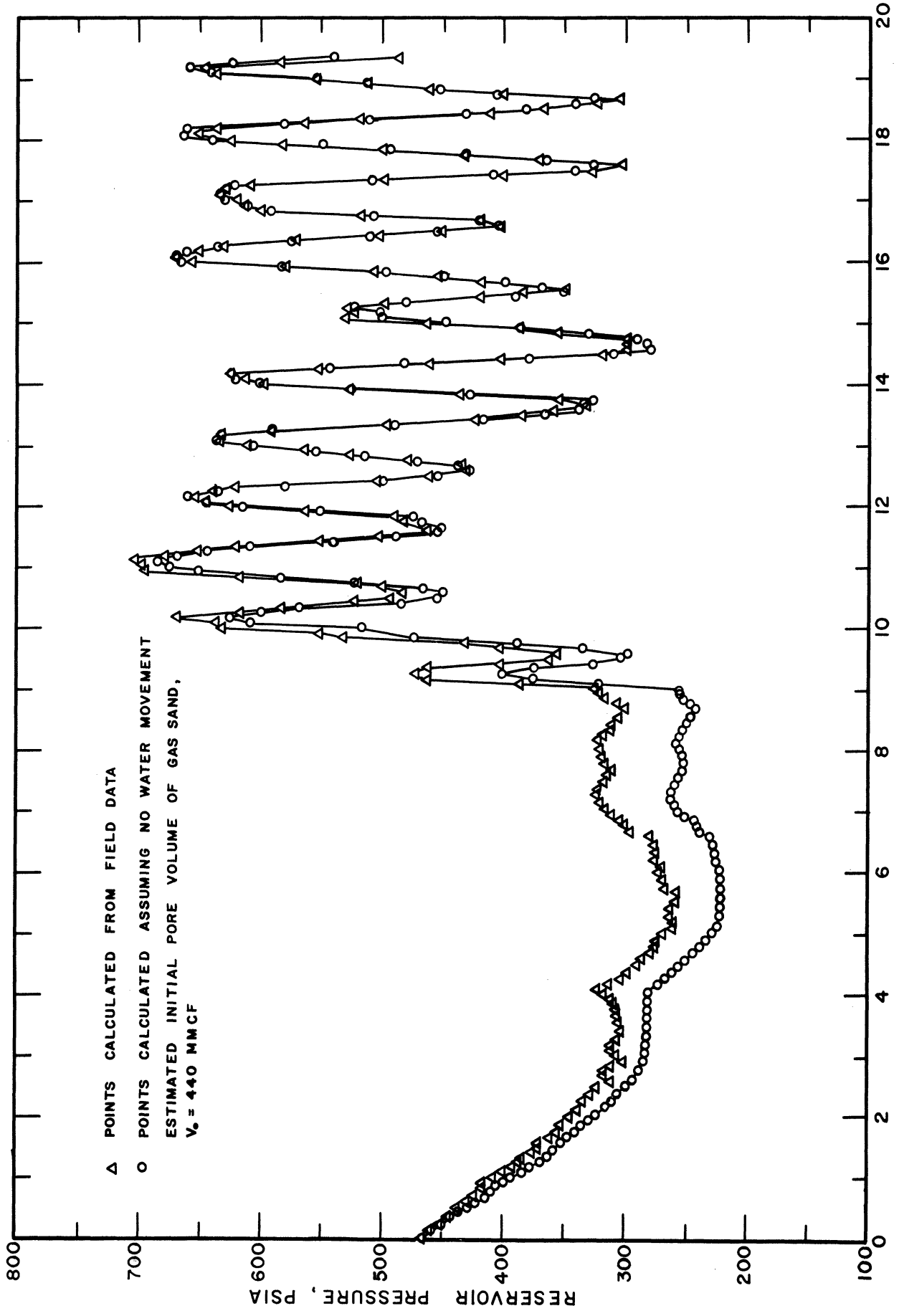

Fig. E-2. Comparison of Field E predicted pressures assuming no water movement with observed pressures for an initial pore volume of 440 million cubic feet.

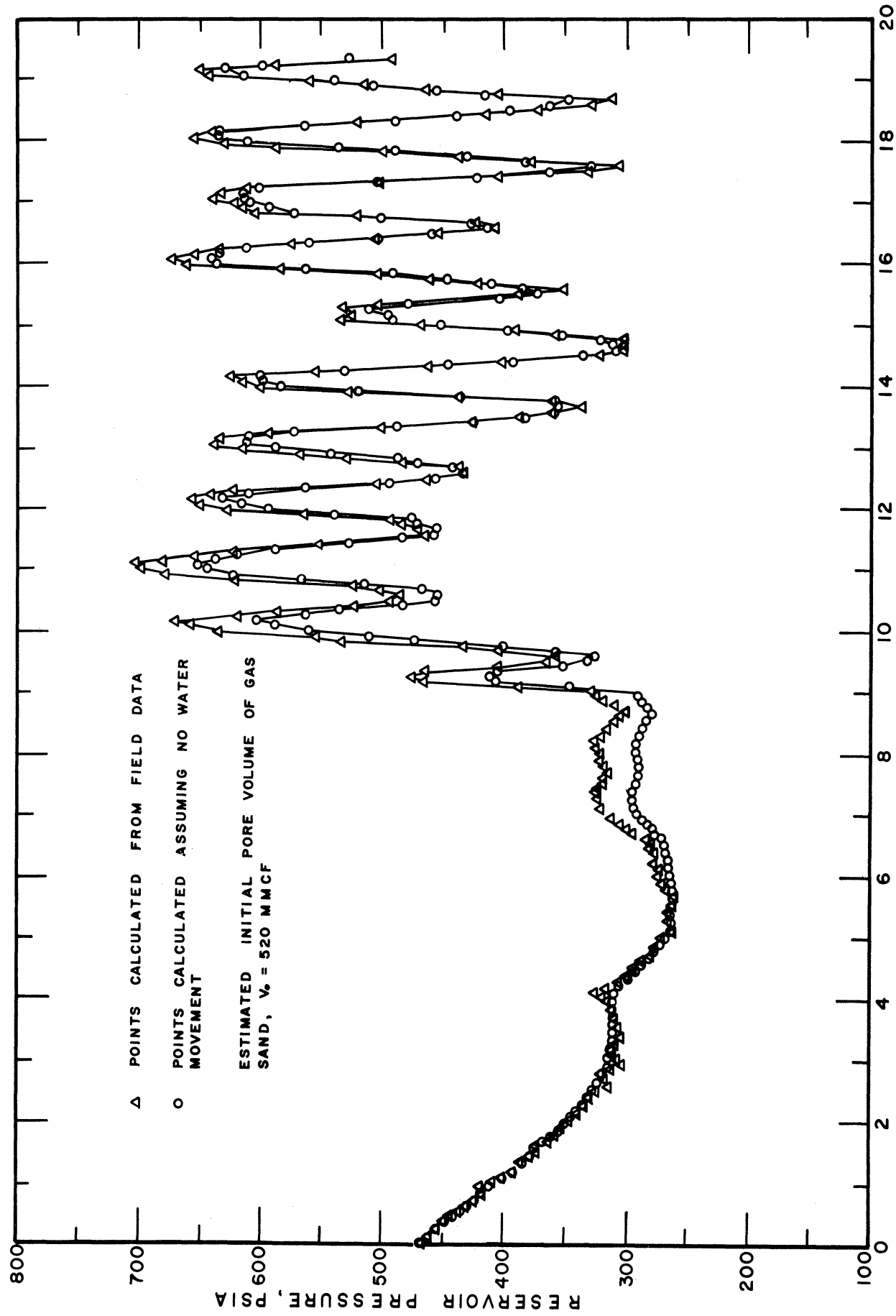

Fig. E-3. Comparison of Field E predicted pressures assuming no water movement with observed pressures for an initial pore volume of 520 million cubic feet.

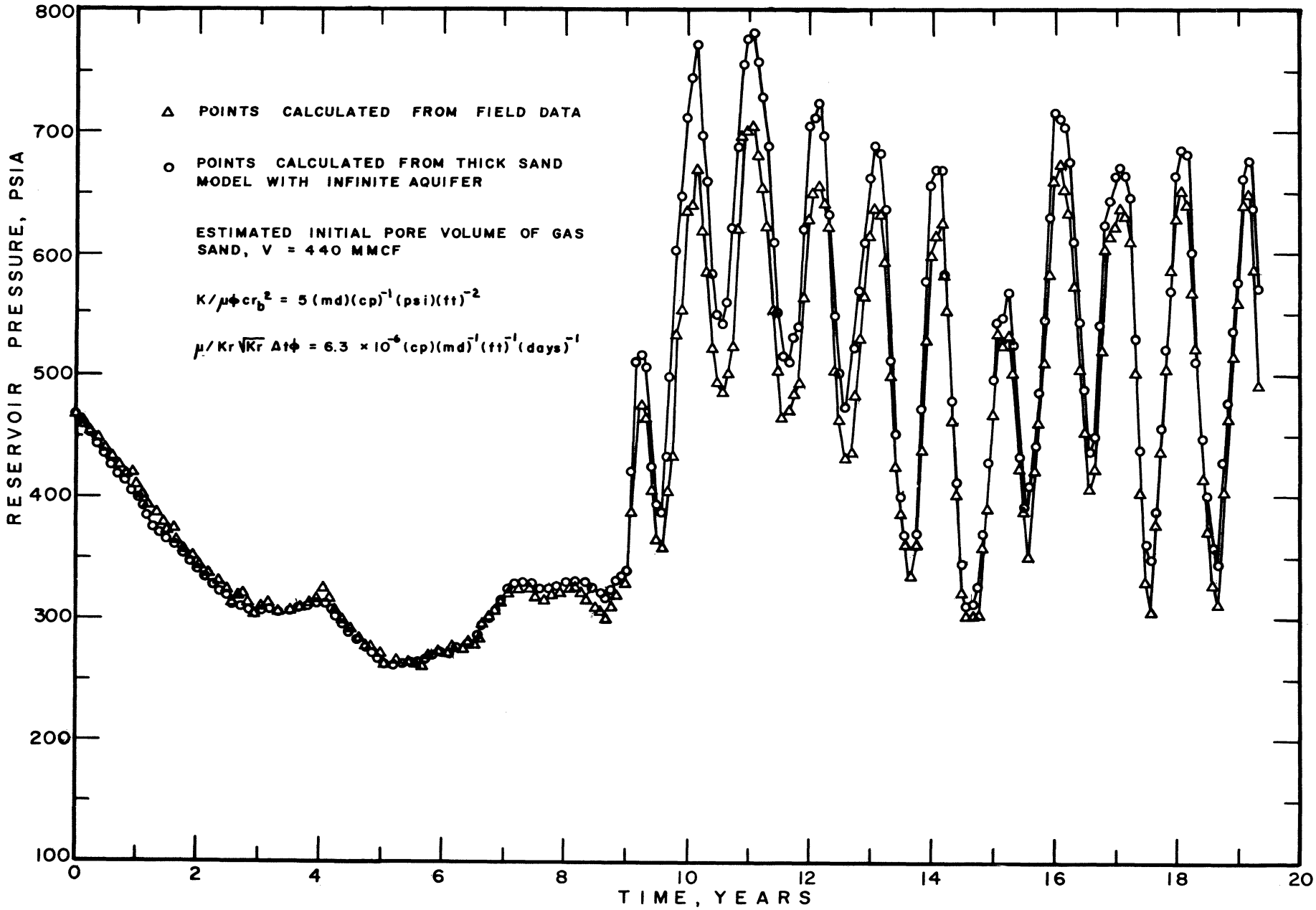

Fig. E-4. Comparison of Field E pressures predicted using thick sand model (infinite aquifer) with observed pressures.

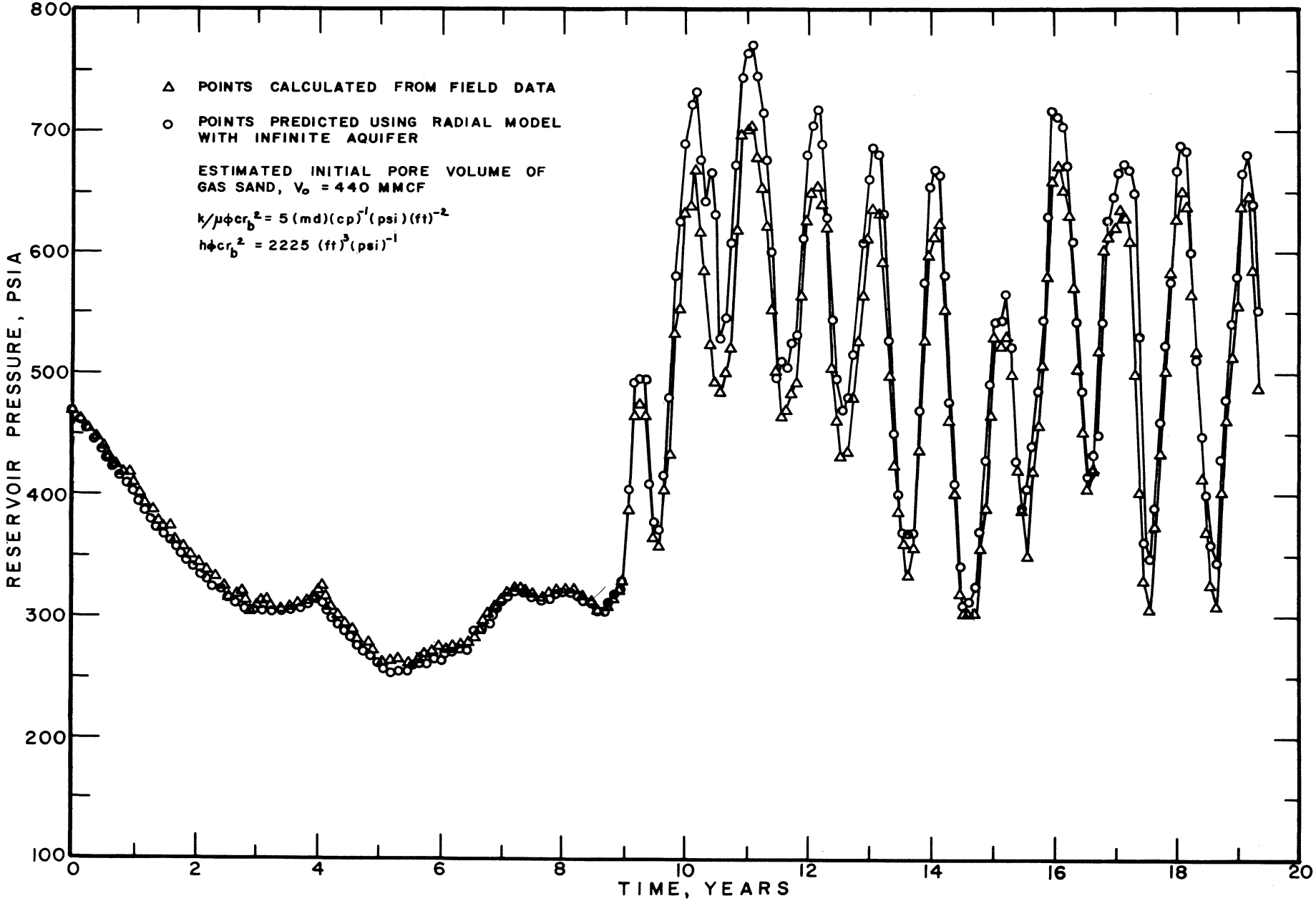

Fig. E-5. Comparison of Field E pressures predicted using radial model (infinite aquifer) with observed pressures.

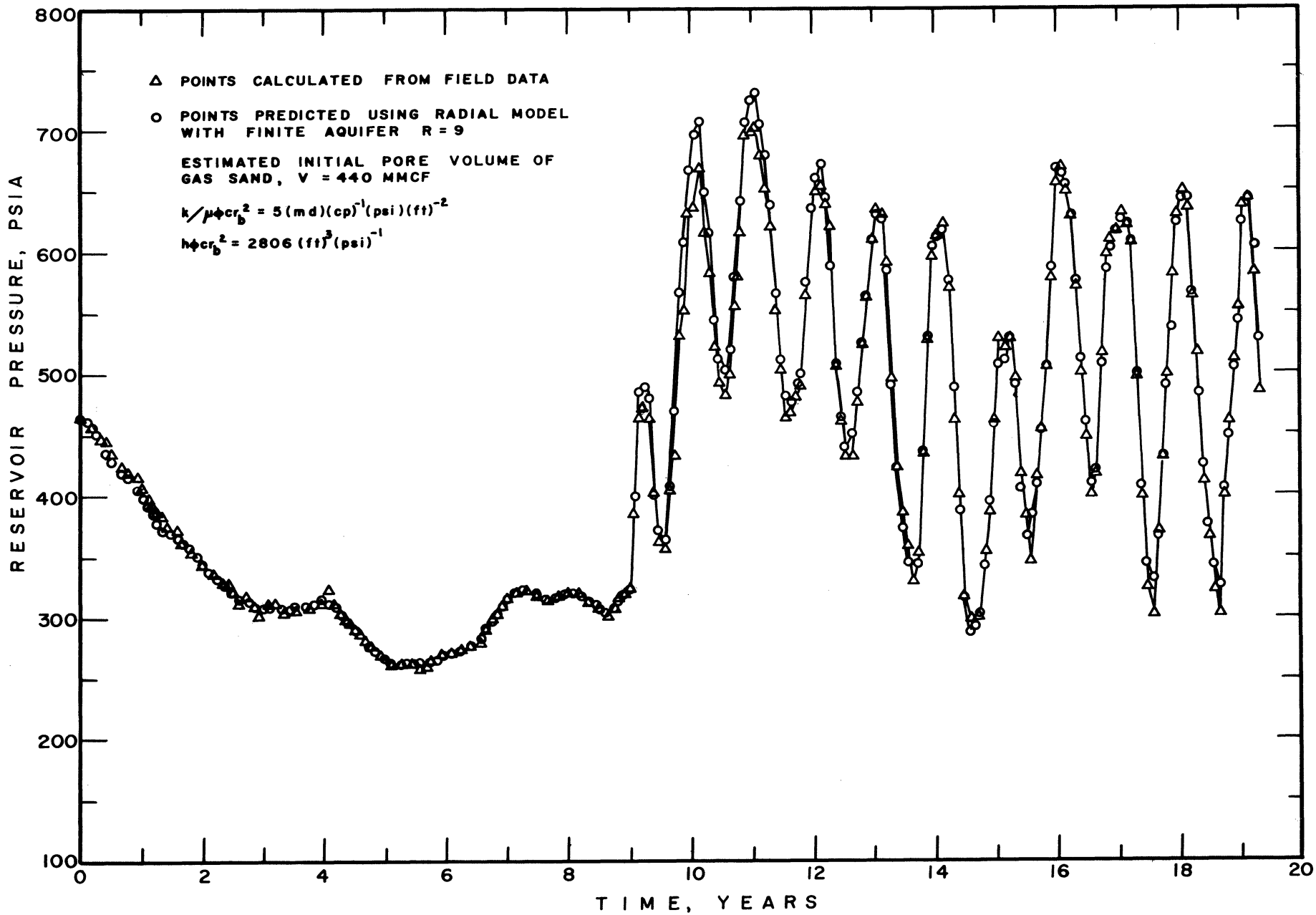

Fig. E-6. Comparison of Field E pressures predicted using finite radial model (R=9) with observed pressures.

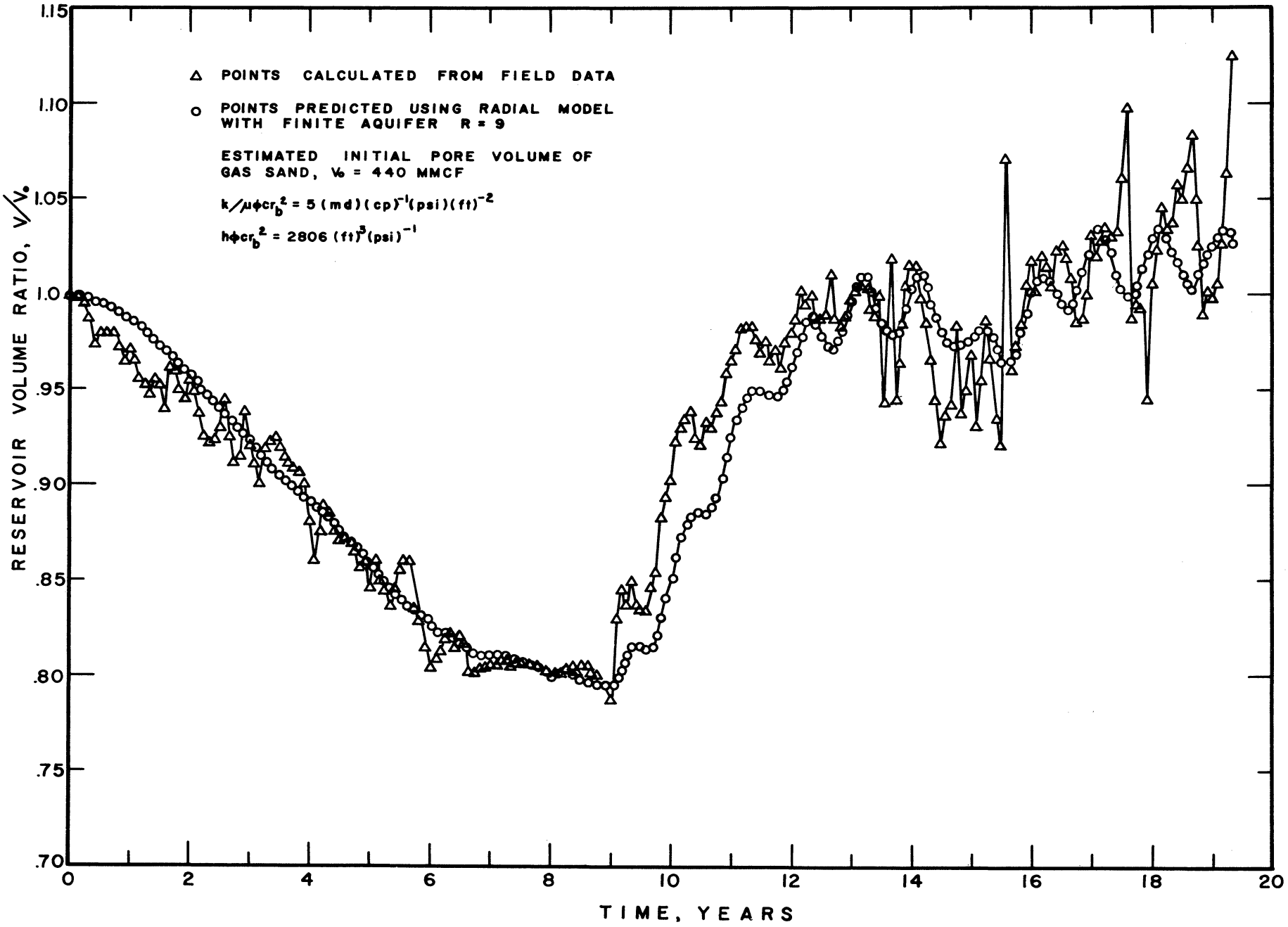

Fig. E-7. Comparison of Field E volume ratio predicted using finite radial model (R=9) with volume ratios calculated from field data.

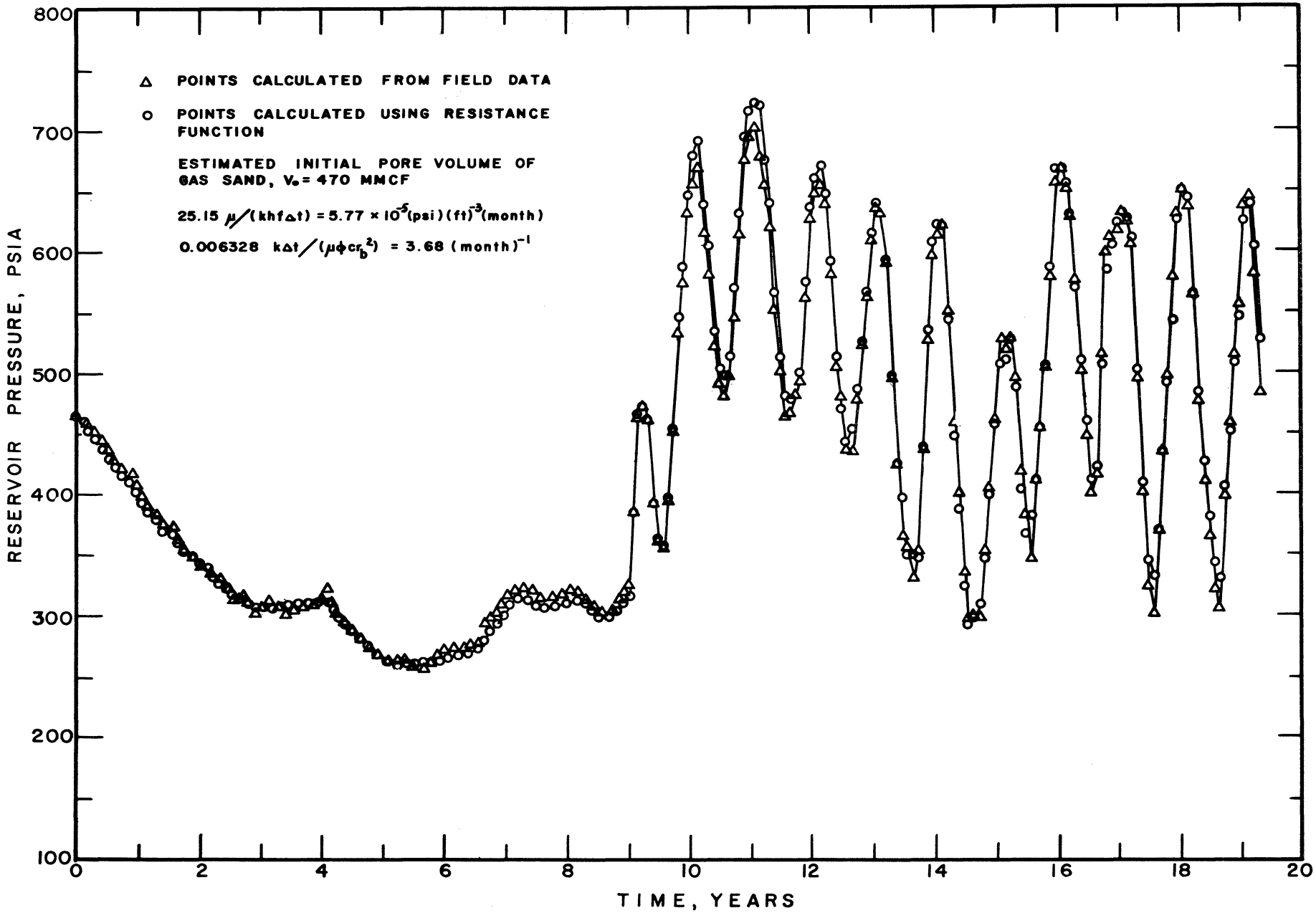

Fig. E-8. Comparison of Field E pressures predicted using resistance function with observed pressures.

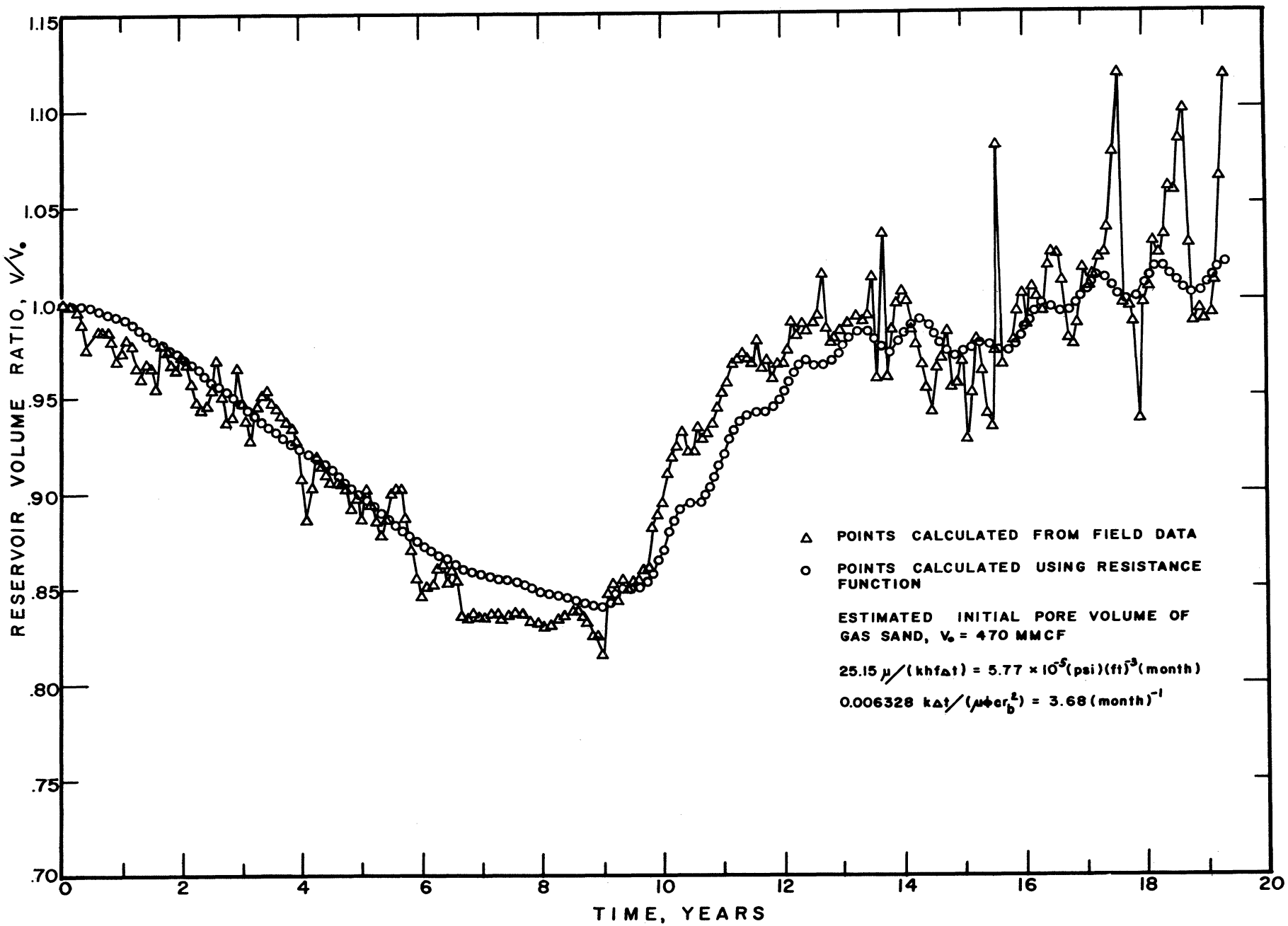

Fig. E-9. Comparison of Field E volume ratio predicted using resistance function with volume ratios calculated from field data.

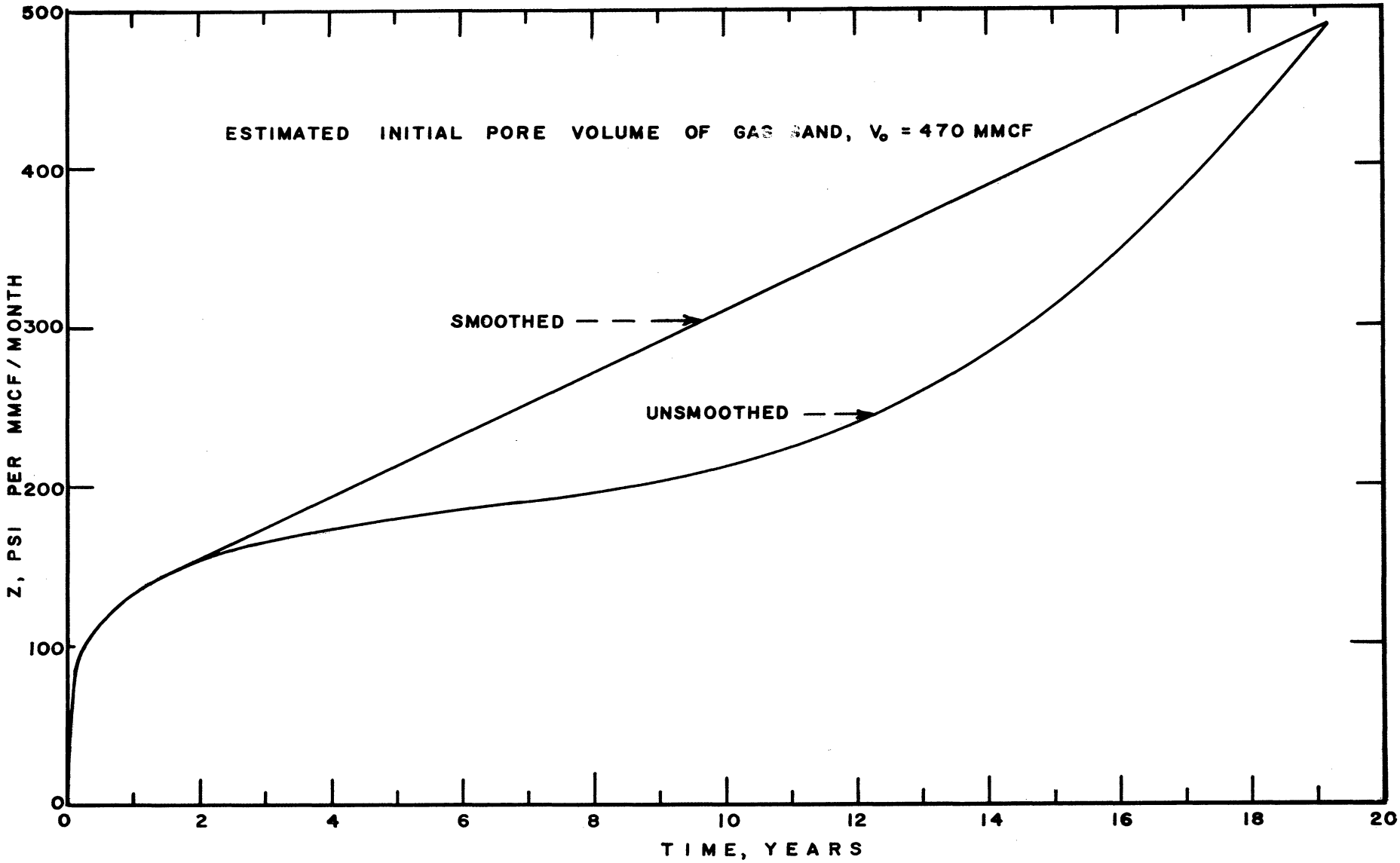

Fig. E-10. Resistance function vs. time for Field E.

FIELD F

Field F, another Michigan storage reservoir discovered in 1933, produced 6.3 billion standard until 1941 when the field was converted to gas storage. During this period, the wellhead pressure dropped from 534 to 301 psia.

1. GEOLOGY

Field F is one of the several Michigan gas reservoirs located in the Michigan Stray Formation. The geology of this formation is dicussed in the geology section of Field E. An areal sketch of this field is given in Fig. F-1.

2. FIELD DATA

Pertinent aquifer and reservoir properties of Field F are listed in Table F-1 and the production-pressure history is tabulated in Table F-2.

3. RESULTS

The shape of this reservoir, as shown in Fig. F-1, indicates the use of either the radial or thick sand model.

Since the lateral extent of the reservoir is large compared to the aquifer thickness, as Table F-1 indicates, the radial model was selected for analyzing the performance of this field.

The pressure variation with time for Field F calculated assuming no water movement is illustrated in Fig. F-2.

Figure F-3 shows the pressure prediction utilizing the infinite radial model. Good agreement is obtained for the first fifteen-year pressure history, but the high prediction for the remainder indicates that the aquifer is finite and that the effect of the outer boundary is being felt.

Therefore, several different values of R, the ratio of the outer to the inner radius of the aquifer, were investigated. The best prediction was obtained with R = 10. This is shown in Fig. F-4. The corresponding volume ratios calculated from these pressures are presented in Fig. F-5. It may be noted that some of the wild fluctuations in the volume ratios calculated from field data are probably due to errors in these data.

TABLE F-1

STORAGE FIELD F DATA

Aquifer Characteristics

Type of formation	Marshall sandstone
Porosity	17%
Permeability	200 millidarcys
Thickness	175 ft
Depth to top of aquifer	1383 ft
Viscosity of liquid in aquifer	1 centipoise
Compressibility of brine and formation	7×10^{-6} vol/vol-psi

Data on Storage Field

a. Field geometry

Location	Michigan
Type of formation	Michigan stray sandstone
Nature of structure	Structural dome

b. Gas-sand formation and fluid properties

Gas compressibility correlation, $z = a + bP$	
Constant a	0.997
Constant b	-1.60×10^{-4}
Reservoir temperature	523.5°R
Reservoir thickness	12.5 ft
Base conditions for gas measurements	P_b = 14.735 psia
	T_b = 520°R

c. History of gas reservoir

Discovery date	1933
Initial discovery pressure	534.4 psia (wellhead)
Initial pore volume	$(270 \text{ to } 290) \times 10^6$ cu ft
Date converted to gas storage	1941

TABLE F-2

GAS INVENTORY AND PRESSURE HISTORY FOR FIELD F

Pressure Base = 14.735 psia
Temperature Base = 520°R

Date	Cumulative Gas Production, MMSCF	P, Wellhead, psia, at End of Month
Initial		534.4
1933 Feb	104.929	-
Mar	209.858	-
Apr	314.785	-
May	315.550	-
June	316.315	-
July	317.080	-
Aug	317.844	-
Sept	318.609	-
Oct	319.374	-
Nov	320.139	-
Dec	320.903	-
1934 Jan	322.127	-
Feb	337.626	-
Mar	354.145	-
Apr	370.664	-
May	387.183	-
June	403.701	-
July	420.220	-
Aug	436.739	-
Sept	453.258	-
Oct	469.777	-
Nov	494.453	-
Dec	510.972	-
1935 Jan	615.424	504.4
Feb	715.767	-
Mar	797.450	-
Apr	866.470	-
May	918.187	-
June	951.410	-
July	978.300	-
Aug	1005.908	492.4
Sept	1045.904	-
Oct	1104.493	-
Nov	1188.949	-
Dec	1322.952	-
1936 Jan	1483.052	-
Feb	1650.409	-
Mar	1781.119	-
Apr	1890.450	-
May	1954.170	454.4
June	2007.105	-
July	2052.912	-
Aug	2111.521	-
Sept	2171.565	-
Oct	2271.022	442.4
Nov	2406.754	-
Dec	2551.897	-
1937 Jan	2714.541	-
Feb	2862.128	421.4
Mar	3005.467	414.4
Apr	2117.671	-
May	3196.288	406.4
June	3256.293	-
July	3305.921	-
Aug	3356.825	406.4
Sept	3423.842	-
Oct	3528.041	-
Nov	3657.543	-
Dec	3827.245	-
1938 Jan	4004.603	-
Feb	4155.721	367.4
Mar	4289.708	-
Apr	4391.712	-
May	4466.455	367.4
June	4518.079	-
July	4558.851	-
Aug	4600.734	-
Sept	4662.932	-
Oct	4728.946	-
Nov	4824.940	-
Dec	4945.975	-
1939 Jan	5077.915	-
Feb	5202.412	-
Mar	5327.239	-
Apr	5424.021	-
May	5475.182	-
June	5509.761	324.4
July	5537.029	322.4
Aug	5568.150	-
Sept	5607.510	-
Oct	5660.082	321.4
Nov	5718.031	-
Dec	5782.258	315.4
1940 Jan	5867.984	313.4
Feb	5939.891	308.4
Mar	6013.479	307.4
Apr	6064.457	307.4
May	6098.632	305.4
June	6111.949	302.4
July	6131.614	302.4
Aug	6149.656	-
Sept	6164.948	304.4
Oct	6174.321	303.4
Nov	6196.179	-
Dec	6219.892	302.4
1941 Jan	6262.580	302.4
Feb	6300.297	302.4
Mar	6329.195	301.4
Apr	6308.537	-
May	6261.992	310.7
June	6200.383	319.7
July	6130.776	326.7
Aug	6075.184	333.7
Sept	6292.098	333.7
Oct	5830.934	345.7
Nov	5662.757	356.7
Dec	5427.396	372.7
1942 Jan	5257.793	381.7
Feb	5098.036	390.7
Mar	4913.288	399.7
Apr	4750.371	409.7
May	4660.273	414.7
June	4484.523	422.7
July	4292.783	432.7
Aug	4089.309	441.7
Sept	3828.507	453.7
Oct	3581.775	464.7
Nov	3366.603	473.7
Dec	3330.217	472.7
1943 Jan	3330.343	471.7
Feb	3330.343	470.7
Mar	3330.343	468.7
Apr	3224.534	472.7
May	3040.791	481.7
June	2859.421	487.7
July	2662.789	495.7
Aug	2481.373	501.7
Sept	2324.826	507.7
Oct	2183.701	512.7
Nov	2067.094	518.7
Dec	2043.586	519.7
1944 Jan	2058.547	515.7
Feb	2125.648	511.7
Mar	2168.632	505.7
Apr	2170.573	505.7
May	2042.566	510.7
June	1891.869	516.7
July	1778.604	521.7
Aug	1778.707	516.7
Sept	1784.541	515.7
Oct	1789.301	517.2
Nov	1812.641	510.7
Dec	1951.831	503.7
1945 Jan	2201.755	494.7
Feb	2308.576	488.7
Mar	2215.053	496.7
Apr	2096.284	502.7
May	2103.501	498.7
June	2013.352	511.2
July	1869.960	512.7
Aug	1724.106	520.7
Sept	1607.629	522.7
Oct	1536.188	524.7
Nov	1580.732	520.7
Dec	1884.749	505.7
1946 Jan	2212.740	488.7
Feb	22545.273	474.7
Mar	2548.177	477.7
Apr	2564.924	477.7
May	2492.619	483.7
June	2299.415	496.7
July	2087.799	509.7
Aug	1904.855	517.7
Sept	1766.045	521.7
Oct	1696.954	522.7
Nov	1814.805	512.7
Dec	2173.093	492.7
1947 Jan	2642.459	467.7
Feb	3152.013	453.7
Mar	3535.242	423.7
Apr	3621.498	423.7
May	3533.473	431.7
June	3225.241	453.7
July	2791.329	480.7
Aug	2350.513	502.7
Sept	2009.456	518.7
Oct	1654.184	533.9
Nov	1686.022	530.2
Dec	1838.973	517.5
1948 Jan	2161.579	498.4
Feb	2409.310	486.9
Mar	2608.787	476.1
Apr	3677.556	433.9
May	3413.051	452.3
June	2494.919	493.1
July	2791.329	521.9
Aug	1091.343	546.2
Sept	510.431	566.6
Oct	574.937	558.6
Nov	679.526	551.2
Dec	1909.645	495.2
1949 Jan	2981.478	449.3
Feb	3472.562	434.7
Mar	4015.939	412.5
Apr	3778.954	433.3
May	3536.310	447.0
June	2861.761	479.9
July	1998.312	512.2
Aug	1364.590	530.7
Sept	1572.336	512.8
Oct	1305.202	531.4
Nov	1321.770	518.9
Dec	1925.154	499.9
1950 Jan	1357.585	522.6
Feb	3357.435	415.9
Mar	4503.945	380.1
Apr	4476.422	395.3
May	3041.999	481.4
June	2034.069	518.7
July	- 296.136	605.0
Aug	-1183.771	627.8
Sept	-1503.596	632.4
Oct	-1540.579	628.2
Nov	-1033.297	600.8
Dec	500.739	537.8
1951 Jan	- 632.275	589.2
Feb	- 318.660	575.6
Mar	198.425	554.0
Apr	609.924	544.9
May	497.678	544.8
June	95.930	562.8
July	27.213	565.5
Aug	-2408.755	662.1
Sept	-2727.598	661.6
Oct	-2783.145	656.9
Nov	-2781.608	653.6
Dec	-1655.208	594.8
1952 Jan	-2950.770	652.7
Feb	-1594.951	595.1
Mar	1070.417	489.6
Apr	1978.102	462.5
May	3239.083	407.8
June	3542.360	403.5
July	3542.382	411.7
Aug	2113.384	490.5
Sept	- 70.716	589.7
Oct	-1469.734	623.7
Nov	-1835.956	624.9
Dec	1883.665	621.1
1953 Jan	-1838.443	615.6
Feb	-1824.777	612.9
Mar	- 649.691	553.9
Apr	1262.722	482.4
May	1342.722	493.2
June	- 451.860	587.7
July	452.260	566.8
Aug	-1262.961	600.1
Sept	-2629.077	650.9
Oct	-3361.325	663.9
Nov	-3382.980	660.4
Dec	-2530.894	618.8
1954 Jan	-1043.168	561.3
Feb	- 974.214	567.5
Mar	556.919	496.5
Apr	1432.722	473.4
May	1744.804	466.6
June	1235.518	495.5
July	170.067	544.8
Aug	- 798.647	578.1
Sept	-2257.816	630.4
Oct	-3402.225	664.0
Nov	-3460.456	657.6
Dec	-3297.078	645.6
1955 Jan	-2582.489	609.8
Feb	-2829.238	625.1
Mar	- 13.847	501.4
Apr	-1594.550	586.6
May	432.867	492.8
June	3697.062	337.2
July	4026.329	338.0
Aug	2367.983	464.6
Sept	107.554	554.9
Oct	-2845.212	657.5
Nov	-2540.963	616.5
Dec	-1755.802	584.2
1956 Jan	-2379.787	627.7
Feb	-1592.806	619.6
Mar	2076.743	401.6
Apr	3586.334	344.4
May	1625.561	493.3
June	1369.218	485.6
July	2893.320	411.7
Aug	3525.462	384.9
Sept	1430.628	524.7
Oct	-2423.435	660.9
Nov	-3161.480	659.6
Dec	-3205.054	651.2
1957 Jan	-1846.768	597.0
Feb	-2401.685	608.6
Mar	2041.525	388.7
Apr	2769.028	396.4
May	3239.111	381.0
June	3241.617	389.2
July	3244.106	393.1
Aug	3246.651	396.7
Sept	768.024	533.5
Oct	-3093.726	676.6
Nov	-3244.760	655.0
Dec	-3269.195	646.9
1958 Jan	-3263.054	642.3
Feb	-1974.590	597.4
Mar	-1012.380	554.2
Apr	- 862.323	544.2
May	393.776	496.3
June	1603.653	447.4
July	305.738	530.9
Aug	- 910.586	569.6
Sept	-1655.590	589.9
Oct	-4287.813	688.3
Nov	-3332.657	611.7
Dec	-2214.954	598.9
1959 Jan	-2609.600	617.1
Feb	-3565.431	683.8
Mar	- 23.423	488.8
Apr	1522.745	432.6
May	3067.589	353.9
June	3569.368	347.0
July	3421.890	368.9
Aug	2143.210	449.3
Sept	-1057.390	601.3
Oct	-3891.675	690.5
Nov	-2921.076	618.8
Dec	-1426.579	542.9
1960 Jan	-3939.747	656.8
Feb	-2439.391	568.7
Mar	1004.883	438.2
Apr	882.228	454.1
May	3240.918	341.9
June	3243.159	353.0
July	1195.468	478.5
Aug	- 999.058	578.8
Sept	-3164.583	647.2
Oct	-3672.215	646.2
Nov	-3698.866	638.5
Dec		

The pressure and volume ratio predictions obtained from the resistance function method are presented in Figs. F-6 and F-7, respectively. The shape of the resistance function itself (Fig. F-8) indicates that the aquifer surrounding Field F is of finite extent, confirming the conclusion of the model study.

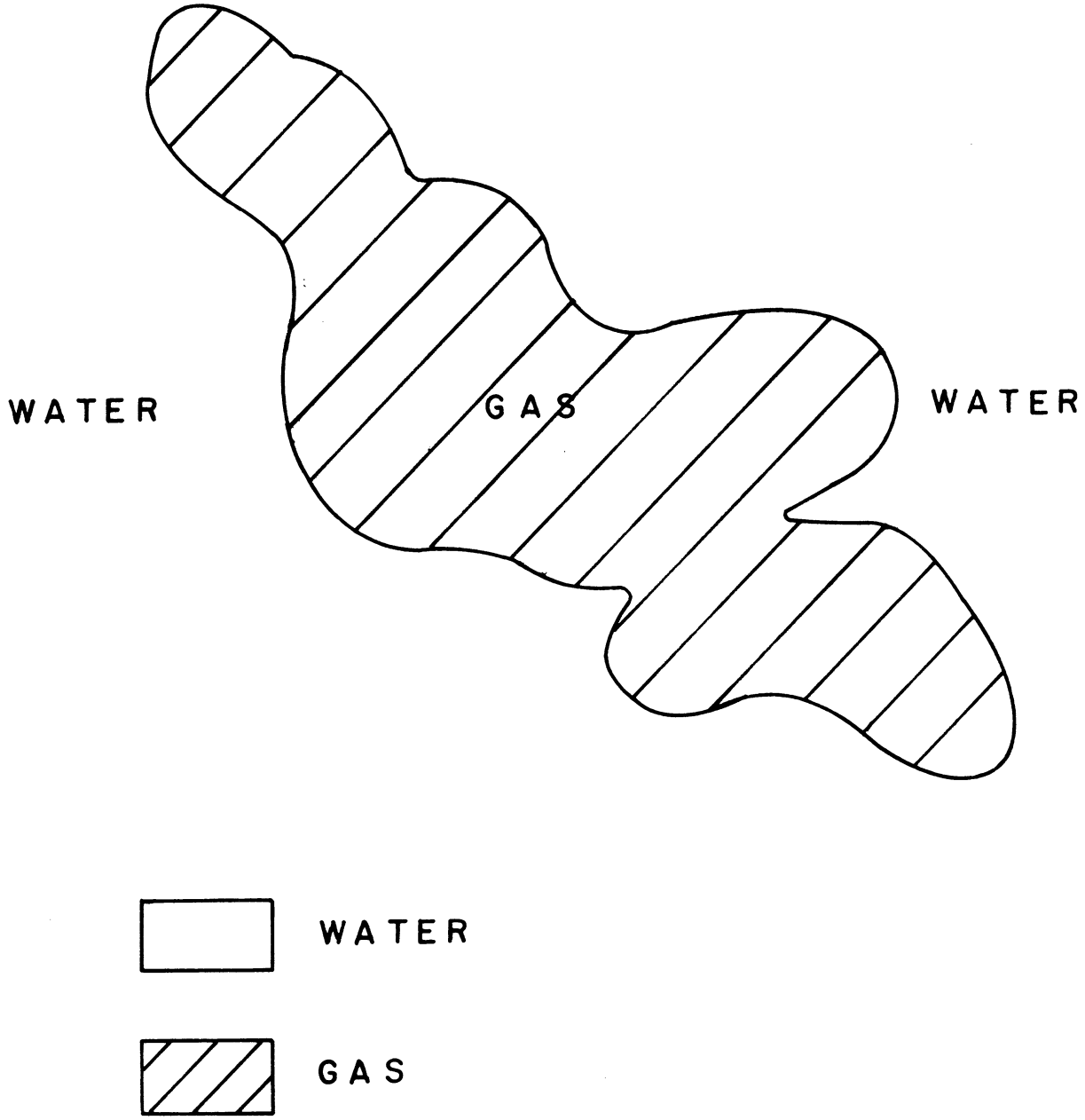

Fig. F-1. Areal sketch showing boundary of Field F.

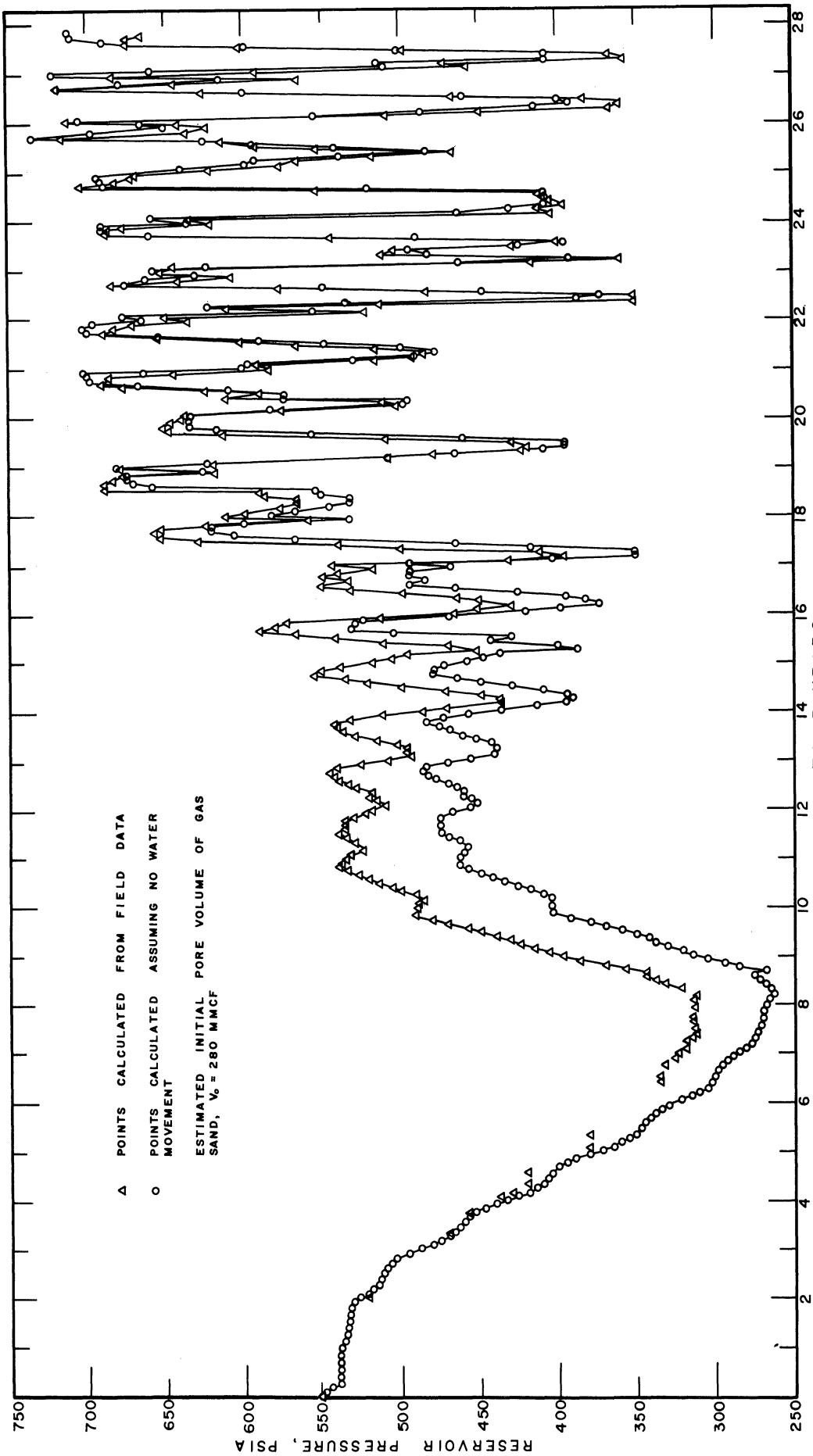

Fig. F-2. Comparison of Field F predicted pressures, assuming no water movement with observed pressures.

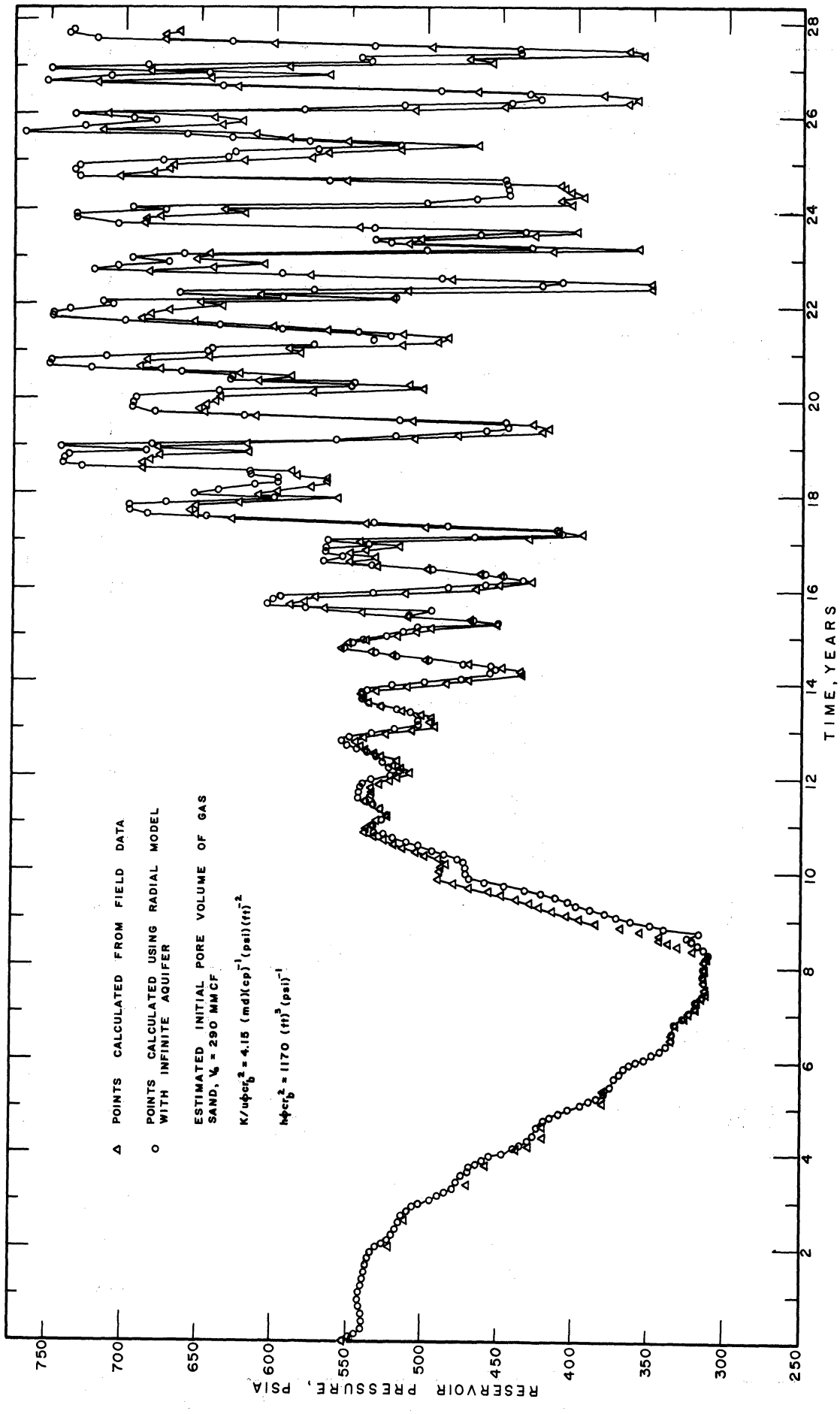

Fig. F-3. Comparison of Field F pressures predicted using radial model (infinite aquifer) with observed pressures.

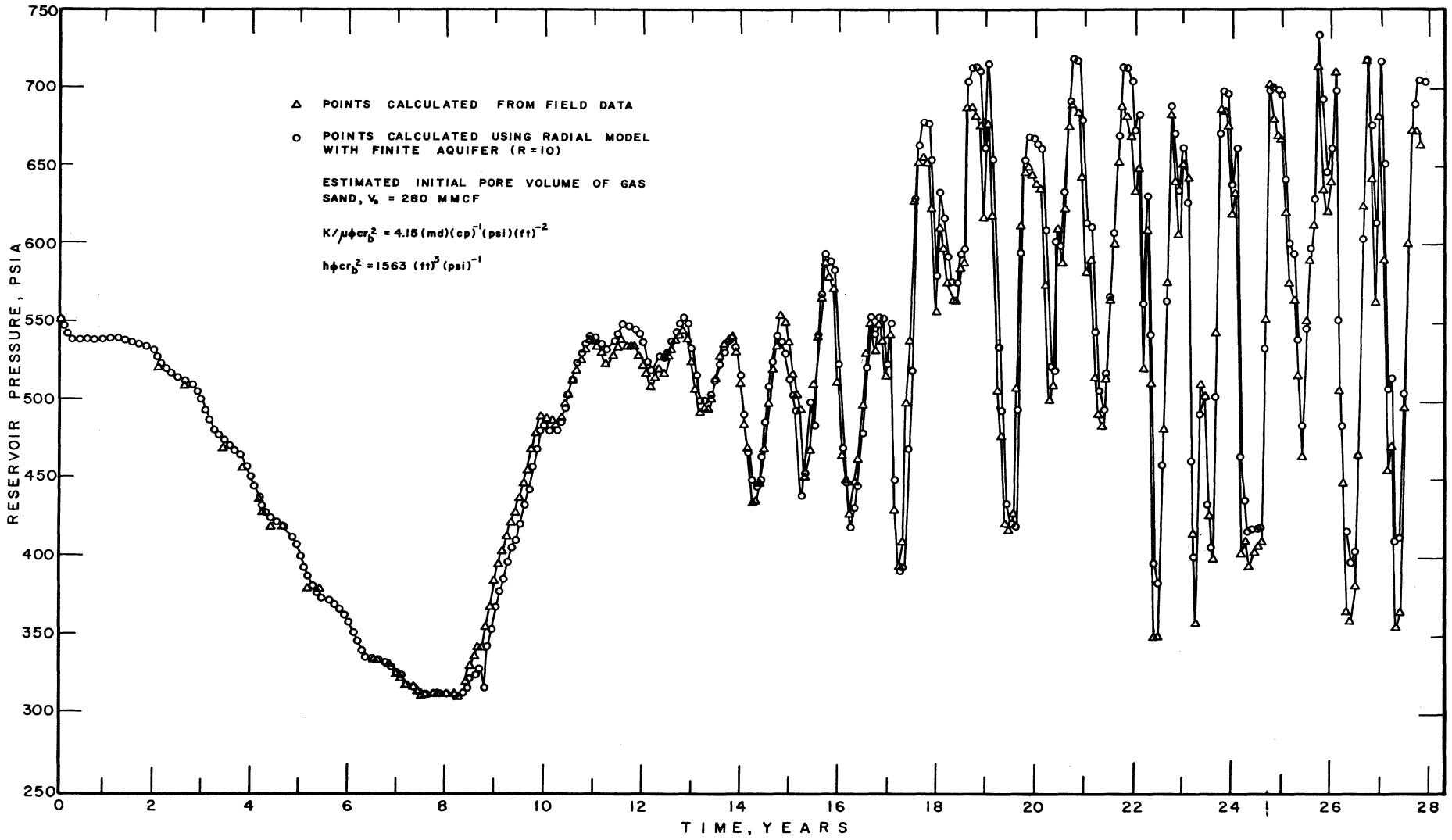

Fig. F-4. Comparison of Field F pressure predicted using finite radial model (R=10) with observed pressures.

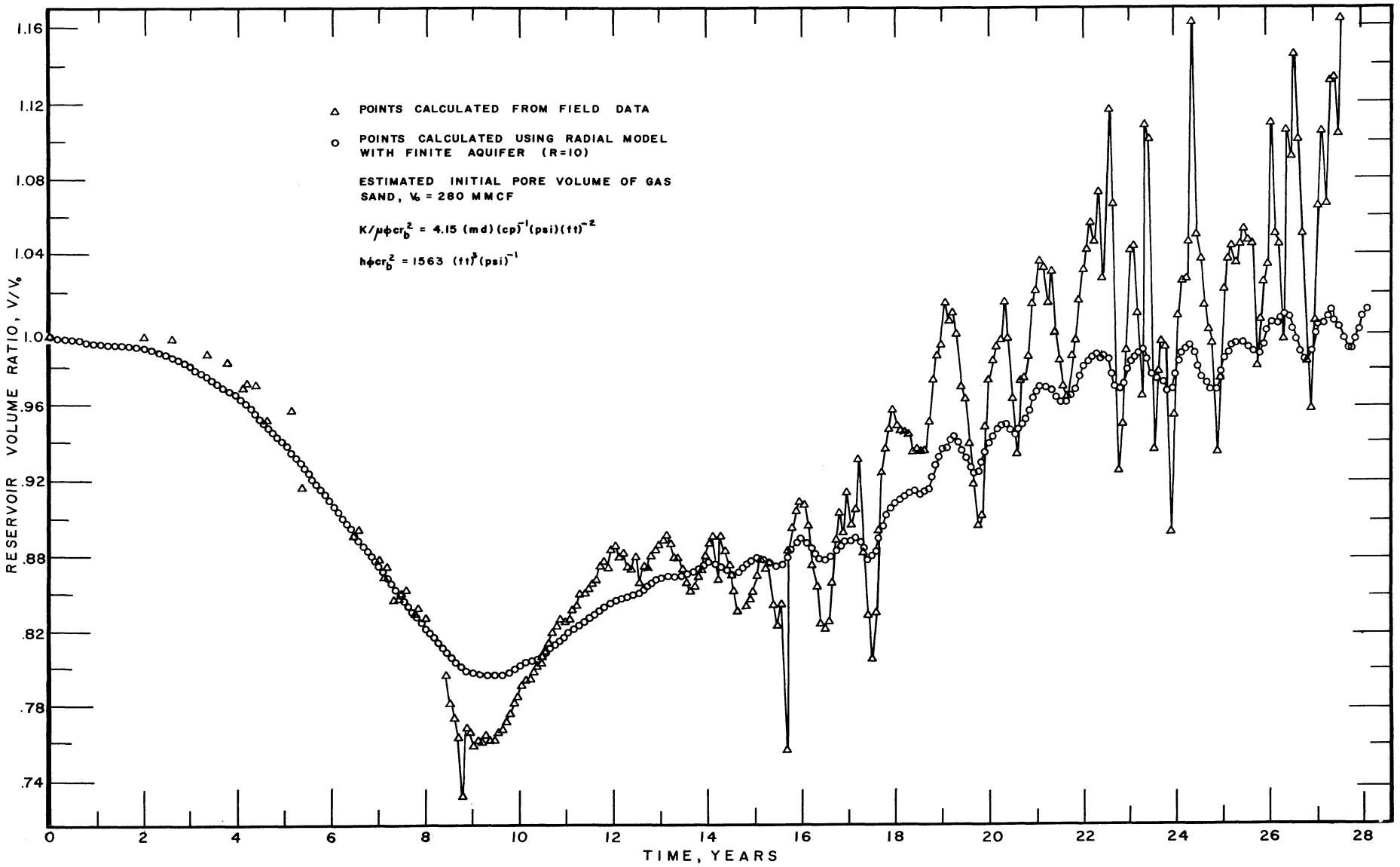

Fig. F-5. Comparison of Field F volume ratio predicted using finite radial model (R=10) with volume ratios calculated from field data.

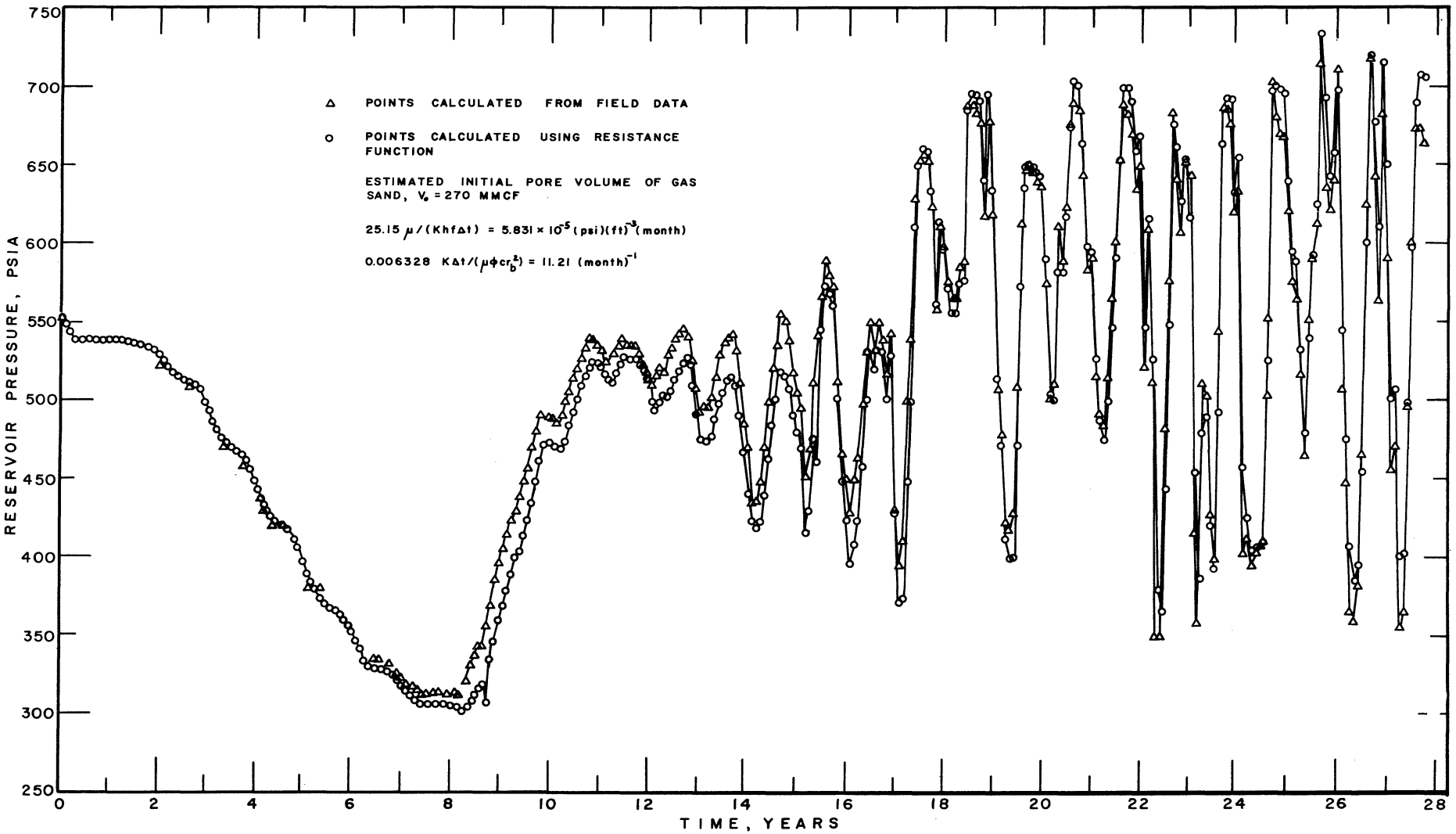

Fig. F-6. Comparison of Field F pressures predicted using resistance function with observed pressures.

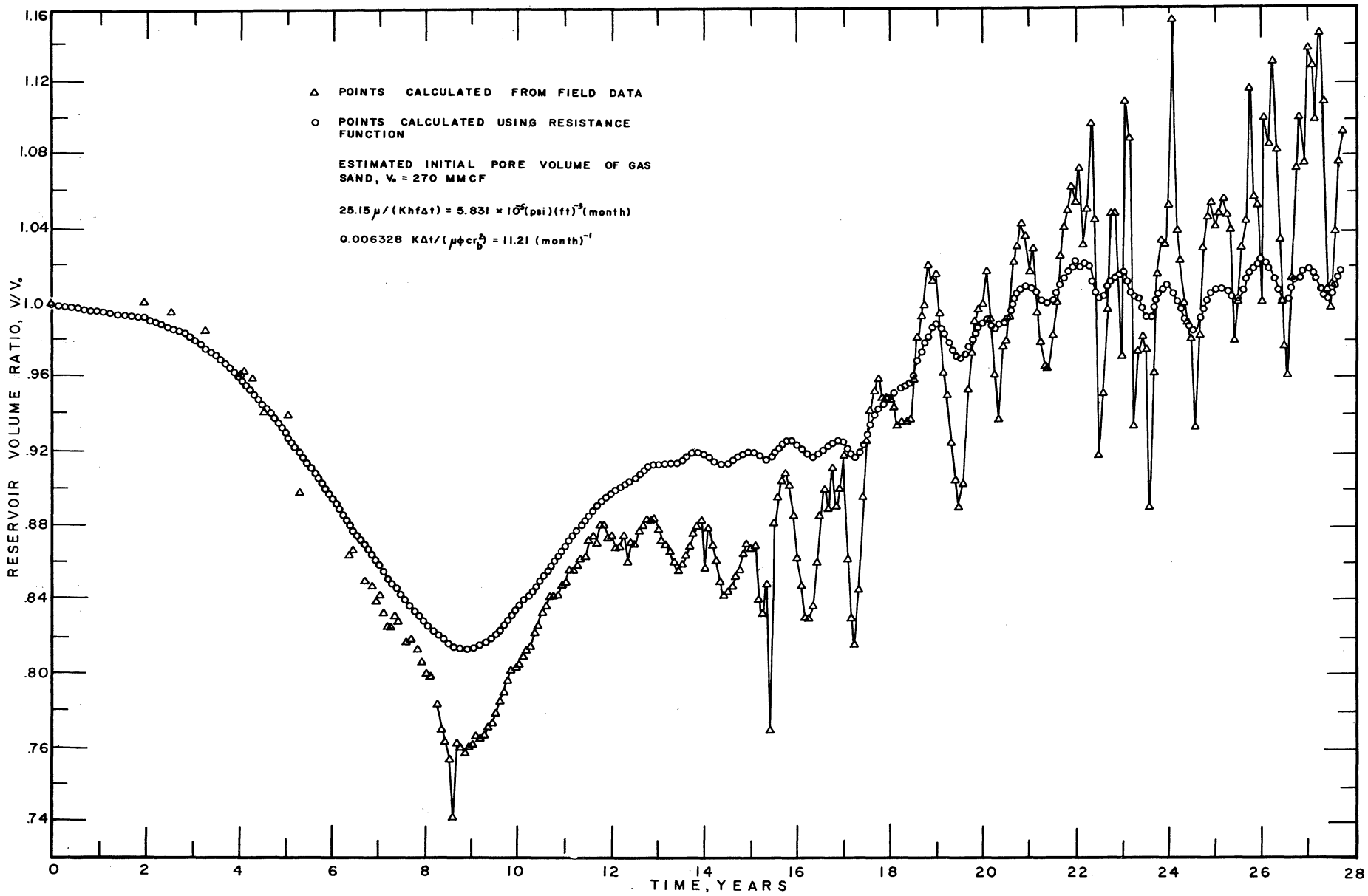

Fig. F-7. Comparison of Field F volume ratios predicted using resistance function with volume ratios calculated from field data.

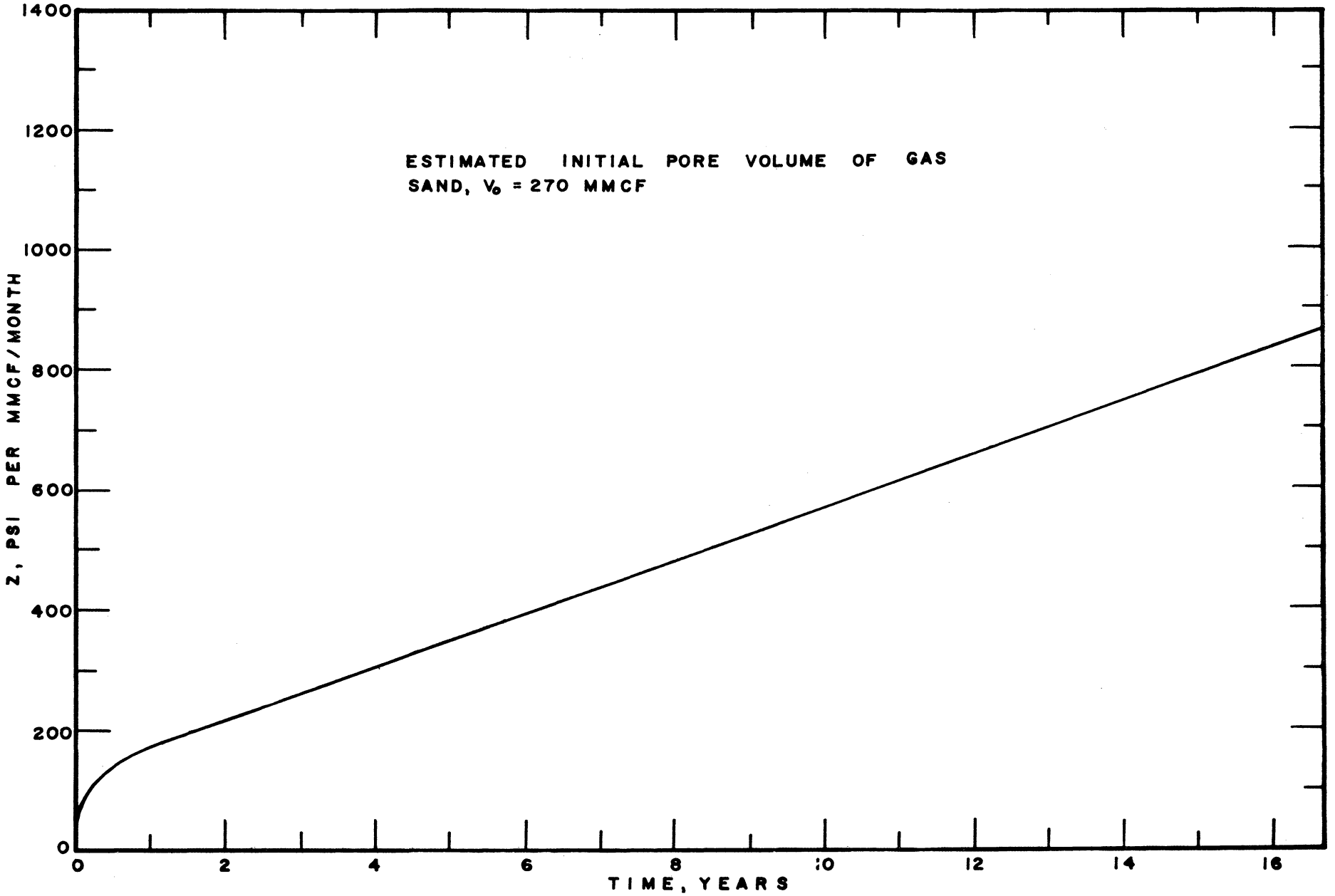

Fig. F-8. Resistance function vs. time for Field F.

FIELD G

Field G is a large gas reservoir under the Gulf of Mexico off the coast of Louisiana. As a result of this gas field's isolation, it is rather doubtful that this field will be used for gas storage.

1. GEOLOGY

As Field G is located in the same sand formation as Field A, the properties of this field consist of fine to medium-grained moderately cemented sandstone with numerous discontinuous shale lenses.

2. FIELD DATA

The reservoir and fluid properties for Field G are summarized in Table G-1 and the production-pressure history, in Table G-2.

The initial pore volume was determined by comparing the predicted and observed pressures for several initial pore volumes. The best estimate for the initial pore volume using the radial model is 950 MMCF while the resistance function's best estimate is 1000 MMCF.

Note that since this has never been used for storage, only primary production data are available.

3. RESULTS

The performance predicted for this reservoir in which the correction for water movement is ignored shows lower pressures than are observed (Fig. G-2).

The radial model, the best representation of Field G based on the reservoir geometry (Fig. G-1), was selected for determining the degree of water movement. With the exception of the last few points, the predicted pressures are in good agreement with the observed pressures as shown in Fig. G-3. The difference between the predicted and observed performance in the last year of the field history may be due to confinement of the aquifer. However, not enough data are available to investigate this possibility with a geometric model. The reservoir volume ratios calculated from this prediction is presented in Fig. G-4.

TABLE G-1

GAS FIELD G DATA

Aquifer Characteristics

Type of formation	Sandstone
Porosity	29%
Permeability	1474 millicarcys
Thickness	100 ft
Depth to top of aquifer	7500 ft
Viscosity of liquid in aquifer	0.5 centipoise
Compressibility of brine and formation	7×10^{-6} vol/vol-psi

Data on Gas Field

a. Field geometry

Location	Gulf of Mexico
Type of formation	Sandstone
Nature of structure	Structural dome

b. Gas-sand formation and fluid properties

Gas compressibility correlation, $z = a + bP$	
Constant a	0.776
Constant b	4.17×10^{-5}
Depth to top of sand	7400 ft
Reservoir temperature	640°R
Reservoir thickness	100 ft
Base conditions for gas measurements	P_b = 14.7 psia T_b = 520°R

c. History of gas reservoir

Discovery date	1951
Initial discovery pressure	3485 psia (well bottom)
Initial pore volume	950×10^6 cu ft

TABLE G-2

GAS INVENTORY AND PRESSURE HISTORY FOR FIELD G

Pressure Base = 14.7 psia
Temperature Base = 520°R

Date	Cumulative Gas Production MMSCF at End of Month	P, Well Bottom, psia, at End of Month
1951 Feb		3485
Aug	747	3458
1952 Feb	2047	3437
Aug	3593	3410
1953 Feb	5146	3397
Aug	6994	3370
1954 Feb	8771	3357
Aug	10620	3335
1955 Feb	12448	3318
Aug	14250	3303
1956 Feb	16100	3282
Aug	18113	3257
1957 Feb	20790	3215
Aug	23352	3170
1958 Feb	21289	3157
Aug	28318	3113
1959 Feb	29689	3105

Application of the resistance function method to the data from Field G resulted in better agreement between the calculated and observed behavior than was predicted by the radial model, as is shown in Figs. G-5 and G-6. The fact that the slope of the resistance curve (see Fig. G-7) decreases for the entire history shows that the reservoir is either infinite or that the effect of the boundary has not been felt.

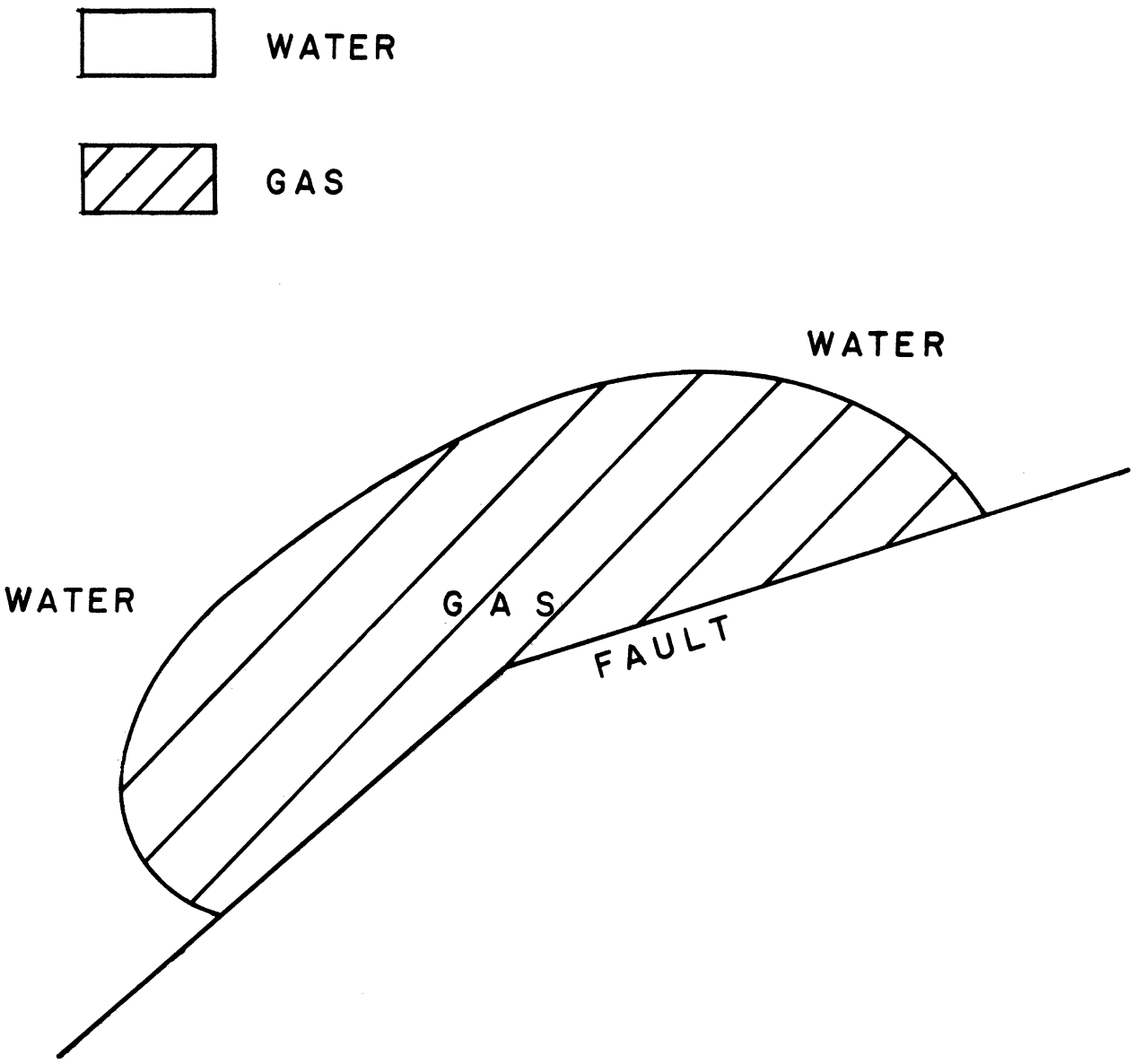

Fig. G-1. Areal sketch showing boundary of Field G.

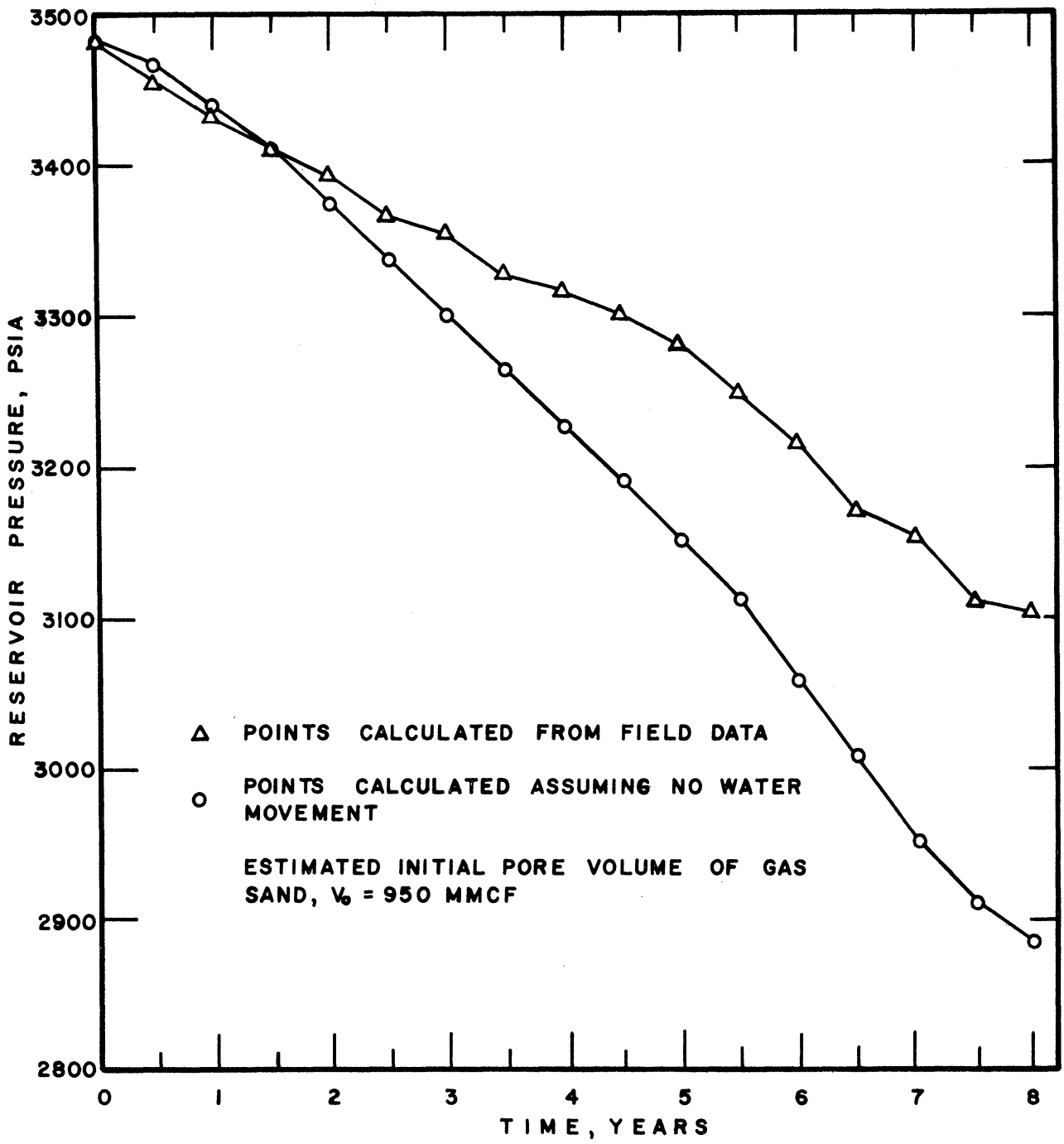

Fig. G-2. Comparison of Field G predicted pressures assuming no water movement with observed pressures.

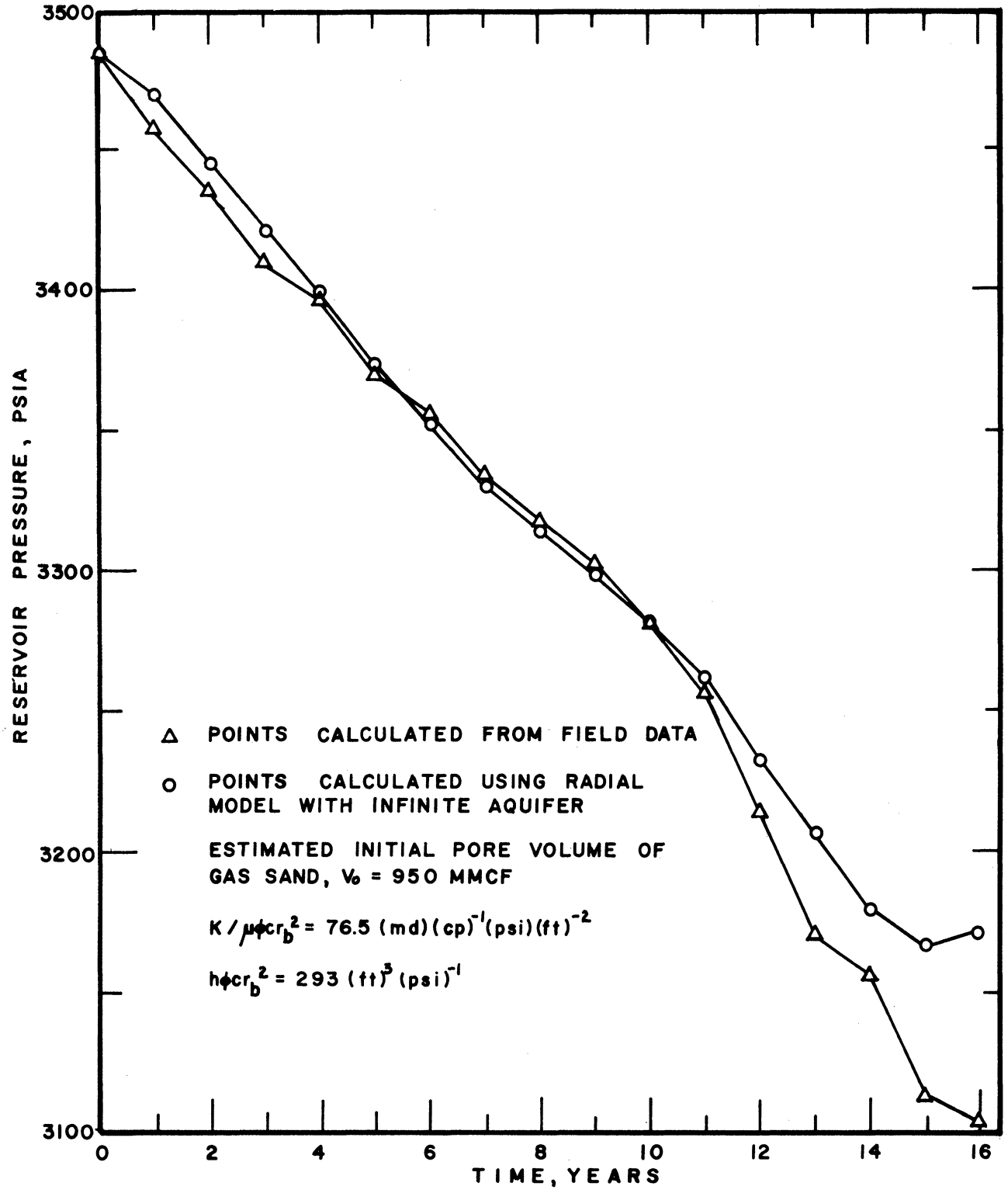

Fig. G-3. Comparison of Field G pressures predicted using radial model (infinite aquifer) with observed pressures.

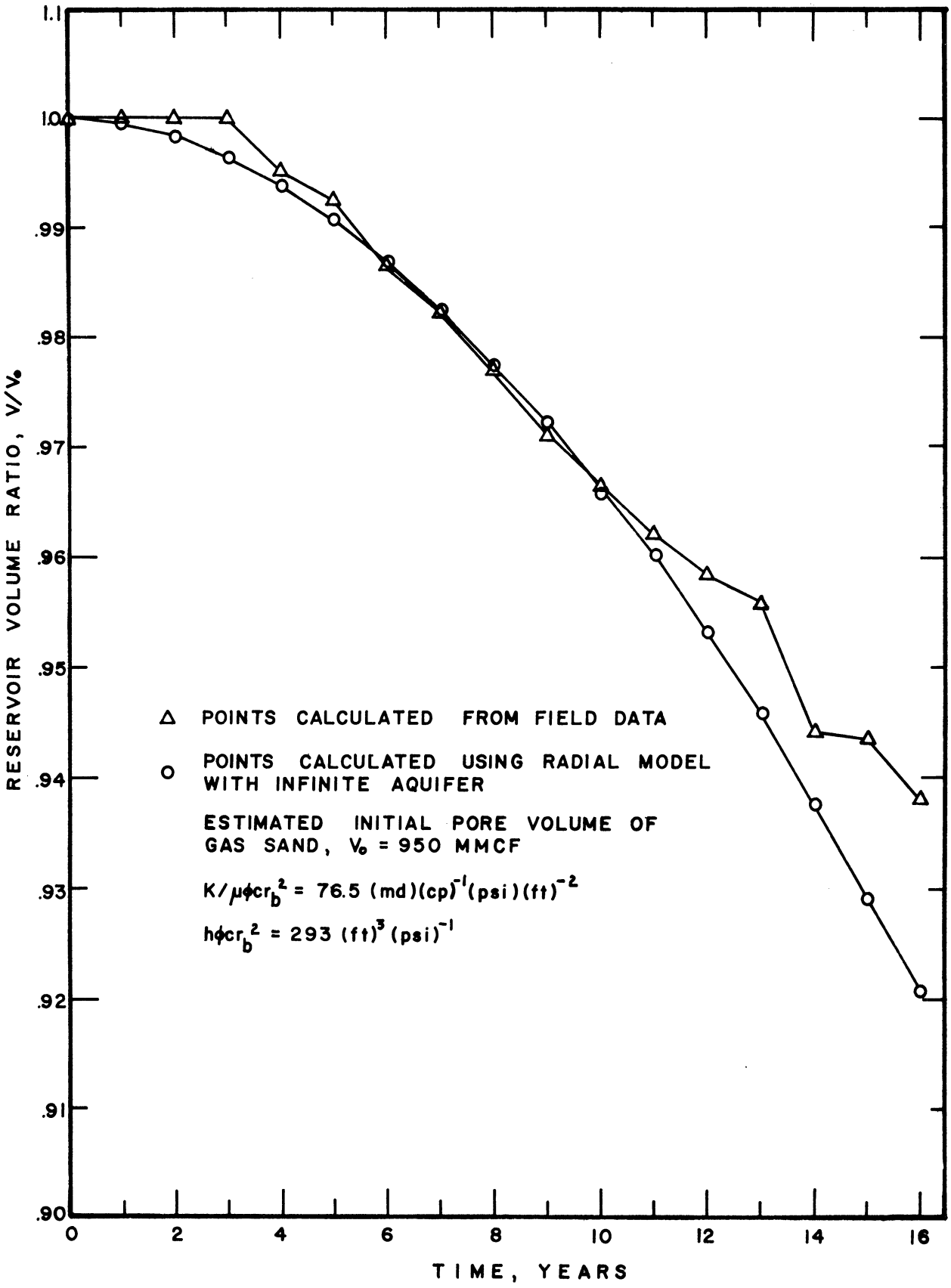

Fig. G-4. Comparison of Field G volume ratio predicted using radial model (infinite aquifer) with volume ratios calculated from field data.

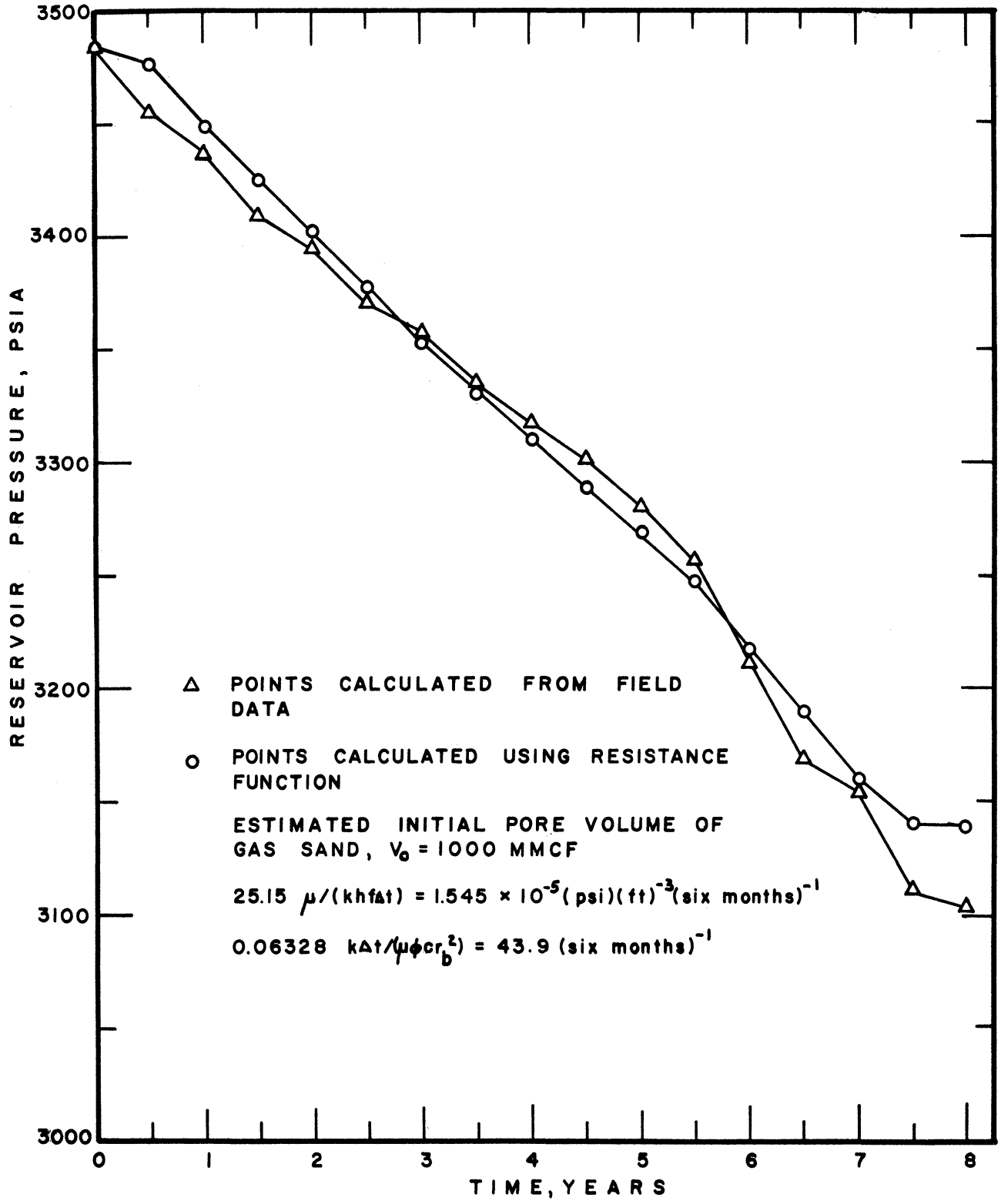

Fig. G-5. Comparison of Field G pressures predicted using resistance function with observed pressures.

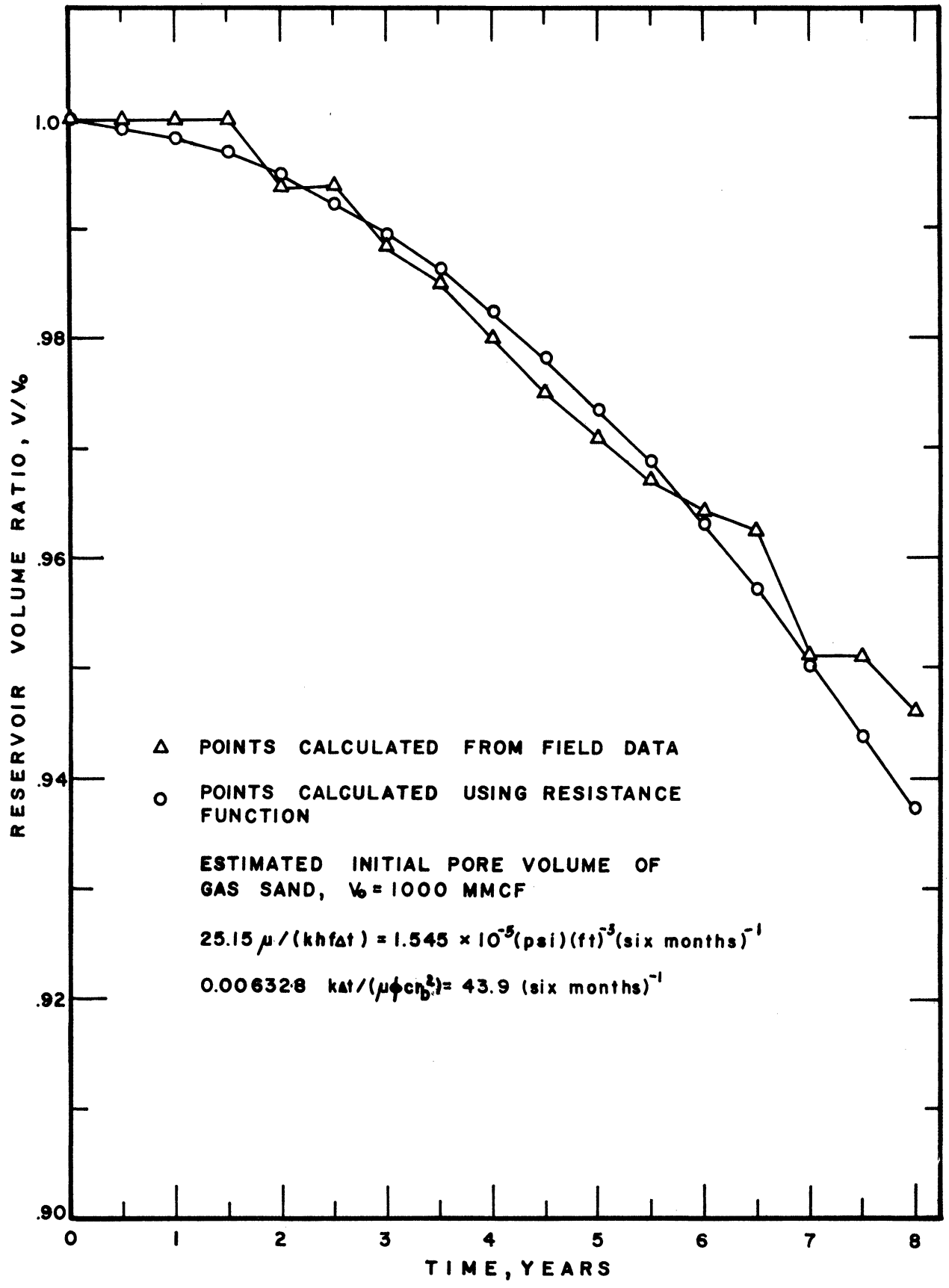

Fig. G-6. Comparison of Field G volume ratio predicted using resistance function with volume ratios calculated from field data.

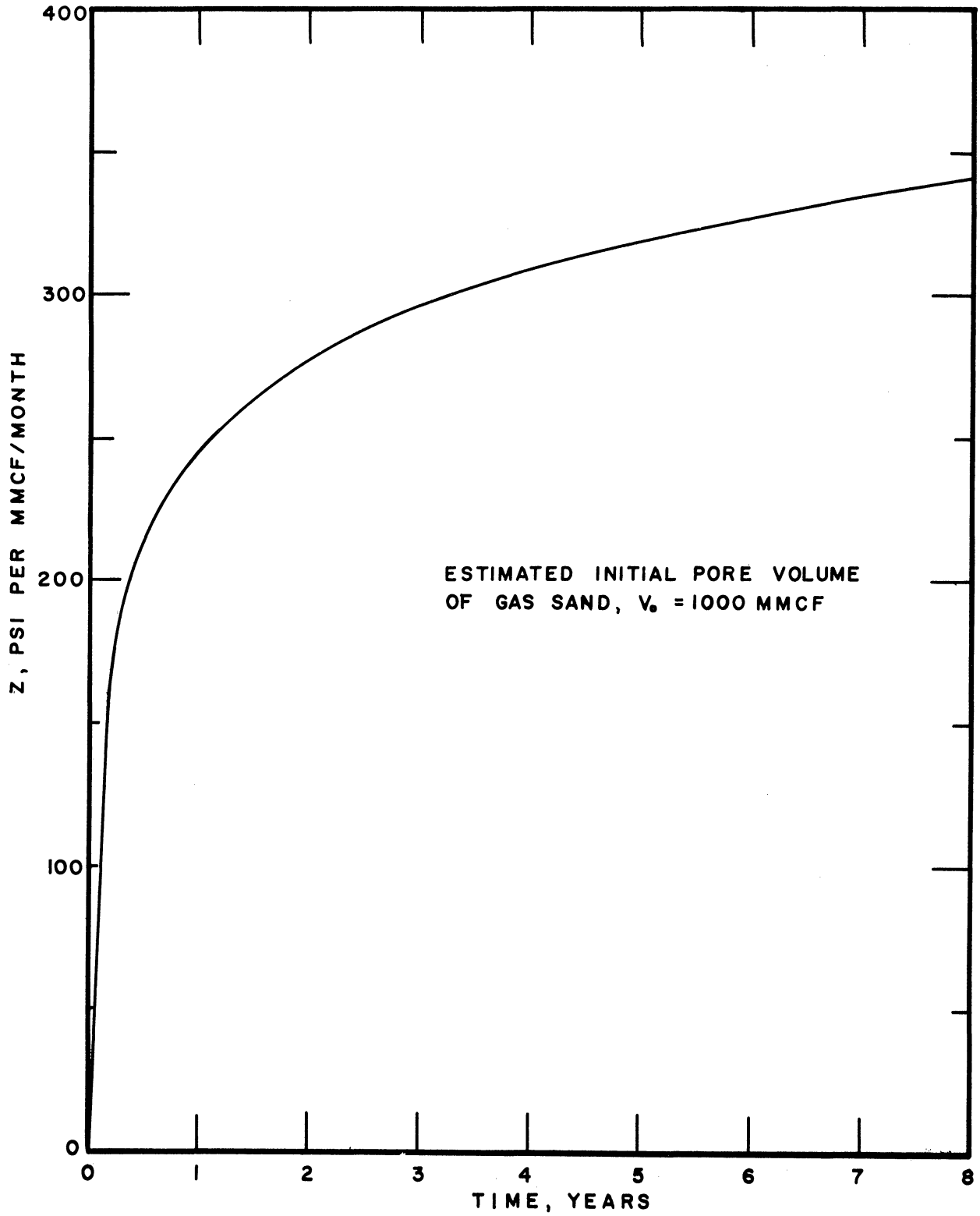

Fig. G-7. Resistance function vs. time for Field G.

FIELD H

Field H is a large gas field discovered in Michigan in August, 1956, with an original void space of 900 million cubic feet and discovery pressure of 1346 psia (well bottom). To date, 111 storage wells and 23 observation wells have been drilled.

Before the field was converted to storage operation in March, 1960, more than 16 billion standard cubic feet had been produced. The acceptibility of this field for storage operation has been in question since the permeability is extremely low (2.4 millidarcys). The answer will be ascertained after operating a few years.

As the available data are rather limited, this study should be considered as preliminary to a more complete investigation to be presented next year after more complete information is available. In addition, corrections due to interference resulting from a neighboring gas field on the same aquifer will be presented.

An areal sketch of this field is shown in Fig. H-1.

1. GEOLOGY

In contrast to the previous fields investigated, the composition of Field H is dolomite instead of sandstone. This dolomite is very "tight" with an estimated permeability of only 2.4 millidarcys. This formation is designated as the A_2 dolomite in the Salina Formation of the Silurian Age.

2. FIELD DATA

The gas and aquifer properties are summarized in Table H-1 and the gas inventory and pressure history is listed in Table H-2.

The value for the initial pore volume which gave the best agreement between observed and predicted pressures for both the radial model and resistence function method was 900 million cubic feet.

3. RESULTS

A comparison of the observed and predicted pressures (Figs. H-2, and H-3) when the assumption of no water movement or water movement in a radial gas bubble, show the predicted pressure are not in agreement with those ob-

TABLE H-1

STORAGE FIELD H DATA

Aquifer Characteristics

Type of formation	Dolomite
Porosity	11.26%
Permeability	2.4 millidarcys
Thickness	19.7 ft
Depth to top of aquifer	2662 ft
Viscosity of liquid in aquifer	1 centipoise
Compressibility of brine and aquifer	7×10^{-6} vol/vol-psi

Data on Storage Field

a. Field Geometry

Location	Michigan
Type of formation	Dolomite
Nature of structure	Anticlinal

b. Gas-sand formation and fluid properties

Gas compressibility correlation, $z = z + bP$	
Constant a	1.0
Constant b	1.9437×10^{-4}
Depth to top of sand	2642 ft
Reservoir temperature	532°R
Reservoir thickness	19.7 ft
Base conditions for gas measurements	P_b = 14.73 psia
	T_b = 520°R

c. History of gas reservoir

Discovery date	1957
Initial discovery pressure	1346 psia (well bottom)
Initial pore volume	900×10^6 cu ft
Date converted to gas storage	1960

TABLE H-2

GAS INVENTORY AND PRESSURE HISTORY FOR FIELD H

Pressure Base = 14.73 psia
Temperature Base = 520°R

Date	Cumulative Gas Production, MMSCF	P, Well Bottom, psia, at End of Month
1957 Dec	--	1346
1958 Jan	457	--
Feb	1009	--
Mar	1491	--
Apr	1713	--
May	1813	--
June	1840	1252
July	1854	--
Aug	1946	--
Sept	2098	--
Oct	2423	--
Nov	2870	--
Dec	3714	--
1959 Jan	4615	--
Feb	5370	--
Mar	5812	--
Apr	5925	--
May	6025	1186
June	6191	--
July	6749	--
Aug	7753	--
Sept	8360	--
Oct	9235	--
Nov	10720	--
Dec	12340	--
1960 Jan	14370	--
Feb	16130	993
Mar	16110	--
Apr	14540	--
May	11820	--
June	9139	--
July	6036	--
Aug	2925	--
Sept	1242	1415

served. The application of the resistance function method (Fig. H-5) improved the prediction considerably, but the disagreement is still large for some points. Part of the disagreement can be rationalized when one considers the pressure gradients within the gas bubble itself. In the previous fields investigated, the permeability of the gas formation is several orders of magnitude larger, thereby allowing use of an average gas pressure for the entire field. As a result of the low permeability in this field, pressure gradients of several hundred pounds within the gas bubble itself have been found. When these gradients are considered, the discrepancy between observed and predicted pressure is not so surprising.

The calculation of pore volume ratios (Figs. H-4 and H-6) show only a slight water movement is present, the void space being reduced by less than 5% prior to gas injection.

The shape of the resistance curve, plotted in Fig. H-7, indicates that the effect of the aquifer boundary has not been felt.

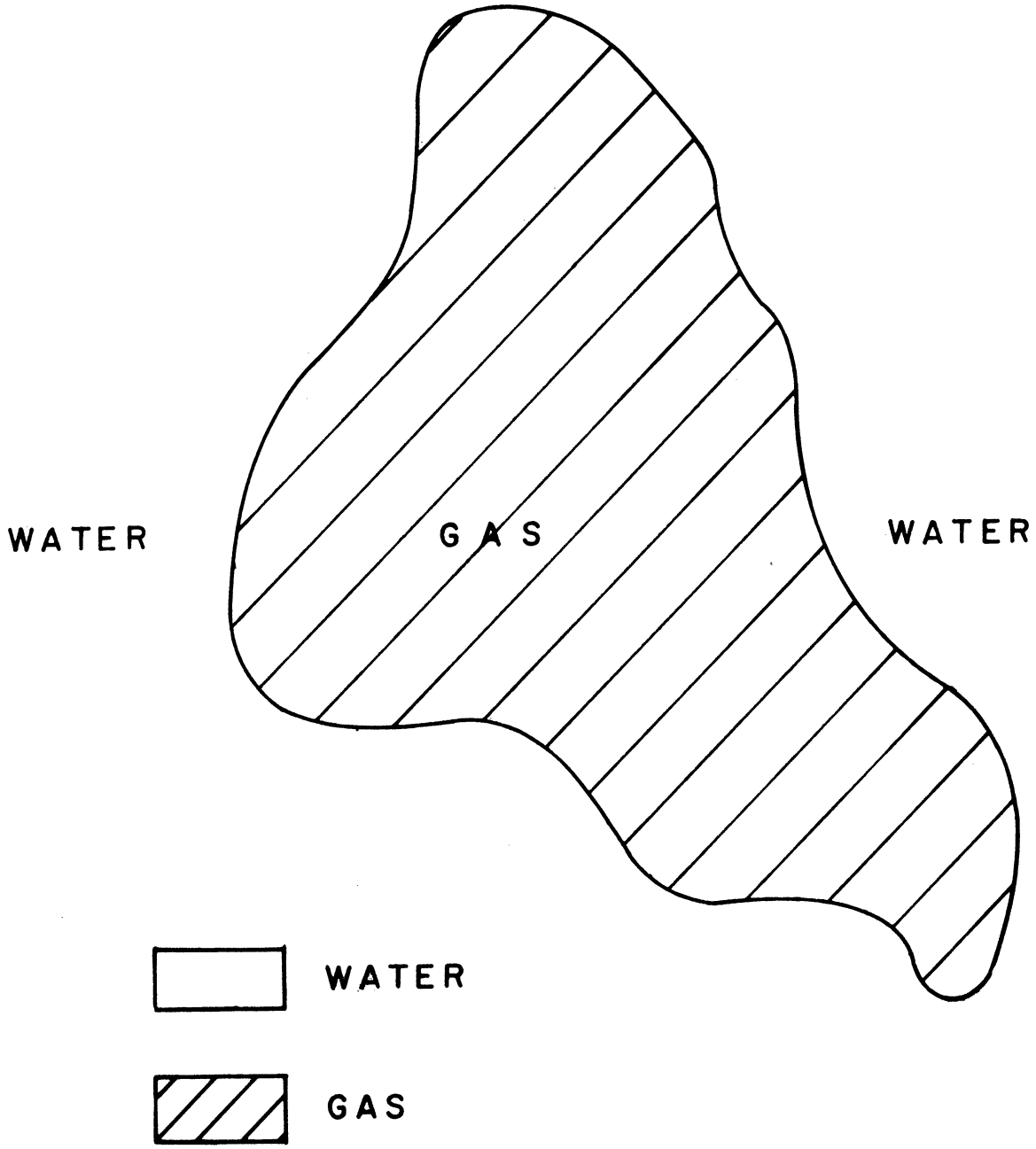

Fig. H-1. Areal sketch showing boundary of Field H.

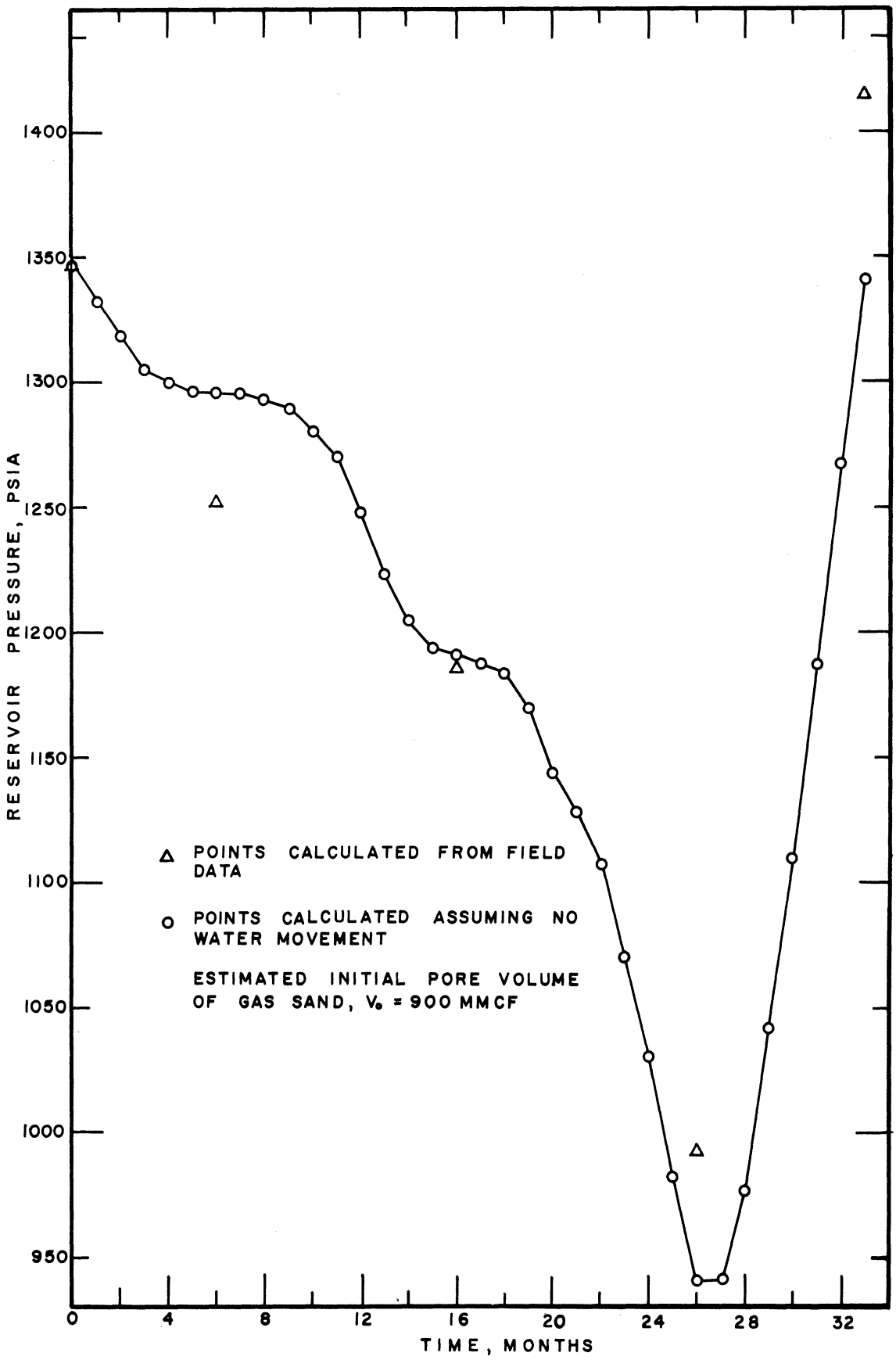

Fig. H-2. Comparison of Field H predicted pressures assuming no water movement with observed pressures.

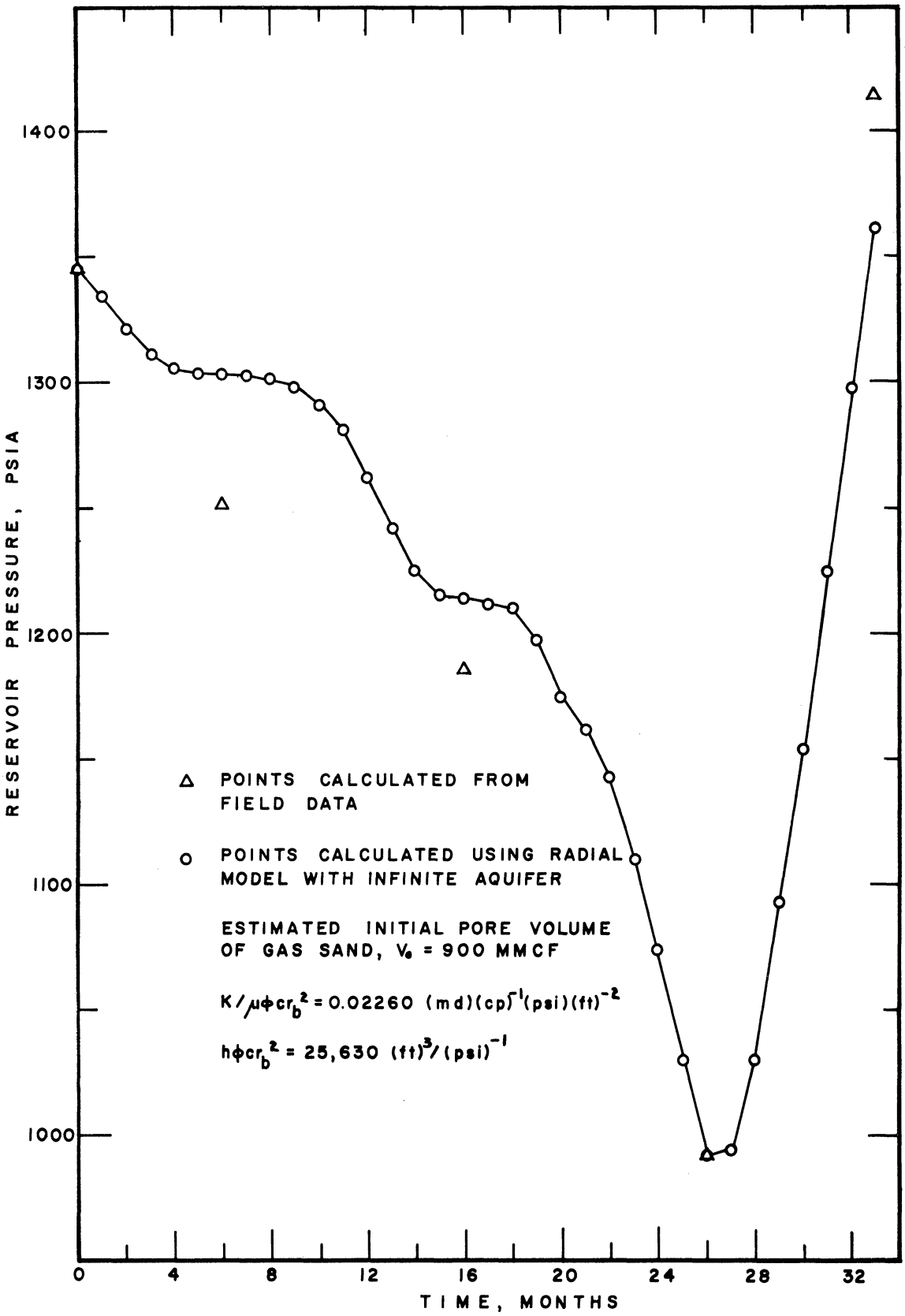

Fig. H-3. Comparison of Field H pressures predicted using radial model (infinite aquifer) with observed pressures.

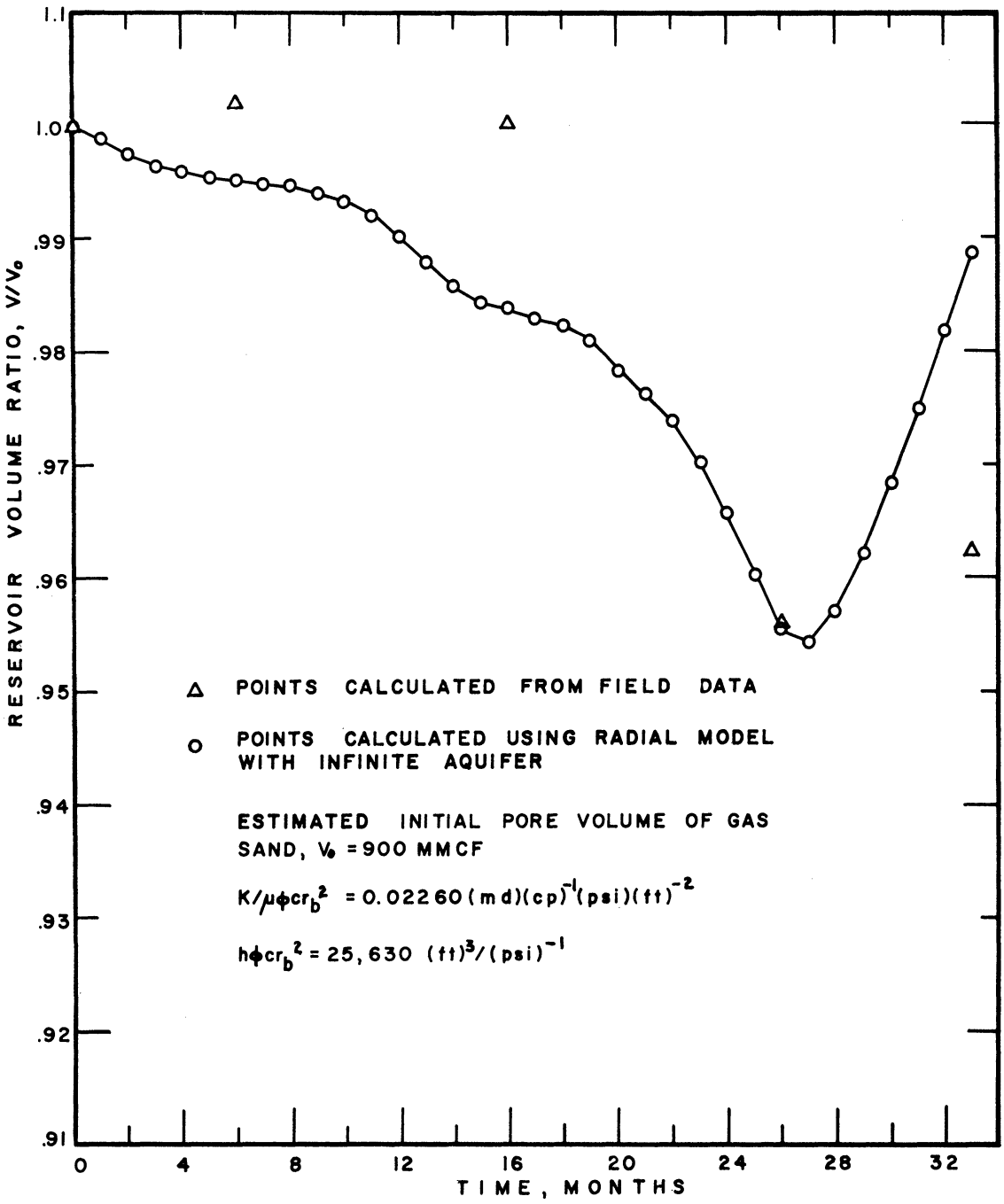

Fig. H-4. Comparison of Field H volume ratio predicted using radial model (infinite aquifer) with observed pressures.

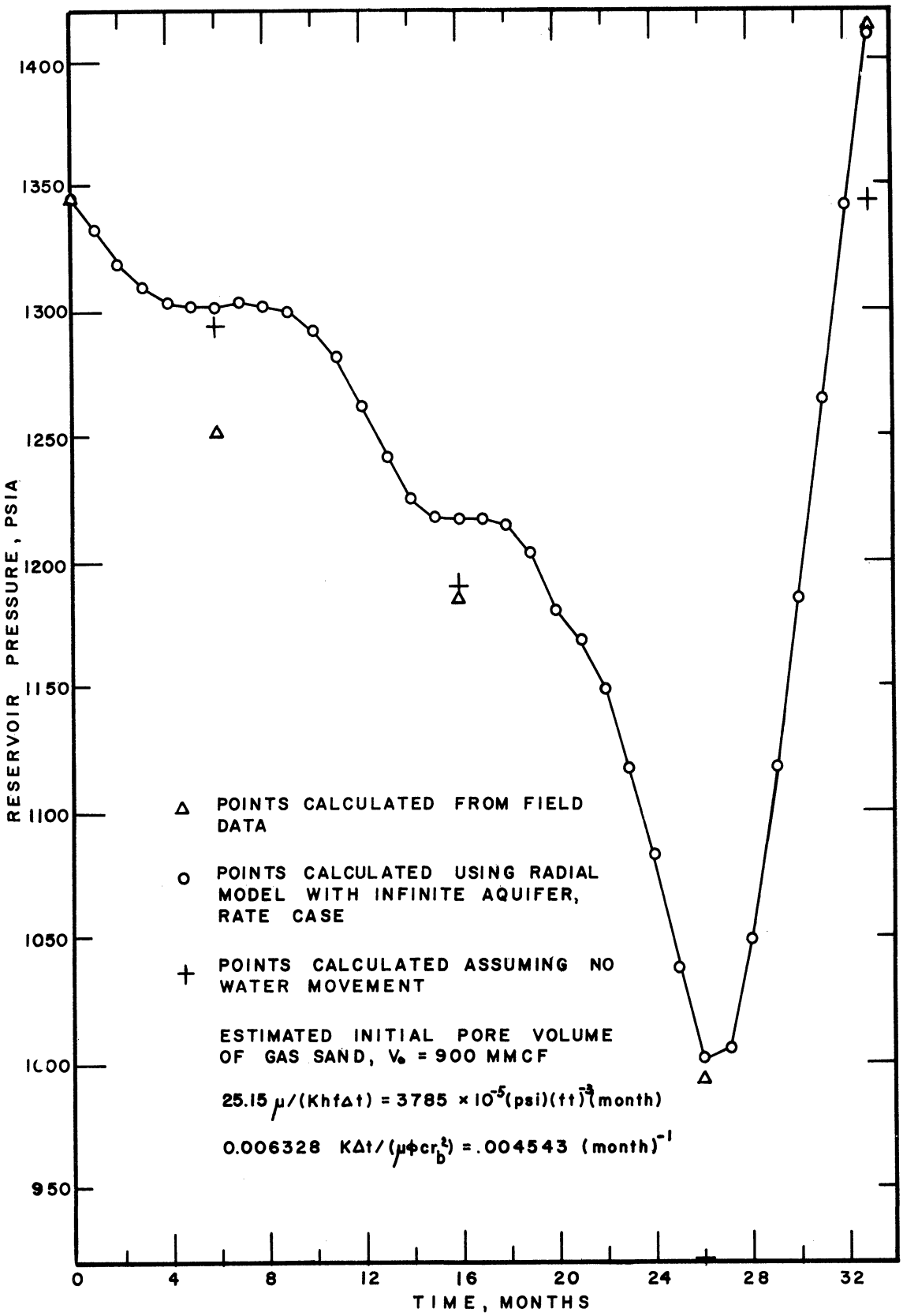

Fig H-5. Comparison of Field H pressures predicted using resistance function with observed pressures and those calculated assuming no water movement.

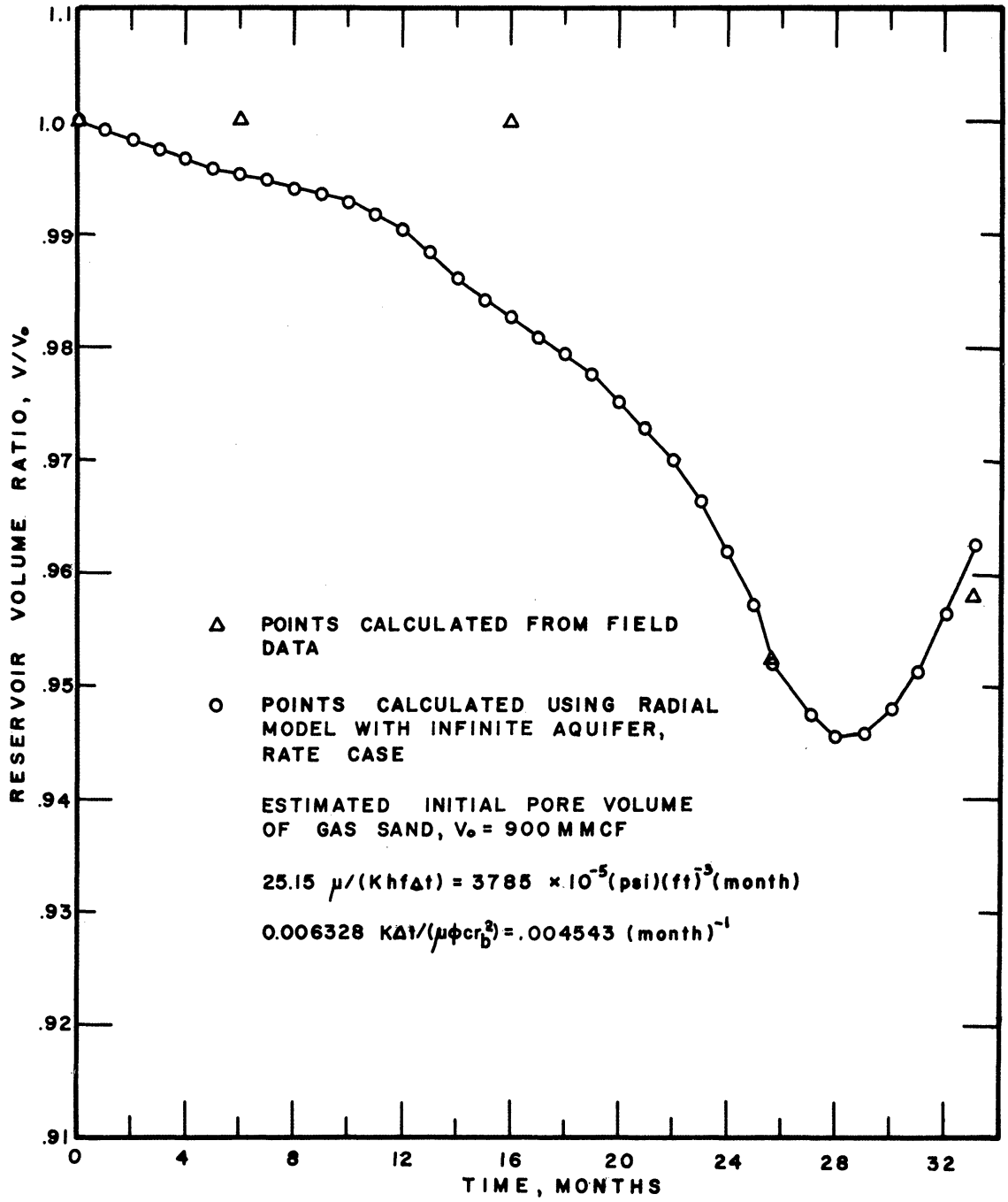

Fig. H-6. Comparison of Field H volume ratio predicted using resistance function with volume ratios calculated from field data.

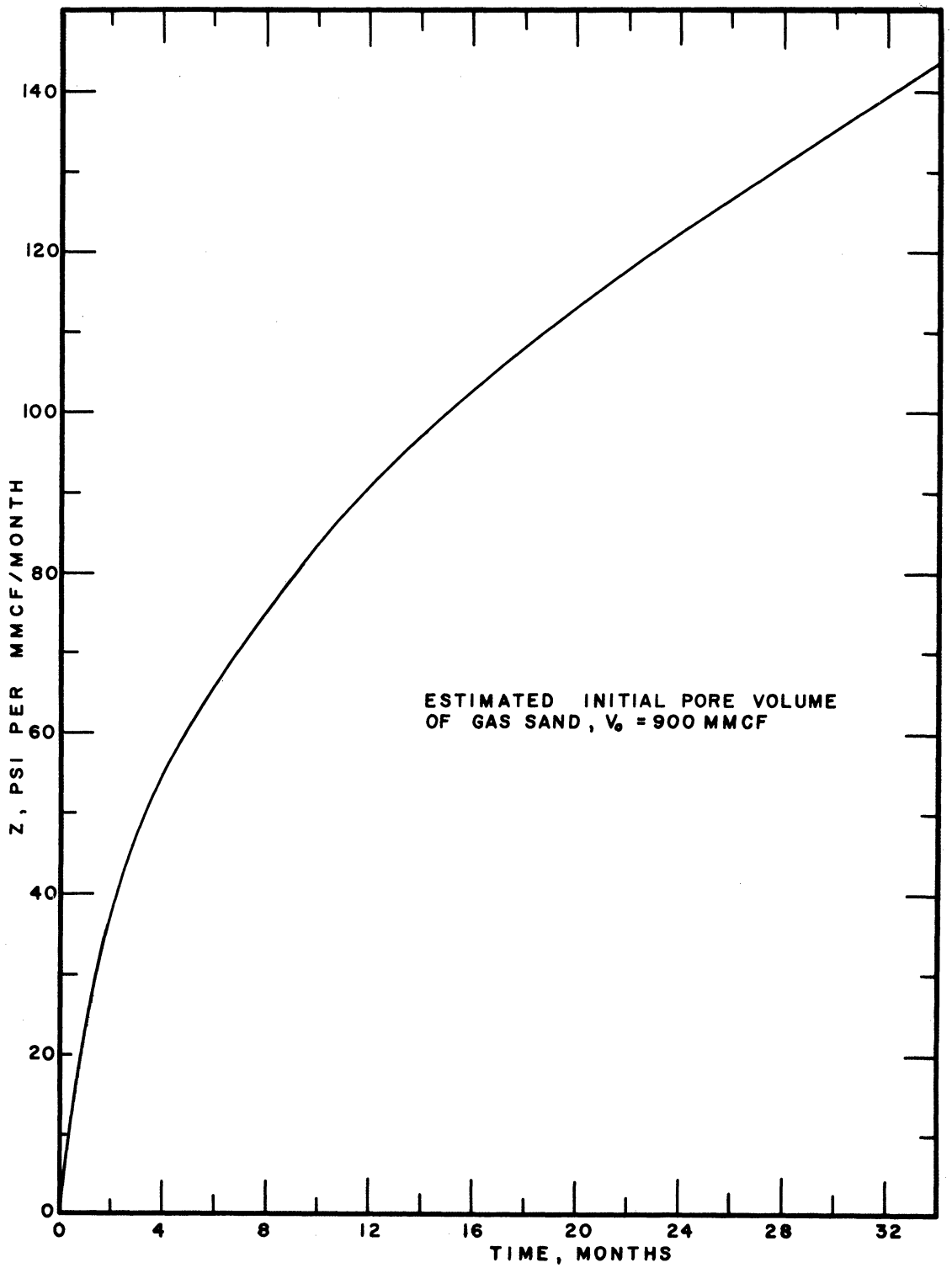

Fig. H-7. Resistance function vs. time for Field H.

TABLE V

PARAMETERS USED FOR FIT AND PREDICTION OF FIELD DATA

Field	Model	Aquifer Radius / Gas Bubble Radius	Initial Pore Volume Occupied By Gas Bubble, V_o, MMCF	K_1, From Estimated Physical Properties	K_1, Adjusted to Give Best Fit of Field Data	K_2
A	Radial	∞	3850	26,600	3,750	19
	Resistance Function	-	3850	1.704×10^{-6}	5.77×10^{-6}	10.88
B	Radial	∞	110	17,400	4,506	14.4
	Thick Sand	∞	110	3.72×10^{-6}	7.6×10^{-5}	14.4
C	Linear	∞*	24	-	689	-
D	Radial	∞	30	5,000	8,150	10
	Resistance Function	-	30	1.652×10^{-4}	6.52×10^{-6}	14.41
E	Radial	∞	440	980	2,225	5.0
	Radial	9	440	980	2,806	5.0
	Thick Sand	∞	440	1.67×10^{-7}	6.3×10^{-6}	5.0
	Resistance Function	-	470	4.13×10^{-5}	5.77×10^{-5}	3.68
F	Radial	∞	290	9,060	1,170	4.15
	Radial	10	280	8,760	1,563	4.15
	Resistance Function	-	270	2.36×10^{-5}	5.83×10^{-5}	11.21
G	Radial	∞	950	3,860	293	76.5
	Resistance Function	-	1000	1.625×10^{-6}	1.545×10^{-5}	43.9
H	Radial	∞	900	2,096	25,630	0.0226
	Resistance Function	-	900	1.747×10^{-2}	3.78×10^{-4}	4.54×10^{-3}

*Aquifer length/gas bubble length.

ACKNOWLEDGMENT

The authors wish to gratefully acknowledge the encouragement, interest and many constructive suggestions from the members of the supervising committee and participating gas and oil companies for Project NO31.

The funds for the research program were made available by the American Gas Association under the auspices of its Pipeline Research Committee.

REFERENCES

1. Chatas, A. T., "A Practical Treatment of Nonsteady-State Flow Problems in Reservoir Systems," Pet. Engr., May, 1953.

2. Katz, D. L., et al., Handbook of Natural Gas Engineering, McGraw-Hill Book Co., Inc., New York, 1959.

3. Katz, D. L., Tek, M. R., Coats, K. H., and Katz, M. L., Engineering Studies on Movement of Water in Contact with Natural Gas, American Gas Association Project NO31, Annual Report, The University of Michigan, September, 1960.

4. Van Everdingen, A. F., and Hurst, W., "The Application of the Laplace Transformation to Flow Problems in Reservoirs," Trans. AIME, 186, 305 (1949).